INTERNAL ENERGY EFFECTS IN TANDEM MASS SPECTROMETRY

By

MARIA DEL PILAR OSPINA

A DISSERTATION PRESENTED TO THE GRADUATE SCHOOL
OF THE UNIVERSITY OF FLORIDA IN PARTIAL FULFILLMENT
OF THE REQUIREMENTS FOR THE DEGREE OF
DOCTOR OF PHILOSOPHY

UNIVERSITY OF FLORIDA

1998

ACKNOWLEDGMENTS

I would like to express my sincere gratitude to my two research advisors, Drs. Richard A. Yost and David H. Powell. Dr. Yost showed patience, support and was always open to discussions when I needed him. He was also so full of options that, although sometimes I felt overwhelmed with them, they definitely opened a whole new world for me. Dr. Powell, not only has been my co-advisor but also a good friend. He always showed me the light at the end of the tunnel when I could not see it.

I also express my appreciation to the rest of the members of my committee, Drs. John Eyler, Sam Colgate and John Toth for taking the time to read and correct this manuscript.

Many thanks to Dr. Gilbert Mattieu (somewhere in Belgium) and Dr. Marta Isabel Paez for introducing me to mass spectrometry when I worked at the Universidad del Valle in Cali, Colombia.

I would like to acknowledge the past and present members of the Yost research group with whom I have had the opportunity to interact. I express my thanks to Dr. Tracie Williams and Alejandra Rodriguez, for the uplifting words that kept me going. I am grateful to Drs. Steve Boue, Chris Reddick, Jon Degnore, and to Joe MacClellan, Jim Murphy, and many others for the great jokes and stories that gathered during the time we shared the office.

Many thanks go to Dr. Jodie V. Johnson for his useful discussions and for always having time to share some stories. I express my appreciation to Dr. Lidia Matveeva for allowing me instrumental time when I needed it and especially because I could see how strong a woman could be when there is a reason to it.

I would like to thank Jeanne Karably and Donna Balkcom for making my life easier during all these years.

Some of the work presented in this dissertation was done in the Protein Core of the Interdisciplinary Center for Biotechnology Research of the University of Florida. I want to acknowledge Dr. Nancy Denslow for allowing me to use her MALDI-TOF and Alfred Chung and Lisa Sapp for training me to use this instrument. Their help was vital to the completion of this work.

My greatest appreciation and gratitude goes to my parents for always encouraging me to take the next step and for their support, not only moral but also economic, even though they live many miles away.

During the time I stayed in Gainesville, my brother came to live with me and I met many people that became part of my circle of friends and social life. Having a family away from the family has been vital to my sanity during these years and has helped me in coping with the stress of graduate school.

Finally, I am in great debt to my fiancé, Roberto Bravo, who not only decided to come with me to the U.S. even though he had no English at all, but also has been my best friend. He is the major inspiration I have. He showed me that perseverance is one of the best virtues one can have, but that being around the right people is what really keeps one on track when pursuing goals.

TABLE OF CONTENTS

Abstract of Dissertation Presented to the Graduate School
of the University of Florida in Partial Fulfillment of the
Requirements for the Degree of Doctor of Philosophy

INTERNAL ENERGY EFFECTS IN TANDEM MASS SPECTROMETRY

By

Maria del Pilar Ospina

December, 1998

Chairman: Richard A. Yost
Major Department: Department of Chemistry

The role of precollisional internal energy on MS/MS spectra was investigated. Several ionization techniques were used to generate the ions employed in these studies. It was shown that the extent of fragmentation and the relative abundance of the fragment ions were dependent on the reagent gas used for chemical ionization (CI) and the matrix used in liquid secondary ion mass spectrometry (LSIMS). Internal energy can be added as thermal energy into the molecules even during fast heating in direct chemical ionization and it can affect the appearance of the tandem mass spectra.

Fragmentation observed in the high-energy (HE) and low-energy (LE) collision-induced dissociation (CID) spectra of ions formed by CI depends on the exothermicity of the proton transfer reaction between the reagent ions and the analyte. It was observed that qualitatively, spectra are similar, but that the

fragmentation efficiencies correlate with energy deposited by the ionization technique for the compounds studied. Although it has been claimed that relative fragment ion abundances in CID spectra are unaffected by internal energy, the results of this study contradict that claim. Even ignoring fragment ions which arise from low activation energy pathways, variation in relative abundances were observed in HE- and LE-CID.

The effect of matrix on matrix-assisted laser desorption ionization post-source decay (MALDI-PSD) spectra was investigated by comparison to LE- and HE-CID spectra. For the compounds employed in these studies, MALDI-PSD spectra are very similar to LE-CID, and structural information can be derived. It was found that ions formed when α-cyanohydroxycinnamic acid (HCCA) was used as matrix generated more lower mass fragment ions than other matrices. It is not clear, however, that merely proton affinity differences between matrix and analyte are responsible for the characteristics of the fragmentation. PSD spectra are much less affected by matrix than are LSIMS spectra or even CI spectra with different reagent gases.

These studies emphasize the importance of understanding and controlling different important parameters in tandem mass spectrometry in order to optimize the information derived from the tandem mass spectrometry experiments.

CHAPTER 1
INTRODUCTION

Mass spectrometry has become one of the most important tools for the analysis and identification of molecules. In a mass spectrometer, ions are formed with a distribution of internal energies; some may be excited to a degree that they may fragment. The extent to which fragmentation takes place and the corresponding reaction rates for the fragmentation reactions are determined by the internal energy imparted to the ion, its structure, and the time allowed between formation and detection.

The introduction of "soft" ionization techniques has been integral to the success of mass spectrometry. So called "soft" ionization techniques generally include fast atom bombardment (FAB)[1] or liquid secondary ion mass spectrometry (LSIMS)[2], matrix-assisted laser desorption ionization (MALDI)[3,4], electrospray ionization (ESI)[5] and chemical ionization (CI).[6] Since ions formed by these ionization techniques typically do not fragment extensively, if at all, the ion current for a given compound is generally concentrated in a single ion. This provides molecular mass information and the number of components in a particular mixture. It also improves the sensitivity and detection limits of mass spectrometric measurements.[7] However, there is a concomitant disadvantage to the simplicity of mass spectra from these ionization techniques. They lack

structural information due to the absence of significant fragmentation. This disadvantage can be overcome by the use of ion activation methods, which impart internal energy to these ions, thus promoting fragmentation and yielding more structural information. The most commonly used method of excitation is collisional activation (CA), whereby additional energy is imparted to the ion by collisions with neutral gas molecules. The overall resulting fragmentation process is called collision-induced dissociation (CID).[8,9] Fragmentation obtained by CA is affected by both the energy deposited during ionization (the precollisional internal energy) and the subsequent energy deposited in the collisional activation event. Most of the studies on CID have been directed towards the latter collisional activation, but a few studies have been reported on the dependence of CID spectra on precollisional internal energy.[10-16] Although the studies on the effect of internal energy have been somewhat controversial, there is supporting evidence[10,12] that a significant dependence of CID spectra on precursor internal energy is only observed for those reactions with lowest critical activation energies such as reactions resulting in metastable ions, which are fragment ions that can also be observed in the absence of any subsequent collisional activation.

The goal of this research work was to understand the role of internal energy on CID spectra, since controlling internal energy in mass spectrometry is crucial to the optimization of the CID process and the amount of information derived from it. This might help to tailor the mass spectral features to a particular need. In this research, the role of precollisional internal energy in CID spectra

was studied. The internal energy deposited by the ionization technique was varied by changing reagent gases in CI and by using different matrices in LSIMS and MALDI. Also, comparison of different ionization techniques and CID processes are addressed in particular sections of these studies.

Overview of the Dissertation

This dissertation is divided into five chapters. The first chapter provides a general review of the principles of tandem mass spectrometry, including ion activation and dissociation, and internal energy. It also discusses briefly some of the instruments associated with MS/MS. Relevant introductions and references to each chapter are included therein.

Chapter two presents a comparison of ionization techniques and their effect on CID spectra. MS/MS spectra were obtained from precursor ions generated by chemical ionization (CI), liquid secondary ion mass spectrometry (LSIMS) and electrospray ionization (ESI). The effect of changing the reagent gas in CI and the matrix in LSIMS is also shown.

The third chapter contains a more detailed study on how, by varying the reagent gas in CI, the internal energy of the precursor ion is changed. The effect of the internal energy on high-energy CID spectra is evaluated for $(M+H)^+$ ions of pyrrole, pyrrolidine, pyridine, and piperidine. Comparison of high- and low-energy CID spectra of $(M+H)^+$ ions of pyrrole as a function of reagent gas in CI is also included in this chapter.

Chapter four provides the results of comparing low- and high-energy CID spectra to post-source decay (PSD) fragmentation for some compounds of biological interest. It also presents data on the effect of the matrix in PSD experiments as a way to control the internal energy of the precursor ion in matrix-assisted laser desorption ionization (MALDI).

The final chapter presents a summary of this work and discusses some future experiments.

Tandem Mass Spectrometry or Mass Spectrometry/Mass Spectrometry (MS/MS)

The basic concept behind tandem mass spectrometry is the measurement of mass-to-charge ratios of ions before and after a reaction within a mass spectrometer[7]. Tandem mass spectrometry and its implications and applications have been the subject of several books and reviews.[7,17-22] MS/MS is widely used for structural elucidation of ions and for the analysis of targeted compounds in complex mixtures.[7,8,19] A simple representation of an MS/MS experiment is shown in Figure 1-1. Once ions are formed in the ion source, at least two stages of mass analysis are considered. The first stage involves the isolation of a precursor ion. The ion selected can dissociate on its way to the second stage, which is used to analyze the ions resulting from the dissociation event. The mass spectrum (MS/MS) obtained is presumed to be characteristic of the structure of the precursor ion, which in turn should allow one to obtain structural information on the neutral compound from which the ion originated.

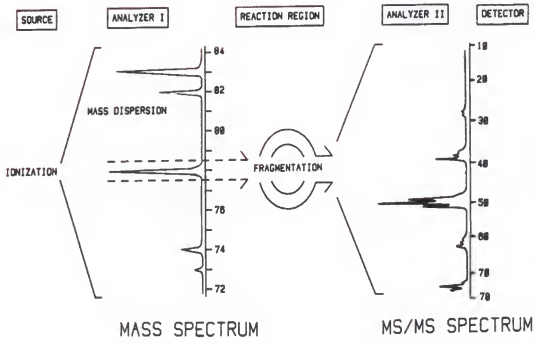

Figure 1-1. Representation of the MS/MS technique. Taken from reference 17.

Ion Dissociation

Unimolecular dissociation

The ionization of neutrals results in the formation of molecular (i e., M^+ ions) and "pseudomolecular" ions (for instance, $(M+H)^+$ or $(M+Na)^+$ ions) with a wide range of internal energies. As a result, a certain fraction of the ions may have enough energy to dissociate. Ionization and dissociation are not spontaneous processes; rather, they occur within certain statistical time frames.

The theory of unimolecular reactions has been referred as quasi-equilibrium theory (QET)[23] and has been the subject of several books.[24-26] The fundamental ideas of QET are: (1) for a polyatomic ion, the time required for dissociation is long compared to the time needed for ionization and excitation or the time for most vibrations, (2) the rate of dissociation is slow compared to the rate of distribution of excess excitation energy over all degrees of freedom, (3) an ion in a mass spectrometer represents an isolated system in the state of internal equilibrium in which energy is distributed over all degrees of freedom with equal probability, and (4) fragmentation products result from a series of competitive and consecutive unimolecular reactions starting with the precursor ion.

The QET has been found to be a good approximation to describe unimolecular dissociation but some of these assumptions are restricted in their applicability. For example, for very large ions ($\geq$ 1000 atoms) assumption (2) probably does not hold.[27] Also, for some Fourier transform ion cyclotron

resonance (FTICR) and ion trap experiments where ions are excited by multiple collisions and thermal equilibrium might be approached, assumption (3) is not valid.[28]

The degree of competition between the different dissociation processes available for an ion can be measured[7] by the rate constant (k) of the process at a given internal energy (E). Thus, the simplest equation for the rate constant of any dissociation reaction is given by the equation:

$$k(E) = \upsilon\left(\frac{E - E_o}{E}\right)^{s-1} \qquad (1\text{-}1)$$

where ν is the frequency factor, E_o is the activation energy of the reaction, and s is the effective number of oscillators in the ion. The rate of decomposition is related to the probability of a given vibrational mode or modes acquiring enough energy to rupture bonds.[29]

Dissociation processes can be recorded in a mass spectrum if they occur within the instrumental time frame, since ion source residence times can vary with the ionization method and the instrumental parameters.[7] In sector instruments, using electron ionization (EI) as the ionization method, ions that dissociate with rate constants greater than 10^6 s^{-1} will dissociate prior to leaving the ion source and can be observed as fragment ions in the mass spectrum. These are called unstable ions since they rapidly fall apart because their internal energy content is sufficient to overcome the activation energy. Ions that dissociate with rate constants less than 10^4 s^{-1} generally do not dissociate in the time frame of the mass spectrometric experiment and are recorded as molecular

or pseudomolecular ions in the mass spectrum. These are called stable ions and have low internal energy content or high activation energies. There are also ions that react with rate constants between 10^4 and 10^6 s^{-1}. These are called metastable ions and can dissociate on their way to the detector after leaving the ion source. Metastable ions generally have lower average internal energies than those decomposing in the ion source and often represent mass spectral reactions of lowest activation energies such as rearrangements.[30,31]

Activation reactions

Since the abundances of ions that are metastable are very low, many techniques have been developed to activate and dissociate polyatomic ions. The most common method of secondary excitation is collisional activation (CA). In this technique ions are activated by collisions with a neutral gas and the resulting fragmentation is called collision-induced or collisionally activated dissociation (CID or CAD).[8,9] This process will be discussed in more detail later. Ions can also be activated by collisions with a surface. The subsequent fragmentation is called surface-induced dissociation (SID)[32,33] and it has shown to deposit large amounts of internal energy (in excess of 7eV for 100 eV collisions). The internal energy distribution of ions excited by SID can be controlled by the translational energy of the incident ion, and it is narrow compared to that obtained by CA. Another method for activation of polyatomic ions is based on the absorption of photons during laser irradiation. The resulting fragmentation process is known as photo-induced dissociation (PID).[34,35] The energy deposited

by this technique is very well defined and can be varied by changing the wavelength of the light source. It has been demonstrated that ion activation is possible by using a high-flux electron beam.[38] This technique, called electron excitation, yields comparable energy deposition to PID without the need for lasers. The most recently introduced type of ion excitation is called electron capture-induced dissociation (ECID).[37-41] In ECID, a keV beam of doubly charged ions (M^{2+}) is collided with various targets (gas or surface), and, among other processes, electron capture can occur resulting in M^{+} ions. The M^{+} ions that contain large internal energies will decompose. This process produces increased fragmentation due to the increase in average excitation energy of the ions. The internal energy of the M^{+} ion can be controlled by selecting target gases with different ionization energies. Collisions with gases of lower ionization energy result in higher excitation energies than collisions with gases of higher ionization energies. The analytical applicability of this method is very promising since generation of doubly charged species is possible with electrospray and other new spray methods.[42]

Collision-Induced Dissociation

The use of CID not only increases the amount of fragmentation, and therefore, the structural information, but also filters out matrix ion contribution when the proper analyte ion is selected.[43]

Many reviews have been written on CID.[44-49] It is not the objective here to discuss the many details of this technique, which has proven to be a very

powerful method to provide structural information. CID allows ions of a particular mass to be selected by a first stage of mass analysis and transmitted into a collision gas cell where ions undergo collisional activation. Collisions increase the internal energy of the ion and stimulate dissociation. The resultant product ion spectrum is observed by a second stage of mass analysis.

For a polyatomic ion, the overall CID mechanism is accepted to proceed in two steps of different time scales.[45] The first step is a fast collision activation process (10^{-15} - 10^{-14} s) in which translational energy of the precursor ion is converted into internal energy of the ion and target molecule. The second step is unimolecular dissociation of the excited ion. These processes are represented in equations 1-2 and 1-3.

$$M_p^+ + N \rightarrow M_p^{+*} + N' \qquad (1\text{-}2)$$

$$M_p^{+*} \rightarrow M_a^+ + M_b \qquad (1\text{-}3)$$

where M_p^+ and N are, respectively, the precursor ion and the collision gas species before collision, and M_p^{+*} and N' are the activated precursor ion and the collision gas after collisions, respectively. M_a^+ and M_b are the dissociation products of M_p^{+*}.

In CID, a fraction of the kinetic energy of the precursor ion is converted into internal energy by collisions with a neutral gas. Collisions between an ion and a neutral gas are easily explained in the center-of-mass (COM) coordinate system. A very detailed explanation of this coordinate system is included in several publications and will not be covered here.[45,48,49]

The maximum collision energy (E_{LAB}) that can be converted into internal energy (E_{COM}) in a single collision is given by the equation:

$$E_{COM} = E_{LAB}\left(\frac{m_{target}}{m_{ion} + m_{target}}\right) \quad (1\text{-}4)$$

where m_{target} is the mass of the neutral collision gas used as target, m_{ion} is the mass of the incoming ion and E_{LAB} is the kinetic energy of the precursor ion in the laboratory frame of reference. As expected, the choice of collision gas[50,51] , its pressure[52-54], the ion kinetic energy[10], and the angle at which scattered products are collected[45] all affect the internal energy deposited in the collected ion by CID.

Collisional activation can be carried in two collision energy regimes, the keV regime (high-energy CID) and the eV range (low-energy CID). Collisions in the keV range are accessible on sector instruments, time-of-flight, and some hybrid mass spectrometers. High-energy (HE) CID spectra (>1keV collision energy) are usually the result of single collisions between the precursor ion and an inert gas. Internal energy deposition in this energy range does not depend significantly on collision energy. The average internal energy deposited in HE-CID ranges from 1-3 eV although the distribution is wide and is characterized by a high energy tail (10-20 eV)[54] which allows large energy transfers of low probability to occur. This is reflected in the low abundance of product ions (~1% yield) and in the observation of a broader range of fragmentation pathways of high critical energy such as charge-remote fragmentation.[55] At several keV

collision energy, the interaction time between a small ion of some hundreds of daltons and a target gas is in the order of 10^{-16} to 10^{-15} s. This is too short to be accompanied by a vibration (typically 10^{-14} sec), but is about the time of an electronic excitation. Thus, collisions at keV are expected to result in excitation of internal electronic modes.[45] Evidence that electronic excitation dominates in HE-CID is given for the highly endothermic charge permutation and charge stripping reactions that are observed in HE-CID and that require electronic excitation.[17,18] On the other hand, the fact that high mass ions undergo CA and dissociate is evidence that vibrational excitation also plays an important role in the dissociation of polyatomic ions at keV.[48]

The most common collision gas used in HE-CID is helium. Its high ionization energy (~ 24 eV) minimizes charge transfer to the target, its small diameter and low mass reduce significant scattering losses. Furthermore, helium has a high cross section which enhances the electronic excitation believed to operate at high energies.[56] It has been demonstrated that the pressure of the collision gas required for 50% attenuation of the ion beam decreases with changing the collision gas from helium to xenon, on HE-CID spectra of substance P and glycol.[50] More recent studies on HE-CID of peptides[43] showed significant reduction or complete disappearance of specific side chain fragmentation (d_n, w_n, and v_n type ions) in CID spectra when helium was used as the collision gas rather than argon. The same studies revealed that argon was more effective in promoting fragmentation as the molecular weight of the peptide increased.

CID in the low energy regime (< 100 eV) is carried out in multipole instruments, Fourier transform ion cyclotron resonance, quadrupole ion trap, and some hybrid mass spectrometers. LE-CID spectra are typically the result of multiple collisions and therefore, multistep cleavage reactions are predominant.[57]

The internal energy deposited during low energy collisions can be very sensitive to changes in collision energy or collision gas pressure.[58-64] The average internal energy is estimated to be between 1 and 10 eV.[64] The distribution of internal energies is much narrower than in HE-CID, which implies that precursor ions are often almost absent or have very low abundance and that fragmentation processes with large critical energies are not frequently observed.

Low-energy collisions do not result in efficient transfer of energy to electronic modes since the typical interaction time is in the order of 10^{-13} s (longer than the period of an electronic excitation, but comparable to the time of vibrational excitation). On the other hand, electronic excitation can not be ruled out, since several LE-CID studies have shown that some fragmentation reactions are the result of significant contribution from electronic excitation.[65-67]

In LE-CID, larger fractions of the maximum available kinetic energy (E_{COM}) can be converted into internal energy of the ion.[68] The efficiency of LE-CID processes can be affected by proton or electron transfer reactions from the ion to the collision gas.[7] Since these reactions compete with CID, it is helpful to use target gases with high ionization energies and low proton affinities to minimize these contributions. Heavy targets are preferred over light targets because they deposit more internal energy.[69-71] A compromise between target mass and

ionization energy is made to obtain high energy transfer without a decrease in the fragmentation efficiency; therefore, argon and nitrogen are usually employed in LE-CID.

Many studies have been published comparing low- and high-energy CID.[72-78] Collisions occurring in these two energy regimes often lead to different fragmentation pathways, which provide complementary structural information. High-energy CID spectra seem to be more reproducible from instrument to instrument than LE-CID where product ion spectra vary more with collision energy and target gas pressure.[60,76]

Instrumentation

The growth of MS/MS as a powerful analytical technique was based on the development of new instruments in which two or more mass analyzers are used in sequence for separation and identification of compounds.[22]

Tandem mass spectrometry involves at least two different stages of mass analysis. The instruments associated with this technique can be classified as tandem-in-space and tandem-in-time instruments. In tandem-in-space mass spectrometers, ionization, selection, excitation and analysis are done in separate regions of the spectrometer. Sequential arrangements of mass analyzers such as magnetic sectors (B), electric sectors(E), quadrupoles (Q) and time-of-flight (TOF) mass analyzers characterize tandem-in-space instruments. In tandem-in-time instruments, all these events occur sequentially in the same physical space, but they are separated in time from one another. Tandem-in-time instruments

are exemplified by ion traps and Fourier transform (FT) ion cyclotron resonance (ICR) mass spectrometers.

Early CID studies were carried out on sector instruments where ions are dissociated at keV energies. Double-focusing mass spectrometers (BE or EB configuration) in which an electrostatic analyzer, used for energy focusing, is coupled to a magnetic sector for directional focusing of an ion beam were especially used for this purposes. Either the magnetic and the electric fields can be scanned simultaneously such that B/E remains constant throughout the scan[79], or E can be scanned with B constant in an instrument of reverse geometry (BE).[80] Neither of these techniques gives good resolving power for both precursor and product ions. The introduction of tandem double focussing mass spectrometers provided an alternative to overcome such limitations. Thus, four-sector mass spectrometers of EBEB[81] and BEEB[82] configuration provided high-resolution precursor ion selection, which eliminates isobaric interferences and allowed study of two or more sequential fragmentation steps.[83] High- and low-energy CID can be obtained in these types of instruments by deceleration of the ion beam.

Studies by Yost and Enke[84] demonstrated that efficient dissociation of ions could be obtained at low collision energies (10-100eV) when several quadrupoles are coupled. They introduced triple quadrupole mass spectrometers for CID experiments, which, nowadays, are the most widely used tandem mass spectrometers. Unit mass resolution is obtained for precursor and product ions because the mass resolution of the quadrupole is essentially

unaffected by changes in ion kinetic energy. These instruments are simple to use, cost much less than tandem sector instruments, and LE-CID experiments can be performed in the rf-only quadrupole (q) or octopole (o) collision cell located between two quadrupole mass filters.

Other instruments used in MS/MS experiments combined the characteristics of double-focussing mass spectrometers (BE and EB geometry) with quadrupoles.[85-87] These hybrid mass spectrometers (e.g., the Finnigan MAT95Q , BEoQ instrument used in these studies) were less complex and more affordable than four-sector instruments. They provided high resolution selection of the precursor ion and unit mass resolution for the product ions, as well as unique capabilities for CID analysis using high- and low-kinetic energy precursor ions.[88] Tandem-in-time instruments are based on ion-trapping devices.[89,90] These devices allow the selection of a particular ion by ejection of all others. The selected ion can be excited and fragmented during a time period, after which a fragment ion mass spectrum can be obtained. Since this process can be repeated several times (MS^n), as far as there are ions to be selected, these are considered the most promising instruments for MS/MS.[19] FTICR instruments present the additional advantage of simultaneous measurements of a broad m/z range of ions, which allows sensitive measurement of trace amounts of material.[91]

A review of combined analyzer technology has been published recently and includes tables with different analyzer configurations and pertinent references.[92] At present, hybrid instruments that combine time-of-flight and ion

traps with other analyzers are expected to replace the sector-quadrupole instruments that were very popular in the 80s since they are cheaper and wider mass ranges are possible.[93] Thus, different configurations such as quadrupole and time-of flight (qTOF)[94], double-focussing sector instruments with ion traps[95] and sector instruments coupled with time-of-flights (EBE-TOF) are now commercially available and are expected to be key in high-mass analysis.[96,97]

Internal Energy and Mass Spectrometry

The appearance of a mass spectrum is a reflection of the internal energy content of the ion. Thus, internal energy controls the available fragmentation channels and the reaction rates as indicated by equation 1-1. Ions with low internal energies will not fragment or will form very few fragments of low abundances. High-energy ions, on the other hand, will produce a wide variety of intense fragment ions. The internal energy of an ion is not a single value, instead, it is characterized by a distribution of internal energies.

Ion internal energy is governed by three factors[98] : (1) the internal energy of the molecule before ionization, (2) the energy gained during ionization, and (3) the environment of the ion. Therefore, the mass spectral pattern is expected to vary with changes in the temperature of the source, the ionization technique, and the conditions under which reactions might occur after ionization.[99] In the absence of collisions, the internal energy of an ion derives from the thermal energy originally in the precursor molecule and the energy deposited during the

ionization process. A schematic representation of the energy terms related to ionization and dissociation of polyatomic molecules is shown in Figure 1-2.[100]

For small molecules (less than 500 Da) the contribution from thermal energy to internal energy is typically much lower than the energy deposited by the ionization technique and is usually neglected.[27] In contrast, thermal energy is very important in large molecules, where it can exceed the energy deposited by the ionization technique at typical mass spectrometric temperatures.[101] For thermally labile molecules, molecular and pseudomolecular ions can be detected if the internal energy of the molecule is kept low. This is possible by performing the analysis at low temperatures and under soft ionization conditions.

Different ionization techniques allow conversion of compounds into measurable ions that reflect the original molecule. Ionization techniques are classified depending on the amount of internal energy resulting from them as "hard" or "soft" ionization methods. "Hard" ionization methods produce a substantial proportion of ionized molecules with such high internal energies that they fragment before leaving the source. A typical example is 70 eV electron ionization (EI), in which ions are produced by electron bombardment at low pressure conditions (10^{-5}–10^{-6} Torr) so that ions do not collide with other molecules before extraction. Therefore, any excess energy provided during ionization leads to ion fragmentation. EI is very convenient for structural interpretation. "Soft" ionization methods, on the other hand, minimize further fragmentation since the average internal energy deposited is low and are useful for characterization of complex mixtures. Soft ionization techniques such as

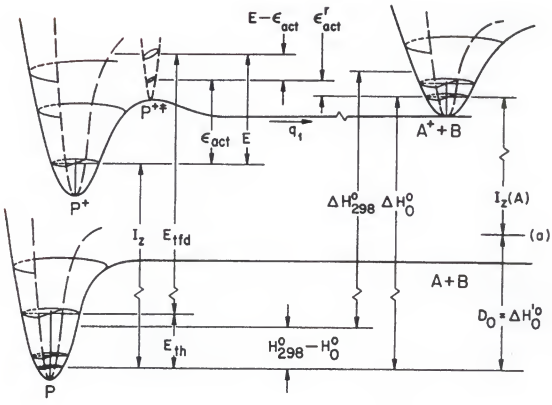

Figure 1-2. Schematic representation of the energy terms related to ionization and dissociation of polyatomic molecule. I_z, ionization energy of molecule P; E_{th}, thermal energy of molecule prior to ionization; E_{tfd}, energy transferred to P during ionization; E, resulting internal energy in the ion; q_1, reaction coordinate for $P^+ \rightarrow A^+ + B$; ϵ_{act}, activation energy (E_o) for $P^+ \rightarrow A^+ + B$; ϵ^r_{act}, activation energy for the reverse reaction $A^+ + B \rightarrow P^+$; ΔH_0^0, ΔH_{298}^0, standard enthalpy change for the dissociation $P \rightarrow A^+ + B$ at 0 K and 298 K, respectively; $D_0 = \Delta H_0'^0$, standard enthalpy change for the dissociation $P \rightarrow A + B$; $I_z(A)$, ionization energy of the fragment A. Only two of the many vibrational degrees of freedom of P, P^+, $P^{*‡}$, and A^+ are represented. The level (a) represents the energy of the dissociated neutral system, A + B, with the species in the ground states. Adapted from reference 100.

chemical ionization (CI) and atmospheric pressure chemical ionization (APCI) produce ions by ion-molecule reactions under high gas pressure conditions. Under these conditions, the mean free path of the ions is short because of collisions with the large excess of reagent gas molecules before they are mass analyzed. Since any excess energy gained during ionization can be lost by collisions with excess neutral gas, there is little energy available for fragmentation and the ions are said to be collisionally equilibrated.[98] In EI and CI, gas-phase ions are formed from gas-phase neutral species. The formation of gas-phase ions from condensed phase neutral species (i. e., solids or liquids) occurs in the so-called desorption ionization (DI) or nebulization ionization (NI) methods. DI methods include fast atom bombardment (FAB), liquid secondary ion mass spectrometry (LSIMS), field desorption (FD), plasma desorption (PD), laser desorption (LD) and matrix-assisted laser desorption ionization (MALDI); while NI methods include thermospray (TSI) and electrospray (ESI). Samples in condensed phases at room temperature have little internal energy and the ionization process typically imparts little excess internal energy so that fragmentation of precursor ion is reduced. In LSIMS and FAB, samples are embeded in a liquid matrix and deposited on a surface where gas-phase ions are produced by bombarding the surface with high energy particles. The names of these techniques are derived from the fact that some particle beams are formed of ions (Ar^+, Xe^+, Cs^+) or neutral atoms (Ar, Xe) with energies of 5-10 keV. Ions produced by these techniques have a wide range of energies so that a great range of fragment ions as well as molecular ions are formed.[102] Heavy

molecules can be ionized by using MeV ions generated from spontaneous fission events occurring in a sample of californium-252[103] or by using tandem accelerators.[104] This technique is known as plasma desorption (PD) and has been used to analyze bigger molecules than in LSIMS and FAB due to much more energetic primary beam particles. Gas-phase ions can also be produced by bombardment of solid samples with photons generated by laser sources (LD). Since power densities in excess of 10^6 W/cm^2 are needed, thermal damage and excessive fragmentation are very critical when analyzing large molecules (>1000 Da).[105] Matrix-assisted laser desorption ionization (MALDI) is used to overcome this mass range limitation. In MALDI, the energy is not directly transfered to the sample; rather, it is initially deposited into an absorbing matrix and is transfered to the analyte, which ionizes into the gas phase by a mechanism not well understood. Thus, non-volatile and thermally labile compounds are gently ionized. Other ionization techniques such as FI and FD involve the application of strong electrostatic fields.[106] In FI, a compound in the gas phase is ionized near or at the surface of an electrode emitter. In FD, the sample is deposited on the emitter. Ionization in these techniques is the result of tunneling of an electron from the sample into the emitter so that the energy required for desorption of the ion is less than the required for evaporation of a neutral molecule. In FI, mostly M^+ and $(M+H)^+$ ions are observed, which indicates a gas-phase process. In FD, it is very common to observe cationized species (e g., $(M+Na)^+$) and $(M+H)^+$ ions if the sample is an electrolyte or contains salts. This process is even less energetic than FI since the extraction of preformed ions requires a weaker field

than is required for electron tunneling. Ions can also be formed by nebulization ionization (NI) techniques such as electrospray and thermospray, which involve a combination of solvent evaporation and low-energy collision processes. In TSI[107] the liquid effluent from a LC or a syringe pump (containing analytes and an electrolyte) is vaporized by applying heat. The superheated mist carries droplets containing the non-volatile molecules. Typically, the solution contains ammonium acetate so that droplets contain a net excess of NH_4^+ and some CH_3COO^-. The excess solvent is removed by rapid pumping and charged species, mostly $(M+H)^+$ and $(M+NH_4)^+$ in positive ion mode, are formed. In electrospray[5,108] ionization occurs at ambient temperature and atmospheric pressure. The compounds are dissolved in aqueous solution and the solution is passed through a capillary tube at a high electric potential (few thousand volts). The emerging liquid is mist of charged droplets, from which solvent is removed by a flow of dry gas. Charge accumulates as a result of decreasing droplet size. For molecules with several basic sites, evaporation produces multiple charged ions. These nebulization ionization techniques produce ions with little excess internal energy.

CHAPTER 2
PRELIMINARY STUDIES OF INTERNAL ENERGY EFFECTS ON LOW- AND HIGH-ENERGY COLLISION-INDUCED DISSOCIATION: THE EFFECT OF THE IONIZATION TECHNIQUE

Introduction

Tandem mass spectrometry is considered a standard method for structure elucidation of organic compounds, especially when the primary ionization process does not introduce sufficient energy for fragmentation. Ions formed in the ion source can undergo fragmentation promoted by the internal energy deposited during the ionization process itself or by some other means of excitation such as collisional activation.

Collision-induced dissociation (CID) experiments are commonly carried out in two energy regimes, high-energy (HE) and low-energy (LE). Spectra obtained by HE CID, in the keV range, are usually the result of single collisions between the precursor ion and the target gas. In contrast, LE CID (less than 100 eV) spectra are typically the result of multiple collisions and multistep cleavage reactions.[57] Although CID spectra obtained under the two energy regimes often show similarities, differences due to the amount of internal energy deposited in the ions during the collision processes are observed.[64] Thus, HE CID often results in a broader range of fragmentation pathways, some of which are not

observed in LE CID. Nevertheless, the complementary value of both techniques in structure elucidation has been documented.[72]

The effect of the ionization technique on tandem mass spectrometry has not been extensively studied. Curtis and coworkers[109] reported important differences and similarities in the four-sector (HE-CID) spectra of valinomycin ions formed by different ionization techniques. Large differences were observed between fast atom bombardment (FAB) and field desorption (FD) tandem mass spectra of $(M+Na)^+$ ions and between FD and electron ionization (EI) tandem mass spectra of M^+ ions of valinomycin. They also showed that $(M+H)^+$ ions of valinomycin formed by electrospray, FAB and methane CI gave very similar tandem mass spectra. Differences in the spectra were attributed to the formation of isobaric ions with different structures. Similarities in the spectra, on the other hand, were considered evidence of a common ion structure (or a similar mixture of structures) and sufficient excitation by the activation method to overcome any differences in internal energies. In a subsequent paper, the same group[110] compared the four-sector FAB tandem mass spectra of $(M+H)^+$ and $(M+Na)^+$ ions of valinomycin, reported in the previous paper, with FAB tandem mass spectra taken on a triple quadrupole mass spectrometer via LE CID. They concluded that CID spectra of $(M+H)^+$ ions show similar fragments under a range of different collision and ionization conditions although the intensities are different. For $(M+Na)^+$ ions, however, the fragments were not the same and did not resemble the FD tandem mass spectra either. It was concluded that for the later case, the

utility of tandem mass spectrometry for structural identification might be determined by the differences in structures formed on ionization.

Some studies have shown the effect of electrospray conditions on low-energy CID of peptide ions with molecular weights less than 1200 Da. By changing the source-skimmer potential, the degree of acceleration of the ions through the skimmer was found to influence the fragmentation observed in tandem mass spectrometry.[111] More extensive fragmentation was observed at higher skimmer potentials, and it was possible to obtain comparable spectra using different combinations of skimmer potential and collision energies.

The effect on fragmentation of the amount and distribution of internal energy deposited during ionization has been recently reported.[16] Tandem mass spectra from M^+ ions of Irganox 1076, an organic polymer additive, were compared in a four-sector mass spectrometer of reverse geometry (BEBE), since these ions could be produced in very high yields by EI, CI, LSIMS and FD. Although all the techniques produced the same product ions, the authors concluded that the variation in relative abundance of various product ions could be used as qualitative estimate of differences in internal energy of the precursor ion resulting from the use of different ionization techniques.

In this chapter, data from preliminary investigations of the effect of internal energy on the CID spectra obtained in high- and low-energy regimes of ions formed by different ionization techniques are presented.

Experimental

Sample Preparation

Isovalerylcarnitine was provided as a 3 mM (about 0.85 µg / µL) solution in a 1:1 methanol/chloroform mixture by Dr. Peggy R. Borum from the Department of Food Science and Human Nutrition of the University of Florida. Leucine enkephalin was purchased from Sigma Chemical Co. (St. Louis, MO) and a 1 µg / µL solution was prepared in methanol.

Mass Spectrometry

Low-energy collision-induced dissociation

Samples were introduced into the ion source by a direct exposure probe (DEP), which consists of a rhenium wire with a small loop for depositing samples that is heated by passing a current through it. One microliter of the sample solution was deposited on the wire and evaporated to dryness. The probe was inserted into the mass spectrometer and heated from 25 to 450 °C at 200 °C/min. The source temperature was 150 °C. Methane (The BOC Group Inc., Murray Hill, NJ), ammonia (Matheson Gas Products, East Rutherford, NJ) and water (MilliQ-purified) were used as reagent gases for chemical ionization (CI). CI was performed at a gas pressure of 1.5 torr. For water DCI experiments, a water reservoir was connected to a variable leak valve (Granville Phillips, Boulder, CO). Water vapor was introduced into the mass spectrometer via this variable leak valve that was connected to the gas chromatograph transfer line. An ice bath was used to cool the water reservoir and avoid boiling. LE-CID experiments

were performed on a Finnigan TSQ 70 triple quadrupole mass spectrometer (Finnigan, San Jose, CA). Argon was introduced in the octopole collision cell until a pressure of one millitorr was measured by a Pirani gauge. The collision energy was varied from 5 to 60 eV for leucine enkephalin and from 5 to 45 eV for isovalerylcarnitine. The fact that precursor ions were absent beyond these upper collision energies accounted for the different ranges. For water and ammonia DCI experiments, only 20 eV collision energy spectra were acquired.

For isovalerylcarnitine, LE-CID experiments were also performed on an ion trap mass spectrometer. Electrospray ionization (ESI) was performed on a Finnigan MAT LCQ instrument. The sample was dissolved in a 1:1 methanol:water solution to a concentration of about 10 pg/μL and infused at a flow rate of 0.2 μL/min and a spray voltage of 2 kV. The capillary was heated to 200 °C. Helium was introduced into the trap not only to improve trapping efficiency, but also as collision gas for CID. Collision energy was varied from 0% to 30% of the maximum available from a 5 V excitation voltage.

High-energy collision-induced dissociation

Compounds were ionized by liquid secondary ion mass spectrometry (LSIMS) and by desorption chemical ionization (DCI). For LSIMS experiments, Cs^+ ions with an impact energy of 15 kV and an emission current of 3 μA were used as the ionization beam. The studies were performed at an acceleration potential of 5kV. 3-nitrobenzyl alcohol (NBA), a 5:1 mixture of dithiothreitol and dithioerythritol also known as "Magic Bullet" in 10% trifluoroacetic acid (TFA)

(Aldrich Chemical Co., Milwaukee, WI) and glycerol (Mallinckrodt, Inc., St. Louis, MO) were used as matrices. Two microliters of sample solution were deposited on a standard LSIMS probe. After solvent evaporation, one microliter of matrix was added on top of the sample and mixed with a glass stick. Scans for pure matrix were recorded so that matrix could be subtracted from the sample scans. For the DCI experiments, 1.5 μl of the sample solution was deposited on the wire of a DEP probe and evaporated to dryness. The probe was heated from 25 to 700 °C at 200 °C/min. CI was performed at a source temperature of 150 °C. Methane, isobutane and ammonia (Matheson) were used as reagent gases. HE-CID studies were performed on a Finnigan MAT95Q (BEoQ configuration) hybrid mass spectrometer. Mass-analyzed ion kinetic energy spectra (MIKES) were obtained with helium as target gas in the second field-free region. The helium pressure was adjusted until the precursor ion beam intensity was reduced to 50 % of its original value.

Results and Discussion

Leucine Enkephalin (Tyr-Gly-Gly-Phe-Leu)

The major fragmentation channels of $(M+H)^+$ ions of leucine enkephaline have been previously reported[112] and are shown in Figure 2-1. For convenience, the nomenclature used is that proposed by Roepstorff and Fohlman.[113]

Desorption chemical ionization-MS

Figure 2-2 shows the spectra of leucine enkephalin obtained by desorption chemical ionization (DCI). As can be seen, it was possible to produce

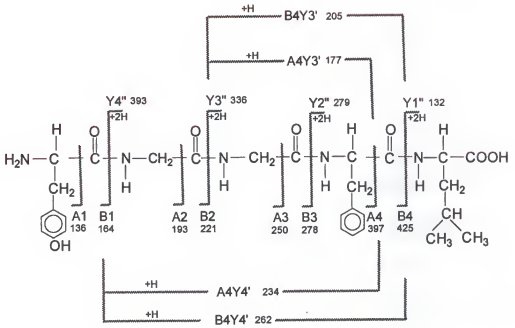

Figure 2-1. Fragmentation pattern of $(M+H)^+$ ion from leucine-enkephalin, H-Tyr-Gly-Gly-Phe-Leu-OH, (m/z 556) adapted from reference 112. The nomenclature used is that proposed by Roepstorff and Fohlman.[113]

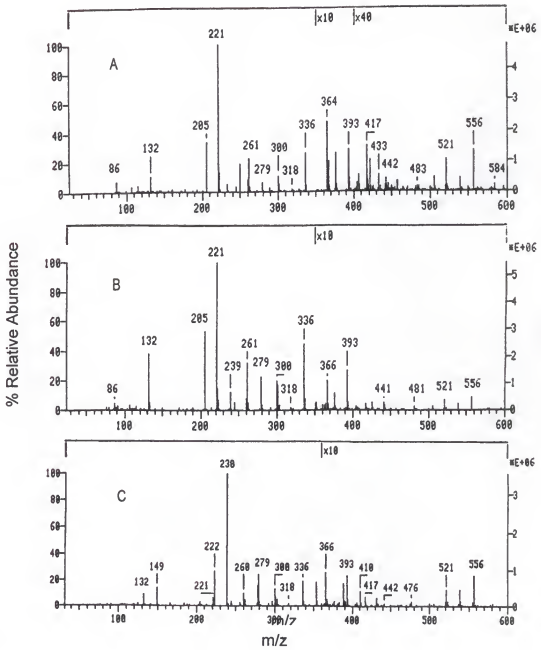

Figure 2-2. MS of leucine enkephalin (MW 555) obtained by DCI with different reagent gases on a TSQ 70. A. Methane, B. Water, C. Ammonia.

$(M+H)^+$ ions of leucine enkephalin using a direct exposure probe on a Finnigan TSQ 70 mass spectrometer with methane, water and ammonia used as reagent gases. There are enough ions in the DCI spectra to obtain the amino acid sequence of the peptide. Most of the ions observed in the spectra originate from cleavages around the amide bonds. The change of reagent gas from methane, which produces a strong proton donor, $[CH_5]^+$, to ammonia, which produces a much weaker proton donor, $[NH_4]^+$, intensifies the $(M+H)^+$ peak. Spectra obtained by methane and water CI are almost identical, showing all the Y-type sequence ions. The base peak at m/z 221 corresponds to the B_2 ion, and a peak at m/z 205 corresponds to the B_4Y_3' ion produced by internal cleavage.

The methane DCI spectra (Figure 2-2 A) presents some peaks at higher masses than the $(M+H)^+$ ion. These peaks, at m/z 584 $(M+29)^+$ and 596 $(M+41)^+$, result from the addition of $C_2H_5^+$ and $C_3H_5^+$ formed during the ionization of methane. Other low-abundance satellite peaks are observed throughout the methane DCI spectrum and were interpreted as the result of peptide decomposition under fast heating followed by adduction with $C_2H_5^+$ and $C_3H_5^+$.

The spectrum obtained under ammonia DCI is also rich in Y-type ions but there are also peaks such as m/z 149, 222, 238 and 410, which are not present in the methane or isobutane DCI spectrum. The complexity of ammonia DCI spectra has been attributed to gas-phase ammonolysis of the peptide bonds at the temperature of the ion source[114] and to adducts of N-terminal acylium ions and unionized ammonia.[115] Thus, peptide amides of the form $(H(AA)_nNH_2 + H)^+$

have been observed at m/z 238, 295 and 442 which correspond to the $(HTyrGlyNH_2+H)^+$, $(HTyrGlyGlyNH_2+H)^+$ and $(HTyrGlyGlyPheNH_2+H)^+$ ions, respectively.

Chemical ionization MS/MS

Figure 2-3 compares low-energy CID spectra of the $(M+H)^+$ ions of leucine enkephalin produced using methane, water and ammonia as reagent gases for DCI. Spectra were obtained in the octapole collision cell of a triple quadrupole mass spectrometer at 20 eV laboratory frame collision energy. As can be seen, the product ions correspond to expected cleavages along the peptide backbone. The product ion mass resolution is approximately unit as indicated by the separation of the m/z 278 and 279 ions. In all three spectra, immonium ions characteristic from phenylalanine (m/z 120) and tyrosine (m/z 136) are observed. The major fragment ions can be assigned to the cleavages shown in Figure 2-1. The spectra in Figure 2-3 agree with the observation[75] that LE-CID spectra are characterized frequently by A- and B-type ions and ions derived from internal cleavages. The latter ions result from multiple collisions, which increase the probability of breaking two amide bonds.[57] In the LE-CID spectra (Figure 2-3) there are more intense low-mass ions in the spectrum obtained by methane CI than in the water and ammonia CI spectra. This is expected since higher internal energies are deposited during ionization with methane ions than by water and ammonia.

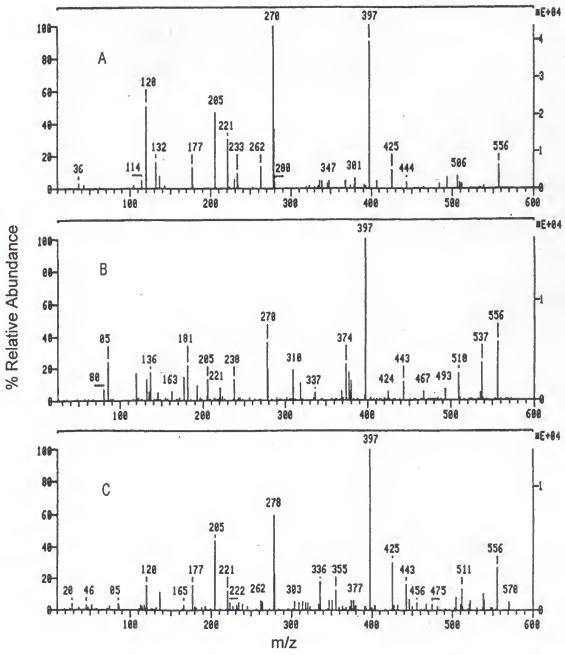

Figure 2-3. LE-CID spectra of $(M+H)^+$ ions (m/z 556) from leucine enkephalin generated by DCI with different reagent gases in a TSQ 70. A. Methane, B. Water, C. Ammonia. 20eV laboratory collision energy.

LSIMS-MS

The actual mechanism of ion formation in LSIMS is not well understood.[116,117] What it is known is that the use of a liquid matrix facilitates the production of ions of a solute by dissipating energy deposited by the primary beam and maintaining a constant supply of fresh analyte ions.[1] Leucine-enkephalin has been previously studied by LSIMS mass spectrometry and CID.[70,112,118,119] As matrix composition has a direct effect on the internal energy of secondary ions,[116] it can therefore be used to modify the MS/MS spectra of the analytes and to optimize the information obtained from them.

Five matrices were used in these experiments: NBA, Magic Bullet/TFA, 2-nitrophenyl octyl ether (NPOE), glycerol and a mixture glycerol/water 50:50 v/v. NPOE did not give a satisfactory signal and pure glycerol only gave a very weak $(M+H)^+$. The other three matrices were used throughout the experiments since they produced strong $(M+H)^+$ signals. Figure 2-4 shows the spectra taken in all three matrices after matrix ions were subtracted from each spectrum. It is evident that these three matrices can be used for sequencing the peptide.

Immonium ions derived from the amino acids present in the peptide are observed in all three matrices as indicated by m/z 30, 86, 120 and 136. These ions are representative of glycine, leucine or isoleucine, phenylalanine and tyrosine, respectively. The signal observed at m/z 91 is also a good indicative of the presence of phenylalanine and tyrosine.

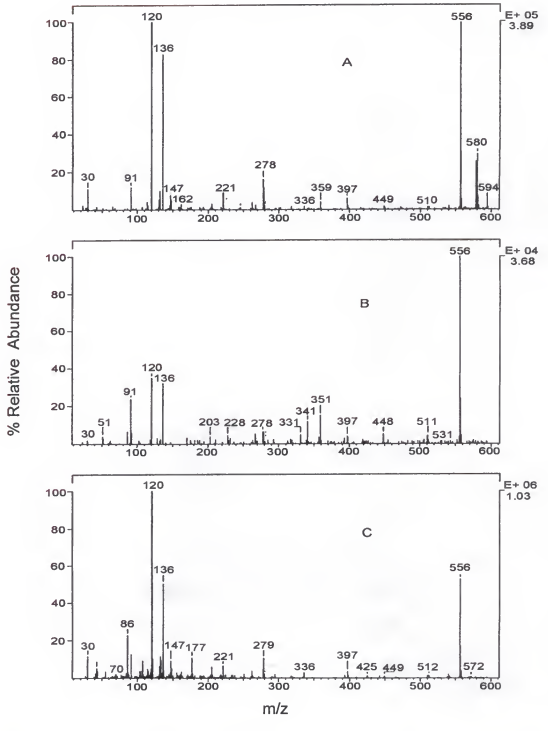

Figure 2-4. MS of leucine enkephalin (MW 555) obtained by LSIMS with different matrices. A. Magic Bullet/TFA, B. NBA, C. Glycerol:water 50:50, v/v.

Spectra obtained in magic bullet/TFA presents some strong signals at masses higher than the $(M+H)^+$ ion. These adducts were identified by high-resolution mass spectrometry as $(M+Na)^+$ for m/z 578 and $(M+K)^+$ for m/z 594. These adducts are almost non existent in the other two matrices (~ 1%), which agrees with previous observations that NBA has low affinity for cations and that the more polar the matrix, the higher the probability for cation attachment.[120] It is evident that $(M+H)^+$ ions are formed with different internal energies when different matrices are used. More intense low-mass ions are observed in glycerol than in NBA, which indicates that $(M+H)^+$ formed in glycerol have higher internal energies than those formed in NBA. Precursor ions formed in Magic Bullet seem to have intermediate internal energies. This agrees with previous reports where glycerol was shown to produce extensive fragmentation of peptides.[116]

LSIMS MS/MS

Collision-induced dissociation experiments for leucine enkephalin $(M+H)^+$ ions generated by LSIMS were performed at a collision energy of 5 keV. For these experiments, the magnetic sector was adjusted to mass select the $(M+H)^+$ ions, which were then directed into the second field-free region of the instrument where collision-induced dissociation occurs upon collisions with helium. The product ion spectra were then obtained by scanning the electric sector voltage. This technique is known as mass-analyzed ion kinetic energy spectrometry (MIKES).

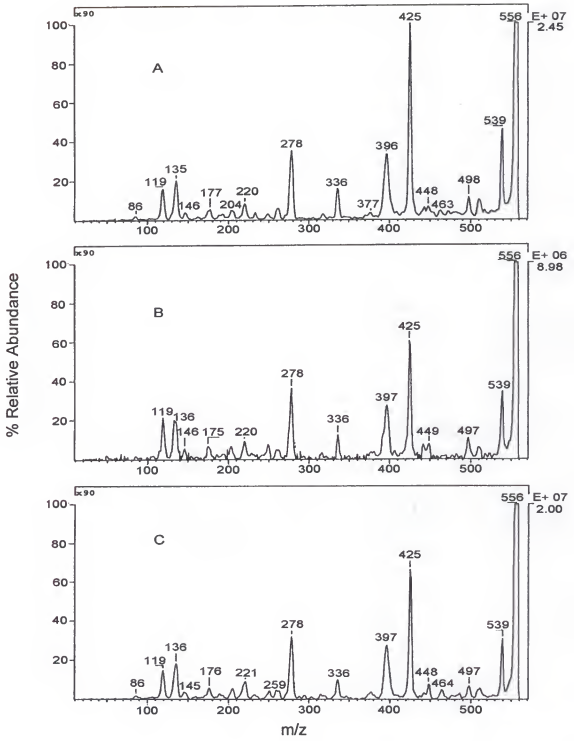

Figure 2-5. HE-CID spectra of $(M+H)^+$ ions from leucine enkephalin (m/z 556) generated by LSIMS with different matrices. A. Magic bullet/TFA, B. NBA, C. Glycerol:water, 50:50, v:v. 5 keV collision energy.

Figure 2-5 shows MIKE spectra of $(M+H)^+$ ions from leucine enkephalin in Magic Bullet/TFA, NBA and glycerol/water 50:50 v/v. The spectra were acquired at 50% attenuation of the precursor ion beam with helium. Notice that the efficiency of the CID process is extremely low, the remaining precursor ion is off-scale by a factor of approximately 90. Peaks are also very wide and it is not possible to separate the m/z 278/279 doublet; this poor product ion resolution arises from partition of the internal energy of the precursor ion into translational energy of the product ions and the use of a kinetic energy analyzer (the electric sector) to analyze the product ions.[121] It can be seen that assigned masses do not necessarily correspond to the masses in the CI spectra. In MIKE spectra, mass assignments are often inaccurate due to kinetic energy losses which can shift the peak away from the center.[122] All three spectra show essentially the same ions. As expected for peptides with no basic amino acids, the HE-CID spectra are dominated by B-type fragment ions[123] with the peak at m/z 425, corresponding to the B_4 ion, being the most intense. Although not shown here, when all spectra were normalized to m/z 425 it was clear that more abundant ions were produced with NBA, followed by those of glycerol/water, in turn followed by Magic Bullet/TFA. These observations indicate that NBA is a "hotter" matrix for HE-CID of leucine enkephalin.

Ionization and CID processes for leucine enkephalin

It was not possible to obtain $(M+H)^+$ ions from leucine enkephalin by DCI in the sector instrument (recall that their intensity was less than 3% of the base

peak in the DCI spectra obtained in the triple quadrupole instrument). Therefore, comparison of high- and low-energy CID of ions generated by chemical ionization can not be made; however, the CID spectra can be compared for $(M+H)^+$ ions produced by LSIMS (for HE-CID) and DCI (for LE-CID). A reasonable explanation for this is that higher internal energies might be deposited in the sector instrument due to ions being accelerated at 5kV during the ion extraction process. Comparing Figures 2-3 and 2-5, it is evident that there are differences between high- and low-energy CID spectra obtained from $(M+H)^+$ ions of leucine enkephalin. The presence of ions originated from internal cleavages such as the ions at m/z 205, 177 and 262 is more noticeable in the LE-CID spectra than in the HE-CID. Internal cleavages are often seen in LE-CID spectra due to the multiple collision conditions and longer time frame of the decomposition in triple quadrupole instruments both of which favor multi-step cleavage reactions.[57] The major difference between HE- and LE-CID spectra of $(M+H)^+$ ions of leucine enkephalin is the relative abundance of the ions at m/z 425 and m/z 397, which correspond to the B_4 and A_4 ions, respectively. Thus, in LE-CID spectra A_4 is predominant, while under HE-CID B_4 is the more intense. These differences can be related to the ionization technique and/or to the collision-induced dissociation process itself. In order to discern the individual contributions of these factors, the data obtained in these experiments were compared to those in previous publications. The literature contains no available CID spectra of leucine enkephalin $(M+H)^+$ ions generated by CI, but there are

many reports on CID of ions generated by FAB and ESI. CID spectra (high- and low-energy) and SID data on leucine enkephalin have also been reported.

Alexander and Boyd[70] demonstrated that the extent of fragmentation of $(M+H)^+$ ions from leucine enkephalin generated by FAB increases as a function of collision energy. Thus, the intensity ratio of low- to high-mass ions increases with increasing collision energy. A similar treatment has been applied in this research for $(M+H)^+$ ions generated by chemical ionization with methane used as the reagent gas. In these experiments, LE CID spectra were taken at different collision energies. For plotting the data, the fragment ion spectrum at each collision energy was divided on two regions, a low-mass region (m/z 20 to 299) and a high-mass region (m/z 300 to 550). The fragment ion intensities were summed for each region and the ratio of high-mass to low-mass ion intensities was calculated and plotted against laboratory frame collision energy. As can be seen in Figure 2-6, there is a rapid change in the high- to low-mass ion intensity ratio as the collision energy increases to a value of 25 eV. Above 25 eV collision energy, the ratio is nearly constant, and no major differences are observed in the spectra. Comparing Figures 2-3 and 2-5, $(M+H)^+$ ions from leucine enkephalin generated by LSIMS appear to be "cooler" (i.e., have less internal energy) than those generated by DCI, since the latter show more intense lower mass ions under the experimental conditions. This may reflect the energy imparted by the desorption process of DCI rather than simply the energy deposited during protonation. The dominant presence of m/z 425 (B_4 ion) in the LSIMS-CID spectra was observed even at 90% attenuation of the precursor ion beam.

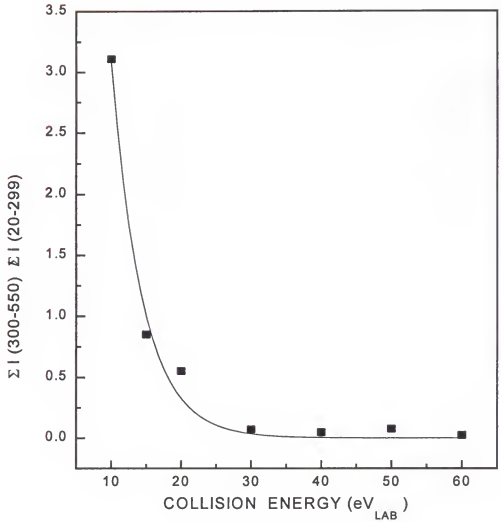

Figure 2-6. Fragment ion distribution from the $(M+H)^+$ ion of leucine-enkephalin as a function of laboratory collision energy. Σ I (300-550) is the sum of all ion intensities in the m/z 300-550 mass range. Σ I (20-299) is the sum of all ion intensities in the m/z 20-299 mass range. Spectra taken on a Finnigan TSQ 70. Precursor ions were generated by methane/CI, and argon was used as the collision gas.

In contrast, in the CI-CID spectra m/z 397 (A_4 ion) is the dominant product ion. It has been noticed[112,70,124,125] that the formation of m/z 397 over m/z 425 is favored by multiple collision conditions and longer reaction times, conditions obtained in quadrupole collision regions, which agrees with the observations made in this research. The presence of a strong m/z 397 in the DCI-CID spectra can also be attributed to thermal dissociation of leucine enkephalin $(M+H)^+$ ions. In order to form $(M+H)^+$ ions in CI, the sample has to be vaporized, which can deposit extra internal energy into the ion. Even under fast heating in DCI, this process can not be ruled out. Thermal decomposition of leucine enkephalin $(M+H)^+$ ions has been studied by Wysocki and coworkers.[125] In these studies the temperature of the heated capillary of an ESI source was gradually increased and SID spectra was recorded. Thermal dissociation of leucine enkephalin was found to lead to intense A_4 ions, which can be formed from B_4 ions by loss of CO. The formation of A_4 from B_4 ions has also been reported by Williams and coworkers[126] in experiments involving blackbody infrared radiative dissociation (BIRD) of protonated leucine enkephalin obtained by electrospray ionization.

Isovalerylcarnitine

Due to their zwitterionic character and the presence of thermally labile functional groups, carnitine and acylcarnitine derivatives are not normally amenable to direct analysis by electron ionization or chemical ionization.[127] Most of the reports on analysis of acylcarnitines are based on gas chromatography -

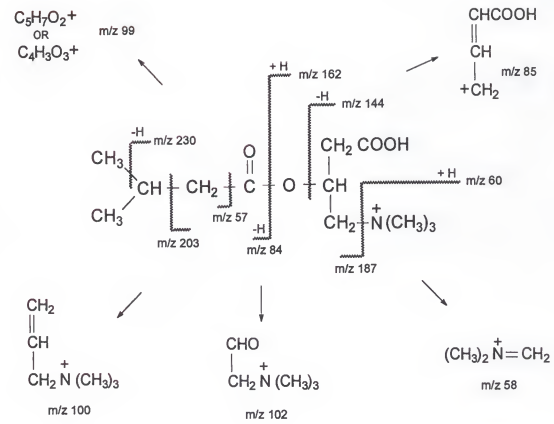

Figure 2-7. Fragmentation pattern of the (M+H)⁺ ion of isovalerylcarnitine (m/z 246). Ions present in high- and low-energy CID. Adapted from reference 72.

mass spectrometry (GC/MS) of suitable derivatives or fast atom bombardment (FAB) mass spectrometry of derivatized and underivatized compounds,[128] although there are a few publications on thermospray[129,130] and DCI.[131] The structure and fragmentation pattern for isovalerylcarnitine is shown in Figure 2-7. The identification of these ions has been supported by high resolution measurements and by linked scan MS/MS techniques.[72]

DCI-MS

The mass spectra of isovalerylcarnitine obtained by DCI using methane, water and ammonia are compared in Figure 2-8. In all cases, $(M+H)^+$ ions of low intensity are observed. The relative intensity of the $(M+H)^+$ ion (m/z 246) increased when the reagent gas was changed from methane to ammonia. Methane and water DCI spectra (Figures 2-8 A, 2-8 B) are characterized by abundant ions at m/z 85, 103, 130, 169, 187, 205 and 232. Cluster reactions are of considerable importance in CI.[132] Ionization of methane produces also $C_2H_5^+$ and $C_3H_5^+$ ions which react to form $(M+C_2H_5)^+$ and $(M+C_3H_5)^+$ ions of low intensity. These ions can undergo demethylation under DCI conditions to form the m/z 260 and 272 observed in the methane DCI spectrum. The water DCI spectrum shows water adducts 18 Da higher than the corresponding ions observed in methane DCI. Thus, ions at m/z 78, 121, 144 and some higher mass adducts separated by 18 Da (m/z 253, 271 and 289) are observed. In the ammonia DCI spectrum (Figure 2-8 C) the characteristic ions are m/z 77, 102, 119, 130, 186, 204 and 232. Differences between the ions in the DCI spectra in

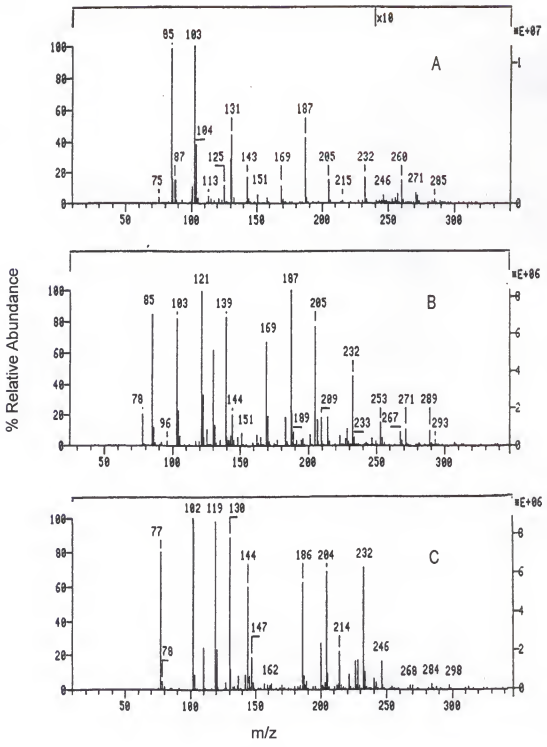

Figure 2-8. MS of isovalerylcarnitine (mw 245) obtained by DCI with different reagent gases on a TSQ 70. A. Methane, B. Water, C. Ammonia.

Figure 2-8, especially between the ammonia DCI spectra and the methane and water DCI spectra, can be explained by the formation of ammonium adducts under ammonia DCI. These ammonium adducts can be seen as signals at 17 Da higher than the corresponding peaks in methane and water DCI spectra (e g., m/z 102 rather than 85, m/z 186 rather than 169, m/z 204 rather than 187). The ion at m/z 102 present in the ammonia DCI spectrum might be accounted for by addition of ammonia with trimethylamine loss from the m/z 144 ion. The m/z 130 ion signal can be accounted for by loss of both acyl and methyl group from intact $(M+H)^+$ ion.[129] The presence of a $(M+H-14)^+$ ion at m/z 232 seems to be an indicative of thermal degradation processes under CI. This ion has been identified in thermospray mass spectra, where the ratio $(M+H)^+$ / $(M+H-14)^+$ has been shown to change as a function of temperature.[130] The formation of this ion is believed to involve a pyrolytic demethylation followed by protonation, since a similar reaction has been reported to occur under pyrolysis for many methyl-substituted quaternary ammonium compounds under CI.[130]

DCI-LE-CID

Low-energy CID mass spectra of $(M+H)^+$ ions from isovalerylcarnitine generated by DCI are shown in Figure 2.9. Fragment ions are essentially the same in the spectra obtained after ionization with methane, water and ammonia and subsequent collisions with argon at 20 eV (laboratory frame). This suggests that the $(M+H)^+$ ions formed with different reagent gases have the same structure and undergo the same decomposition reactions upon collisions. As can be

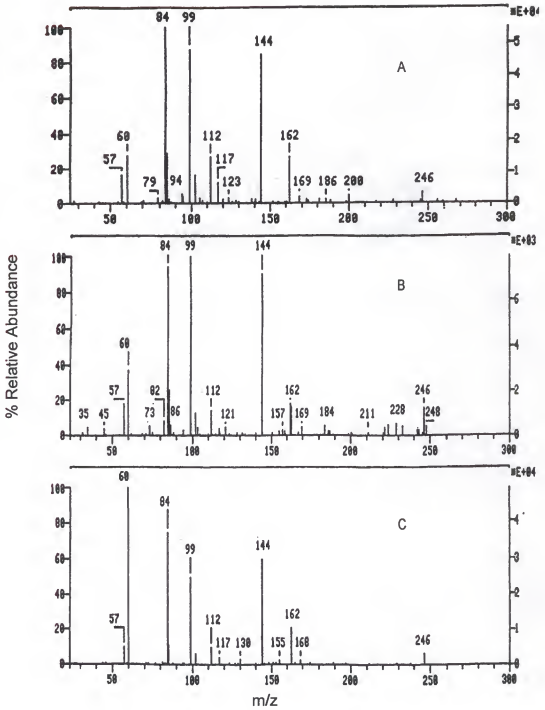

Figure 2-9. LE-CID spectra of $(M+H)^+$ ions from isovalerylcarnitine (m/z 246) generated by DCI with different reagent gases in a TSQ 70 at 20eV collision energy. A. Methane, B. Water, C. Ammonia.

observed in Figure 2.9 more fragment ions of low abundance are present in the methane and water DCI LE-CID spectra. The intensities of the major fragments ions are higher in the ammonia DCI LE-CID spectrum. It is important to notice that the signal-to-noise ratio in the ammonia spectrum is also much higher. The fewer ions and better signal-to-noise ratios observed in Figure 2-9 C indicate that, as expected, cooler ions are formed during ionization with ammonia than when stronger proton transfer reagents such as methane and water are used.

DCI-HE-CID

One of the goals of this research is to be able to compare not only different ionization techniques but also different collision energy regimes. For this last purpose, $(M+H)^+$ ions from isovalerylcarnitine were formed in the ion source of the hybrid sector instrument to perform HE-CID. As shown in Figure 2-10, it was possible to form $(M+H)^+$ ions by DCI with methane, isobutane and ammonia as reagent gases. As expected and as observed in the triple quadrupole instrument, the relative intensity of the $(M+H)^+$ ion increased as the proton transfer reaction was less exothermic. The $(M+H)^+$ ion was very weak, almost non-existent, with methane DCI; with isobutane DCI a more intense signal was observed and, with ammonia DCI the most intense $(M+H)^+$ was obtained. It is evident from the scale of the spectra that methane DCI produced the most intense fragment ions, followed by isobutane DCI, which in turn is followed by ammonia DCI. This is again indicative that methane DCI $(M+H)^+$ ions are more energetic and fragment more easily than the corresponding

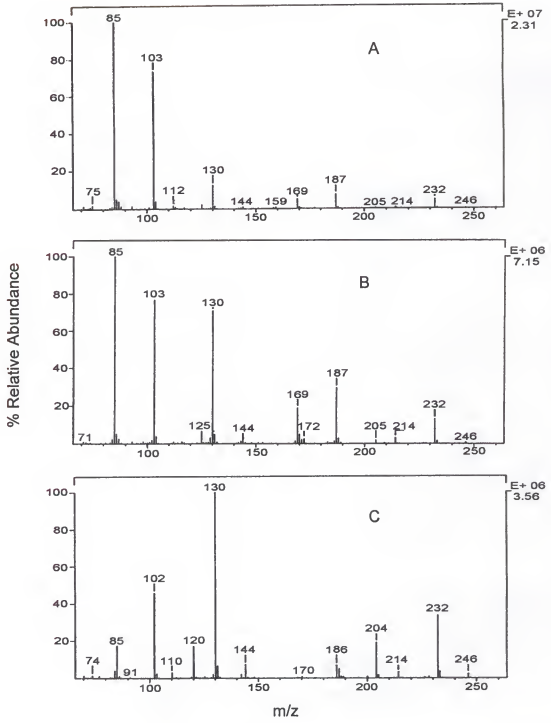

Figure 2-10 . MS of isovalerylcarnitine (mw 255) obtained by DCI with different reagent gases on a MAT 95. A. Methane, B. Isobutane, C. Ammonia.

$(M+H)^+$ ions generated by isobutane and ammonia DCI. It is important to notice that all three DCI spectra show a peak at m/z 232, which as explained previously appears to be a pyrolysis product obtained by demethylation followed by protonation. Adduct formation was also observed for DCI experiments in the sector instrument. Although not shown in Figure 2-10 A, a weak ion corresponding to $(M+C_2H_5)^+$ at m/z 274 was identified in the methane DCI spectrum. For isobutane DCI, ions at m/z 289 and 274 of formula $(M+C_3H_7)^+$ and $(M+C_2H_5)^+$ were observed. No adduct corresponding to the $(M+NH_4)^+$ was present in the ammonia DCI spectrum.

Comparing Figures 2-8 and 2-10, in which DCI spectra are shown from two different instruments, the spectra obtained in the hybrid instrument (Figure 2-10) are simpler and have better signal-to-noise ratios than the DCI spectra obtained in the triple quadrupole instrument (Figure 2-8). In a similar way to the results obtained in the quadrupole instrument, the ions obtained with methane and isobutane DCI are similar, with some differences in relative abundance. As on the triple quadrupole, ammonia DCI (Figure 2-10 C) forms ions such as those at m/z 102, 120, 186, and 204 that are ammonium adducts of the corresponding ions observed in methane and isobutane DCI. Although it was possible to form $(M+H)^+$ ions by DCI in the sector instrument, they are so low in absolute intensity (and CID is so inefficient) that HE-CID spectra with acceptable signal-to-noise were only obtained under ammonia DCI. This spectrum will be compared later to those produced by LE-CID.

LSIMS-MS

Figure 2-11 shows the LSIMS spectra of isovalerylcarnitine in Magic Bullet/TFA, NBA and glycerol. To facilitate the identification of peaks belonging to the compound of interest, matrix ions were subtracted. In all three matrices, the LSIMS spectra exhibit very intense $(M+H)^+$ ions due to the presence of a quaternary nitrogen in isovalerylcarnitine, which is a basic functional group. Furthermore, the solubility of isovalerylcarnitine in these matrices is high, which helps in the production of intense sample ion peaks.[133] The spectra in Figure 2-11 are rather simple; the ions at m/z 58, 85, 100, 144, and 162 are consistent in all three cases, corresponding to the structures shown in Figure 2-7. Compared to the DCI spectra (Figures 2-8 and 2-10), there is far less fragmentation, indicating that LSIMS is a gentler ionization process than DCI for isovalerylcarnitine.

LSIMS MS/MS

High-energy CID spectra of $(M+H)^+$ ions of isovalerylcarnitine generated by LSIMS with three different matrices are shown in Figure 2-12. In general, spectra were reproducible, although the mass resolution was not adequate to make accurate mass assignments based solely in these spectra. Note as well the inefficiency of HE-CID; with the helium pressure set to attenuate the precursor ion beam by 50%, the most abundant product ion is still at least 450 times less intense than the remaining precursor ion. As can be observed, the same fragment ions were present in Magic Bullet / TFA, NBA and glycerol. The

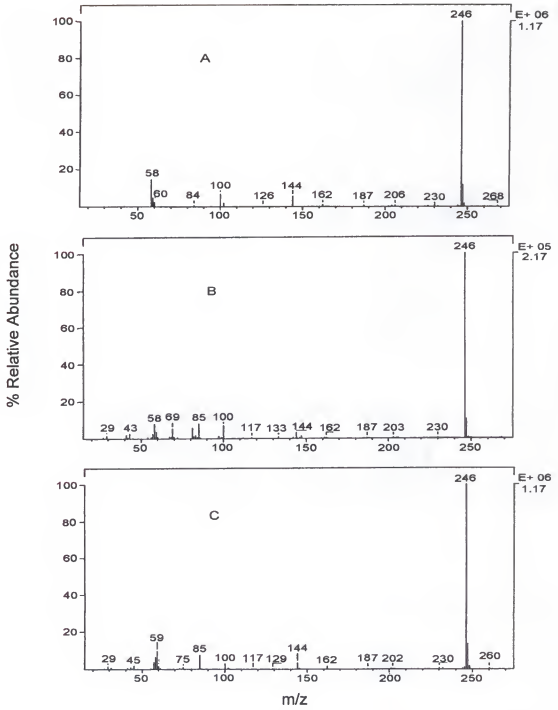

Figure 2-11 MS of isovalerylcarnitine (mw 245) obtained by LSIMS with different matrices on a MAT 95. A. Magic Bullet/TFA, B. NBA, C. Glycerol.

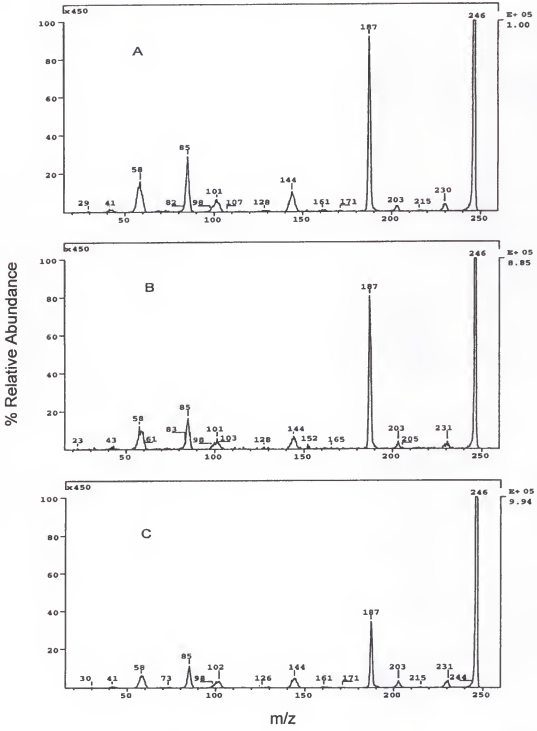

Figure 2-12. HE-CID spectra of (M+H)+ ions from isovalerylcarnitine (m/z 246) generated by LSIMS with different matrices. A. Magic bullet/TFA, B. NBA, C. Glycerol. 5KeV collision energy.

most abundant fragment ion, m/z 187, has been interpreted[72] as the $(M+H-59)^+$ ion, formed by loss of the trimethyl amine. More abundant fragment ions were observed in Magic Bullet/TFA, followed by NBA and glycerol. Under HE-CID, the presence of fragment ions such as those at m/z 203 and 230 from isovalerylcarnitine allows unequivocal differentiation of isomeric acylcarnitines.[72] These ions are the result of charge-remote fragmentation reactions in the alkyl chain, reactions predominantly observed at high collision energies.[134]

Ionization and CID processes for isovalerylcarnitine

Figure 2-13 compares CID spectra of $(M+H)^+$ ions from isovalerylcarnitine taken under different ionization techniques and collision energy regimes. HE-CID at 5 keV of ions generated by LSIMS and by ammonia DCI are shown in Figures 2-14 A and B. Notice that under the conditions of the experiments, m/z 187 is virtually absent in the DCI spectra, while it is the predominant product ion in LSIMS. These differences might indicate that for isovalerylcarnitine, the collisional activation process at this collision energy did not impart sufficient internal energy to override internal energy differences due to ionization. An alternative possibility is that different structures or mixture of structures at m/z 246 are being formed by LSIMS and by DCI. Similar conclusions have been drawn from experiments involving valinomycin ions in which differences in the HE-CID spectra were attributed to different structures formed by different ionization techniques.[109]

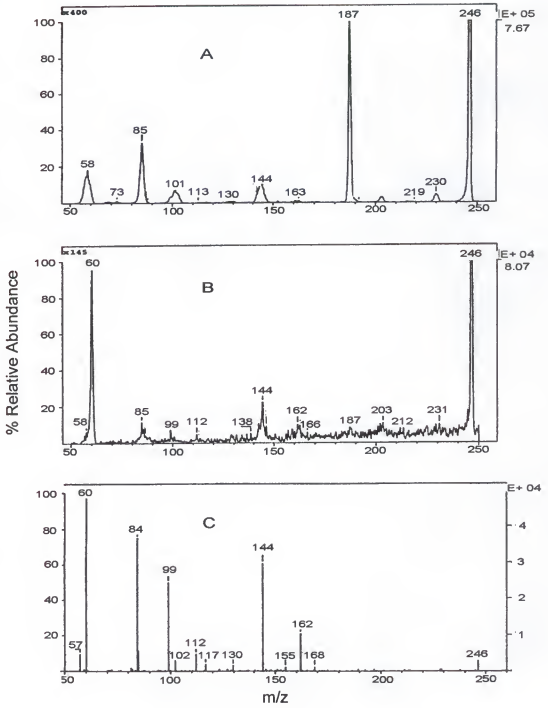

Figure 2-13. CID spectra of $(M+H)^+$ ions of isovalerylcarnitine (m/z 246). A. LSIMS-HE-CID (5 keV) helium 50% attenuation, matrix: Magic Bullet/TFA B. Ammonia-DCI HE-CID (5keV) helium 50% attenuation, C. Ammonia-DCI LE-CID (20 eV) argon 1mtorr, TSQ 70.

CID spectra of $(M+H)^+$ ions from isovalerylcarnitine generated by DCI were obtained at laboratory frame collision energies of 5 keV (on the MAT 95)and 20 eV (on the TSQ 70), as shown in Figures 2-14 B and C. It is evident that m/z 187 is almost non existent in the CID spectra of the $(M+H)^+$ ions produced by DCI regardless of the collision energy regime. This ion was not present, or at least not appreciable, in any of DCI LE-CID spectra obtained with different reagent gases (see Figure 2-9). M/z 60 is the predominant ion signal in Figures 2-14 B and C, as well as m/z 144. As can be seen, the efficiency of the HE-CID process is very poor (< 1%) as indicated by the scale of the spectrum and by the intensity of the precursor ion. In contrast, LE-CID is a very efficient process in which most of the precursor ions has been converted into product ions. The baseline in the HE-CID spectrum in Figure 2-13 B is noisy although several scans were averaged to obtain the spectrum shown; notice also that peaks are broad since spectra were acquired by the MIKES technique previously described. In the LE-CID spectrum (Figure 2-13 C), approximately unit mass resolution was obtained and signal-to-noise ratio was remarkably better than in the HE spectrum due to higher CID efficiency.

In order to help understand the differences in the fragment ions generated by CID of $(M+H)^+$ ions produced by LSIMS and DCI, especially the presence of m/z 187 in HE-CID spectra of $(M+H)^+$ ions generated by LSIMS, electrospray ionization (ESI) was used to generate precursor ions and CID was carried out. Figure 2-14 shows the LE-CID spectra, taken on an ion trap mass spectrometer at 15% of the maximum voltage, of isovalerylcarnitine $(M+H)^+$ ions generated by

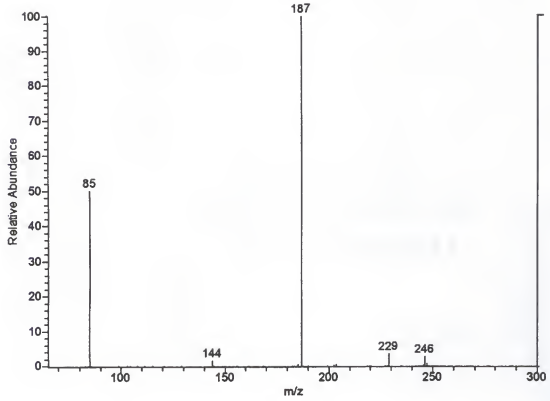

Figure 2-14. LE-CID spectrum from $(M+H)^+$ of isovalerylcarnitine (m/z 246) generated by ESI on an ion trap mass spectrometer.

ESI. As can be seen, the ESI-MS/MS spectrum is rather simple. It is similar to HE-CID spectra of LSIMS precursor ions (Figure 2-13 A), although the mass resolution is much better and the efficiency of the CID process in the ion trap is remarkably higher. The major peak observed at m/z 187 corresponds to the loss of trimethylamine. Ions at m/z 85 and m/z 144 are also present, as in the LSIMS MS/MS spectra. Unfortunately, due to CID occurring in the ion trap at a Mathiew q parameter of 0.25, the lowest product ion mass that can be stored for a precursor ion of 246 is m/z 65. Notice that there is a signal at m/z 229, which is not seen in the DCI and LSIMS spectra. To identify this ion, two other carnitines, hexanoyl and isobutyroylcarnitine were analyzed by ESI LE-CID. Loss of 17 Da from the $(M+H)^+$ ions of these two compounds was not observed. This suggests that m/z 229 might form from isobaric interferences in the isovalerylcarnitine solution.

Low-energy CID is a very efficient process; it is possible to transfer most of the kinetic energy into internal energy so that small changes in ion kinetic energy can have great effect on the appearance of product ion spectra.[59] Plots of relative abundance of the fragment ions observed as a function of collision energy produce energy-resolved breakdown curves that are useful for the determination of fragmentation pathways, isomer differentiation and for the optimization of CID conditions for trace analysis.[135] The LE-CID energy-resolved curves for the $(M+H)^+$ ion of isovalerylcarnitine formed by methane DCI and by ESI are shown in Figure 2-15. As can be seen, the curves are significantly

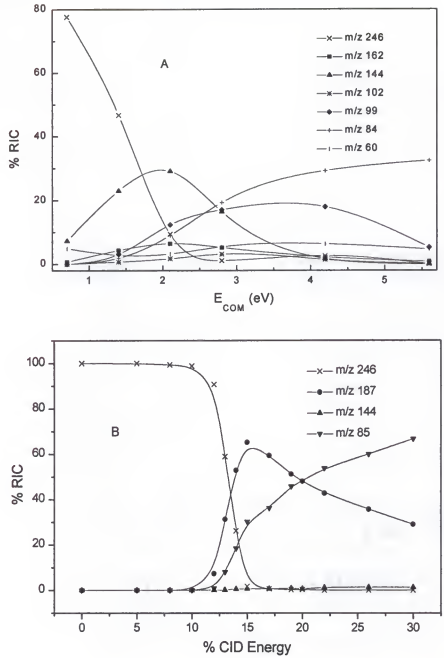

Figure 2-15. LE-CID energy-resolved breakdown curves for $(M+H)^+$ ions (m/z 246) from isovalerylcarnitine generated by: A. Methane DCI, TSQ 70 (1.0 mtorr Ar). B. ESI, LCQ. E_{COM} represents the center of mass collision energy. % CID Energy represents the porcentage of a maximum 5 V excitation voltage available for CID.

different for the ions generated by the two ionization techniques. Note that for the experiments performed in the triple quadrupole instrument, there is some CID occurring already at E_{COM} =0.7 eV (5 eV in laboratory frame). This has been indicated[136] to be due to penetration of the electric fields of the lenses on both sides of the collision cell. As for CID in the ion trap, because CID occurs in the same space as ionization, the ions only need to be sufficiently excited to decompose. Thus, relatively sharp increase in product ion intensity occurs once the appearance energy is reached. In Figure 2-15A, the formation of m/z 144 requires less energy than the formation of m/z 99 and m/z 84. The higher abundance of m/z 144 in the triple quadrupole indicates that the internal energy of the precursor ion is higher in this instrument than in the ion trap. Under the conditions of the curves shown in Figure 2-15B, m/z 187 (loss of trimethyl amine) requires less energy than m/z 144 and m/z 85. The loss of trimethyl amine to form m/z 187 is not observed in the LE-CID spectra of precursor ions formed by methane DCI, which suggests that structures (or mixture of structures) of $(M+H)^+$ ions formed by methane DCI and ESI are different. Also, thermal effects might play an important role in favoring a fragmentation pathway over another.

Conclusions

Leucine Enkephalin

It was possible to observe $(M+H)^+$ ions of leucine enkephalin in DCI/MS spectra on the triple quadrupole instrument. Spectra obtained with methane and water as reagent gases were very similar. Ammonia DCI spectra showed

ammonia adducts at 17 amu higher than the corresponding ions in methane and water DCI. For DCI LE-CID spectra, methane DCI produced the most intense low-mass signals, which indicates higher energy deposition in the precursor ion when methane is used as reagent gas. Less intense low mass ions were obtained with water and with ammonia as reagent gases. These observations agree with different amounts of the internal energy deposited during chemical ionization with different reagent gases.

Ion intensity in LSIMS spectra was found to be dependent on matrix composition. Thus, glycerol/water (50:50 v/v) was the most effective in promoting fragmentation and NBA the least, while Magic Bullet/TFA was the most prone to cation adduction. As for LSIMS HE-CID, spectra were very similar in all the matrices used, although NBA showed more intense product ions, followed by glycerol/water, in turn followed by Magic Bullet/TFA.

Comparison of HE- and LE-CID spectra, obtained for $(M+H)^+$ ions of leucine enkephalin generated by LSIMS and DCI, respectively, showed that the formation of the A_4 ion is favored over the B_4 ion in LE-CID, while B_4 is more intense in HE-CID. This seems to correlate with longer reaction times for the LE process and with thermal decomposition of the $(M+H)^+$ ion of leucine enkephalin which favors formation of A_4 by loss of CO from B_4 under DCI.

Isovalerylcarnitine

DCI-MS spectra of isovalerylcarnitine with methane and water as reagent gases showed abundant ions throughout the mass range. The ammonia DCI

spectrum exhibited ions corresponding to ammonia adducts of the ions observed with the other reagent gases. An ion at m/z 232 present in all three spectra was attributed to thermal degradation processes occurring in DCI. In this case, pyrolytic demethylation, followed by protonation seems to be a reasonable explanation. For DCI LE-CID, spectra of $(M+H)^+$ ions obtained with different reagent gases showed similar ions. More intense low-mass ions were obtained with methane DCI, while fewer ions and better signal-to-noise ratios were observed with ammonia DCI, which agrees with the internal energy deposited during chemical ionization with the reagent gases used in these experiments. DCI HE-CID spectra were also obtained, but only precursor ions generated by ammonia DCI produced enough fragmentation to be recorded and averaged. HE and LE-CID spectra of DCI ions were very similar.

LSIMS spectra of isovalerylcarnitine showed a very intense $(M+H)^+$ ion signal and only a few fragments in the three matrices used. HE-CID spectra were characterized by loss of trimethylamine. The most intense fragmentation was observed with Magic Bullet/TFA, followed by NBA and by glycerol. Charge-remote fragmentation was also observed in HE-CID.

Comparing HE- and LE-CID of LSIMS and DCI-generated ions, the fragmentation patterns were more complex in DCI. The intense ion observed in LSIMS from loss of trimethylamine was not observed in DCI under any of the collision energy regimes. This suggests different ions are formed by the two ionization techniques. ESI LE-CID data was also compared to LSIMS and DCI CID and a similar pattern to LSIMS was observed. This indicates again, that

different structures or mixtures of structures can be formed by different ionization techniques. Condensed-phase in contrast to gas-phase processes might play an important role in these observations.

CHAPTER 3
INTERNAL ENERGY DEPOSITION IN CHEMICAL IONIZATION / TANDEM MASS SPECTROMETRY

Introduction

During the early years of mass spectrometry, most research focused on fundamental studies of ionization and dissociation. The development of mass spectrometry as an analytical tool was mostly due to the utility of electron ionization (EI) for structural elucidation of small organic molecules. Although 70 eV EI spectra were very reproducible and predictable, thermally labile compounds were not amenable to EI. It is estimated that about 20% of EI spectra fail to show molecular ions[17] since too much energy is deposited into the ions during this process.

In 1952, Talrose and Lyubimova[137] found that CH_5^+ ions existed and could be produced by introducing methane into a mass spectrometer at pressures around 1-2 torr. Field and coworkers[138] put these ideas into their ion-molecule reaction experiments with ethylene and multiple-order reactions (as high as sixth-order) to produce the $C_7H_{13}^+$ ion from ethylene were observed. Later on, ion-molecule reactions in methane,[139] ethane, propane and butane[140] were studied.

The biggest breakthrough was finding that the extensive ion decomposition observed in EI spectra of hydrocarbons was not occurring with this new type of ionization, and that $(M+H)^+$ or $(M-H)^+$ ions were appreciable in

the spectra. The ions produced by hydride abstraction from a hydrocarbon were even-electron species, whose stabilities and decomposition paths are very different from odd-electron ions formed by EI. It was also very likely that the amount of energy transferred to the pseudomolecular ion in these ion-molecule reactions was smaller than in EI.[141]

Munson and Field[6] introduced the term chemical ionization (CI) in 1966 after application of these ion-molecule reactions with methane to the analysis of different compounds was successfully carried out. For chemical ionization to occur, a gas (called the reagent gas) or mixture of gases at a pressure of about 0.2-1.0 torr is introduced into an ion source and bombarded with electrons. Ionization of the reagent gas (usually present in large excess (hundredfold or more)) is followed by ion-molecule reactions with reagent gas neutrals to produce CI reagent ions. Collisions of these reagent ions with sample molecules produce ions characteristic of the sample.[132] Ionization in CI can occur by charge exchange, proton transfer, hydride or other anion abstraction and electrophilic addition; these techniques have been reviewed in several books.[17,132,142] For this dissertation, only proton transfer reactions for positive ions will be reviewed.

Proton transfer reaction from a reagent ion $(B+H)^+$ to a sample molecule M, is shown by the equation

$$(B+H)^+ + M \rightarrow (M+H)^+ + B \qquad (3\text{-}1)$$

The ΔH of the reaction is given by the difference in proton affinity (PA) of the reactants according to the equation

$$\Delta H = PA\,(B) - PA\,(M) \qquad (3\text{-}2)$$

Brønsted acids are used as reagent gases in CI. The fragmentation of the $(M+H)^+$ ion observed in the CI spectra depends on its internal energy, which can be controlled by varying the reagent ion and, therefore, the exothermicity of the proton transfer reaction. In general, fragmentation increases when the exothermicity of the proton transfer reaction increases.

It is possible to predict which proton transfer reactions will occur in a particular system, since values of PA of a large number of compounds are tabulated.[143] Selective ionization can be obtained by the choice of reagent ion. Thus, proton transfer from NH_4^+ occurs to compounds with PA's greater than that of ammonia, such as amides and amines,[144] but not to most organic compounds. Protonated methane, on the other hand, can be used to protonate a great variety of compounds.

Spectra obtained by CI are often simple, frequently giving only molecular weight information; therefore, activation techniques such as collision with a neutral gas are commonly used to increase the internal energy of the ion and promote fragmentation. The fragmentation observed in collision-induced dissociation (CID) depends upon the internal energy present in the ions prior to collision as well as the energy deposited during collisional activation. The limited publications on the role of precollisional internal energy on CID spectra show conflicting results. Some studies[10,12,109,110] indicate that precursor ion internal energy has a negligible effect on the CID spectrum, except for product ions formed through processes with the lowest activation energy. Alternatively, there

is supporting evidence that CID spectra are highly dependent on initial energy of the precursor ion and/or angular momentum.[11,13-15]

The effect of internal energy on the relative rates of the reactions competing in CID processes has been studied by varying the electron energy in electron ionization (EI).[10] It was found that precursor ion internal energy has a negligible effect on the ion CID spectrum except for product ions formed through the processes of lowest activation energy. The effect of the degrees of freedom of the analyte on ion internal energy has also been investigated.[11] In these experiments, the differences in CID spectra of benzoyl ions formed from a series of homologous compounds were attributed to different internal energy distributions in the fragmenting ion. McLafferty and coworkers[12] reviewed these results by forming the ions by electron ionization at 14 and 70 eV. They concluded that the CID spectra of benzoyl ions were independent of their internal energy and mode of formation since no differences were observed. An ingenious experiment was designed by Beynon's group[13] in which different portions of a metastable peak were sampled. They were able to select ions with different internal energies and let them to undergo CID. It was shown that the position of an ion within the metastable peak correlated with its internal energy. Thus, the ions sampled from the edges of the metastable peak were the least excited and the ions taken from the center were the most excited, as reflected in the CID spectrum. Bowers and coworkers[14] showed that ions generated by selected ion-molecule reactions could have energies that vary over several electronvolts and that the CID spectrum depends on the internal energy of the ions prior to

collision. Later studies performed in the same group[15] included charge-stripping reactions and showed that the charge stripping spectra of the ions studied were strongly dependent on internal energy. The most recent studies on the role of precollisional internal energy on CID spectra were reported by Scrivens and coworkers.[16] They obtained CID spectra of ions formed by various ionization techniques from irganox 1076, a polymer additive. It was demonstrated that the variation in relative abundance of various fragment ions present in the CID spectra was correlated to differences in the internal energy transferred to the precursor ion during ionization.

Although there are several studies that indicate the importance of internal energy on CID spectra, it is still often assumed that the ions have no memory of where and how they were formed, as implied by the quasi-equilibrium theory. We are interested in understanding the effects of internal energy on CID spectra. In the present work, $(M+H)^+$ ions of several heterocyclic amines were formed with different internal energies via chemical ionization using different reagent gases. The effect of precollisional internal energy on the subsequent CID spectra of these amines is reported.

Experimental

Pyridine, piperidine, pyrrole and pyrrolidine (Aldrich Chemical Co. Milwaukee, WI) were used for the experiments presented here. All compounds (Figure 3-1) were used as received, except for pyrrole, which was passed through a silica gel column to remove oxidation products. The compounds were introduced into the mass spectrometer through a variable leak valve (Granville

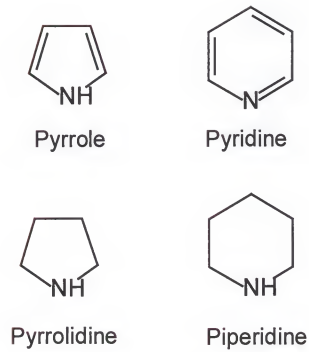

Figure 3-1. Five- and six-membered heterocyclic compounds.

Phillips, series 203). The valve was placed inside the oven of a gas chromatograph so that its temperature could be regulated as needed.

High- and low-energy CID and metastable experiments were performed on a Finnigan MAT95Q hybrid sector mass spectrometer of BEoQ configuration (Finnigan MAT, San Jose, CA). The ions studied were generated by chemical ionization (CI). Methane, isobutane and ammonia were used as reagent gases, with their pressure adjusted to obtain a $(M+H)^+ / (M)^+$ ratio of 10 ± 3.

High-energy CID (HE-CID) and metastable ion spectra were measured at a collision energy of 5 keV in the second field-free region, between the magnet and the electric sector, of the mass spectrometer. Mass-analyzed ion kinetic energy spectra (MIKES) were obtained with helium as target gas. Twenty scans were acquired at each collision gas pressure; the collision gas pressure was increased until 97% or more of the precursor ion intensity was attenuated.

Low-energy CID (LE-CID) product ions were formed in the octopole collision cell and mass analyzed with the quadrupole mass analyzer of the MAT95Q. Argon was used as collision gas. The collision energy was varied from 5 to 95 eV in 10 eV increments at each collision gas pressure by changing the offset voltage applied to the octopole. Ten scans were acquired at each collision energy value.

High- and low- energy CID experiments were performed three times, taking an average of three-and-a-half hours to generate the triplicates with each reagent gas. Approximately half-an-hour was allowed to evacuate the gas lines and the ion source after changing reagent gases. An average of the three

analyses was used for all the calculations. Most of the graphs shown here include error bars equivalent to one standard deviation.

The kinetic energy release (KER) associated with unimolecular decomposition was determined by mass-analyzed ion kinetic energy spectrometry (MIKES). In this technique, the ion of interest is mass selected by the magnetic sector and the products of unimolecular decomposition reactions occurring in the field free region between the magnet and the electric sector are measured by scanning the electric sector. The KER values were calculated according to the equation[30]

$$KER = \frac{y^2 m_1^2 E}{16 m_2 m_3}\left(\frac{\Delta E}{E}\right)^2 \qquad (3\text{-}3)$$

where m_1 is the mass of the precursor ion, m_2 is the mass of the product ion, m_3 is the mass of the neutral loss, y is the charge of the product ion, E is the accelerating voltage and ΔE is given by:

$$\Delta E = \left[\Delta E_{50\%}^2 - \Delta E_{m_1}^2\right]^{1/2} \qquad (3\text{-}4)$$

where $\Delta E_{50\%}$ is the width in volts of the product ion peak at half height and ΔE_{m1} is the width in volts of the precursor ion peak at half height.

Results and Discussion

A list of the proton affinities of the compounds and reagent gases used in these experiments is shown in Table 3-1. If the exothermicity of the proton transfer reaction is calculated with equation 3-2, it can be seen that the ionization process with methane CI is the most exothermic, and therefore, the $(M+H)^+$ will have the most internal energy. On the other hand, proton transfer reactions

Table 3-1. Proton affinity values for species of interest

SPECIES	REACTANT ION	PA (EV)*
C_4H_5N	SM**	9.07
C_4H_9N	SM	9.82
C_5H_5N	SM	9.63
C_5H_9N	SM	9.89
CH_4	CH_5^+	5.63
C_4H_8	$C_4H_9^+$	8.31
NH_3	NH_4^+	8.84
C_2H_4	$C_2H_5^+$	7.05
C_3H_4	$C_3H_5^+$	8.48

* Values obtained from reference 143 and converted from kcal/mol to eV
** SM – sample molecule

involved in ammonia CI will be the least exothermic and the ions produced will have the least internal energy.

The composition of reagent gas plasmas is sensitive to pressure and temperature of the ion source. Ideally, the maximum sensitivity should be obtained at minimum source pressure to minimize competing reactions in the ion source. At low pressures, however, a significant number of sample ions are typically formed by electron ionization, not by ion-molecule reactions. Under typical CI conditions, several different reagent ions may be formed from a given CI reagent gas. Primary ions of methane react rapidly with methane neutral gas at virtually every collision to give predominantly CH_5^+, $C_2H_5^+$, and $C_3H_5^+$. Of these ions, CH_5^+ and $C_2H_5^+$ react mostly by proton transfer reactions, while $C_3H_5^+$ reacts typically by hydride abstraction. $C_2H_5^+$ and $C_3H_5^+$ ions frequently produce $(M+C_2H_5)^+$ and $(M+C_3H_5)^+$ adduct ions of low intensity in the spectrum[6]. In isobutane CI, primary fragment ions react by hydride abstraction with isobutane to form an intense $C_4H_9^+$, presumably the t-butyl ion.[132] The major positive ions present in the source during ammonia CI are NH_4^+ and $NH_4^+NH_3$. Proton transfer and association reactions are commonly observed in ammonia CI. If the proton transfer reaction from NH_4^+ to an analyte is exothermic, the reaction will be fast. Proton transfer occurs more readily from NH_4^+ than from $NH_4^+NH_3$ because the thermochemical stability of solvated ions increases with the extent of clustering, which causes proton transfer to be more difficult.[114]

Metastable Ions

A metastable ion is one that is sufficiently stable to survive the ionization conditions of the ion source, but is not stable enough to reach the detector before dissociating.[30] Excess internal energy imparted during ionization may be released upon dissociation as translational energy of the dissociation products. This causes a spread in the velocity of the product ions, resulting in broadening of the metastable ion decomposition peak shape. Thus, measuring the kinetic energy release (KER) of the product ions allows precise estimation of a quantity related to the internal energy distribution of the precursor ion.[145] Kinetic energy releases for the metastable decompositions of the $(M+H)^+$ ions of the four compounds in Figure 3-1 formed by CI with different reagent gases were measured in order to correlate the amount of internal energy deposited by the ionization technique with its effect on tandem mass spectra. A summary of the metastable ions observed in the second field-free region and the kinetic energy release values for the corresponding metastable transition is shown in Table 3-2.

As can be seen, no metastable transitions were observed for $(M+H)^+$ ions of pyrrole generated by isobutane or ammonia CI, which implies low internal energies for ions produced by these reagent species. A metastable ion at m/z 41 was observed only when methane was used as the reagent gas. This corresponds to the neutral loss of HCN from protonated pyrrole. The KER for this metastable transition is 50 meV. The error in this value is large due to low signal-to-noise ratio of the metastable peak, which made it difficult to measure.

Table 3-2. Kinetic energy release for metastable ions.

COMPOUND	METHANE/CI			ISOBUTANE/CI			AMMONIA/CI		
	ΔPA[a]	m/z	KER[b]	ΔPA[a]	m/z	KER[b]	ΔPA[a]	m/z	KER[b]
Pyrrole	3.44	41	50±20	0.76	-	-	0.23	-	-
Pyridine	4.00	-	-	1.32	-	-	0.79	-	-
Pyrrolidine	4.19	30	56±3	1.51	30	79[c]	0.98	-	-
Piperidine	4.26	30 69	45±11 34±1	1.58	-	-	1.05	-	-

[a] Difference in proton affinity between the compound and the conjugate base of the predominant reactant ion in eV.
[b] In millielectronvolts (meV) ± one standard deviation (three replicates)
[c] Intensity too low in two of the replicates to measure KER.
- No metastable ions observed.

For pyridine, no metastable ion decomposition is observed to occur for the $(M+H)^+$ ion (m/z 80) even with methane CI, which imparts 4 eV of internal energy. For pyrrolidine, methane CI and isobutane CI produce ions with enough internal energy to allow metastable decompositions to be observed, as indicated for the peak at m/z 30. The KER value obtained for isobutane CI might not be accurate, since only one of the three replicates could be evaluated (the peaks in the other two replicates were of low signal-to-noise ratio and it was not possible to determine a reasonable value for the peak width at half maximum). For piperidine, the metastable ion spectrum of the $(M+H)^+$ ion generated by methane CI shows two ions, m/z 69 and m/z 30, which correspond to neutral losses of 17 amu (NH_3) and 56 amu (C_3H_6N), respectively.

In all compounds the studied, the relative intensities of the metastable ions were very low (< 0.03% of the normalized precursor ion intensity). Ammonia CI does not impart enough energy into the $(M+H)^+$ ions (≤ 1.05 eV) to allow metastable ions to be observed in any of the compounds studied here. The absence of metastable ions indicates that the internal energy of the precursor ion prior to collisions must be less than the critical energy for the pathway of lowest dissociation energy.[7] The peak at m/z 30 in the metastable ion spectra of piperidine and pyrrolidine is common for secondary amines and corresponds to $NH_2CH_2^+$ produced by rearrangement.[146]

Correlation of internal energy deposited by proton transfer reactions from various reagent gases with metastable kinetic energy release was not possible due to the lack of metastable ions with reagent gases other than methane.

Fragmentation Efficiency / HE-CID

One way to estimate the energy deposited by the ionization technique and its effect on HE-CID is to compare the fragmentation efficiency for the $(M+H)^+$ ions formed by CI with the different reagent gases.

The fragmentation efficiency (E_f) is simply the fraction of detected ions that are fragment ions[22] and is given by

$$E_f = \left(\frac{\Sigma F_i}{\Sigma F_i + P} \right) \qquad (3\text{-}5)$$

where ΣF_i is the sum of the intensities of all the fragment ions and P is the remaining precursor ion intensity. In these studies, fragmentation efficiency was monitored as the collision gas pressure was increased. Because the pressure of the collision gas is typically not measured directly in the collision cell of a sector mass spectrometer but rather at a nearby location, it has been suggested that precursor ion transmission (P/P_o) or attenuation ($1\text{-}P/P_o$) be measured instead of pressure.[22,42] P_o is defined as the parent ion intensity when no collision gas is introduced. Although measuring attenuation takes care of differences in collision cell designs and pressure gauges and facilitates comparison of data taken in different instruments,[22,42] it will be shown in this chapter that for these studies pressure graphs provide more revealing information.

The dependence of HE-CID fragmentation efficiency on the collision gas pressure (plotted as attenuation and as pressure measured directly in the analyzer region) and on the reagent gas used for chemical ionization is shown in Figure 3-2 for the 6-membered ring heterocycle piperidine. As can be seen for

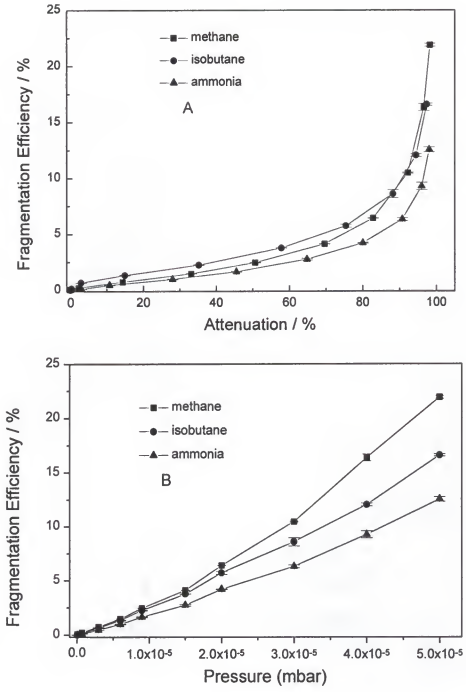

Figure 3-2. Fragmentation efficiency curves for the HE-CID of $(M+H)^+$ ions of piperidine produced CI with methane, isobutane and ammonia as a function of A. Attenuation, B. Analyzer pressure.

each curve, as collision gas pressure is increased, the amount of internal energy deposited into the precursor ion increases due to increasing probability of collisions and therefore the fragmentation efficiency increases. Note that for the fragmentation efficiency curve plotted against attenuation (Figure 3-2. A) there is some overlap between the methane and isobutane CI curves up to about 90% attenuation. The highest fragmentation efficiencies were observed for $(M+H)^+$ ions generated with methane CI, the lowest for ammonia CI, and in between for isobutane CI. In contrast, as can be seen in Figure 3-2 B, the fragmentation efficiency curves plotted as a function of collision gas pressure (measured as analyzer pressure) for the $(M+H)^+$ ions are consistent throughout the pressure range, with the fragmentation efficiencies for the $(M+H)^+$ ions generated by methane CI the highest, followed by those of isobutane CI, in turn followed by those of ammonia CI. The pressure graphs indicate that, as expected, methane CI produces $(M+H)^+$ ions with more internal energy than those formed by isobutane CI, which are in turn more energetic than the ions produced by ammonia CI. Even under multiple collision conditions, the fragmentation efficiency is still affected by the energy deposited by the ionization technique; the HE-CID process does not impart enough energy to mask these internal energy differences.

For a better understanding of the differences observed in the graphs shown in Figure 3-2 A and B, the relationship between attenuation and collision gas pressure needs to be established. Figure 3-3 shows the relationship between attenuation of $(M+H)^+$ ions of piperidine produced by chemical ionization

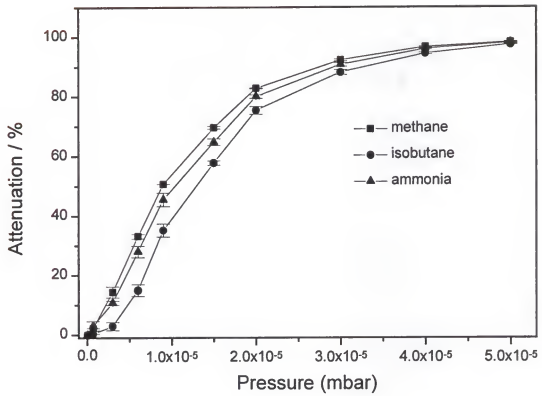

Figure 3-3. Measurement of precursor ion attenuation as a function of analyzer pressure for HE-CID of $(M+H)^+$ ions of piperidine generated by CI with methane, isobutane and ammonia.

with methane, isobutane and ammonia and the analyzer pressure, which is the parameter measured. As can be seen, the attenuation at a given pressure is consistently less for isobutane CI than for methane or ammonia CI. Although the origin if this difference is not clear (it is not seen in some of the other compounds studied), it has the effect of shifting the isobutane curve in Figure 3-2 A to the right, causing it to cross the methane curve. Thus, the data presented in this chapter are plotted versus analyzer pressure, not attenuation.

As shown in Figure 3-2 B, increasing the collision gas pressure increases the fragmentation efficiency; the collection efficiency, however, decreases as the collision gas pressure increases due to scattering and neutralization losses. The collection efficiency (E_c) represents the ratio of ions leaving the collision region that are collected to those entering the collision cell[22] and is given by the equation:

$$E_c = \left(\frac{\Sigma F_i + P}{P_o} \right) \tag{3-6}$$

Figure 3-4 shows how the collection efficiency of piperidine ions changes as a function of attenuation or collision gas pressure (measured as analyzer pressure) and chemical ionization reagent gas. As can be seen, the collection efficiency is 100% when there is no collision gas present. For the ions formed by CI with methane, isobutane and ammonia, the collection efficiencies decrease almost linearly and are virtually undistinguishable from one another when beam attenuation increases due to scattering and neutralization reactions of the ions occurring in the collision cell. As has been noted before, the use of attenuation

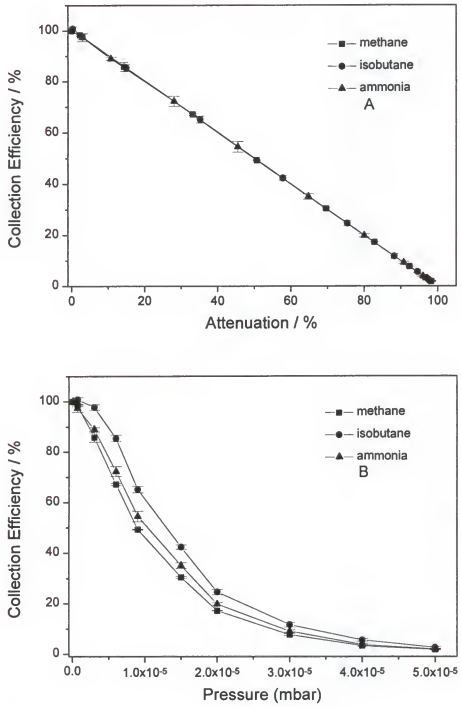

Figure 3-4. Collection efficiency curves for the HE-CID of $(M+H)^+$ ions of piperidine produced by CI with methane, isobutane and ammonia as a function of A. Attenuation, B. Analyzer pressure.

hides the true nature of the collection efficiency.[22] For collection efficiency evaluated as a function of pressure in the analyzer (Figure 3-4 A), at a given pressure, the collection efficiency is highest for ions formed by isobutane CI, followed by the collection efficiency of ions formed by ammonia CI, in turn followed by those generated by methane.

As was mentioned before, as fragmentation efficiency increases, the collection efficiency decreases. The product of these two values is called the overall CID efficiency (E_{CID}). It accounts for fragmentation, neutralization and scattering losses during the CID process. The real value for the current study of plotting overall CID efficiency, however, is that it provides a much better way to view differences in efficiencies at low attenuations than does plotting fragmentation efficiencies. The overall CID efficiency has been defined as the fraction of initial precursor ion that is converted to collected product ions or the total fragment ion current divided by the ion current of the precursor ion entering the collision cell[22] and can be written as:

$$E_{CID} = \frac{\Sigma F_i}{P_o} = E_f \times E_c \qquad (3\text{-}7)$$

The overall CID efficiency plots for $(M+H)^+$ ions of piperidine generated by CI with methane, isobutane and ammonia as a function of attenuation and analyzer pressure are shown in Figure 3-5 A and B, respectively. As collision gas pressure is increased, overall CID efficiency curves typically show an increase, then level off. A decrease is observed at high pressures due mostly to scattering losses. As can be observed, by evaluating the overall efficiency of the

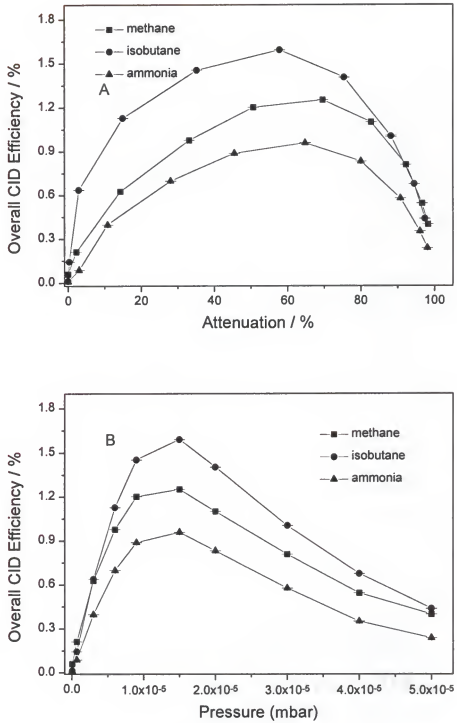

Figure 3-5. Overall CID efficiency curves for the HE-CID of $(M+H)^+$ ions of piperidine produced by CI with methane, isobutane and ammonia as a function of A. Attenuation, B. Analyzer pressure.

HE-CID process as a function of either attenuation or pressure, the highest values are obtained for ions generated by isobutane CI, followed by those of methane CI. The lowest overall efficiencies are observed for ions produced by ammonia CI. Note that the high values of the collection efficiency for isobutane CI generated ions are amplified in these graphs.

The primary goal of this study is to evaluate the effect of internal energy on the fragmentation process. Thus, it is most informative to examine the fragmentation efficiency curves rather than the collection or overall efficiency curves, both of which are affected by scattering and neutralization losses. Furthermore, it is preferable to plot fragmentation efficiency versus analyzer pressure rather than attenuation, since attenuation is also affected by scattering and neutralization losses.

Figure 3-6 shows how the fragmentation efficiencies for HE-CID of $(M+H)^+$ ions of pyridine, pyrrolidine and pyrrole change as a function of collision gas pressure and CI reagent gas (for comparison, the corresponding curves for piperidine are shown in Figure 3-2 B). As anticipated, fragmentation efficiency increases as collision gas pressure is increased; the internal energy of the $(M+H)^+$ ions increases as the number of collisions increases, resulting in more fragmentation. In all cases, the $(M+H)^+$ ions generated by methane CI produced the highest fragmentation efficiencies, followed by those produced by isobutane CI, in turn followed by those formed by ammonia CI; this is in agreement with the large internal energy deposited into the $(M+H)^+$ ions by CI with reagent gases of lower proton affinities. Notice that the fragmentation efficiencies at any given gas

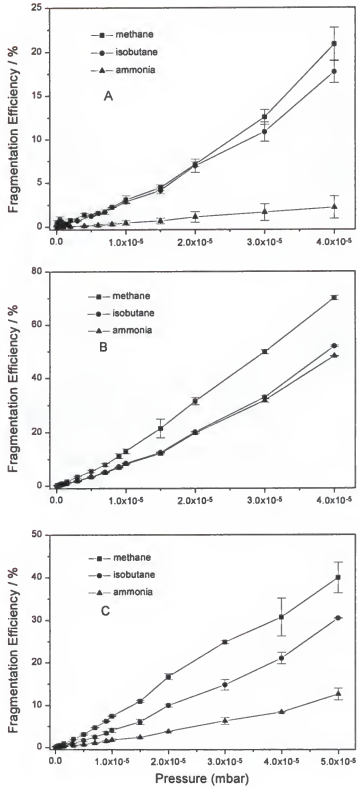

Figure 3-6. The effect of collision gas pressure (measured as analyzer pressure) and CI reagent gas on fragmentation efficiency of $(M+H)^+$ ions from A. Pyridine, B. Pyrrolidine, C. Pyrrole.

gas pressure of the five-membered heterocycles pyrrolidine and pyrrole (Figure 3-6 B and C, respectively) are much higher than those of the six-membered compounds piperidine (Figure 3-2 B) and pyridine (Figure 3-6 A), independent of the saturation of the ring. This is expected since in general, six-membered ring compounds are more stable than five-membered rings.

It has been claimed[10] that a unique advantage of CID spectra for ion structure determination is their insensitivity to ion internal energy, if the peaks resulting from low activation energy pathways are ignored; if that assumption is valid, the CID spectra of precursor ions of the same structure formed with different internal energies will have the same relative abundances within statistical error. The results presented here indicate that fragmentation efficiencies of the heterocyclic compounds are a function of the internal energy deposited during ionization. Note that the fragmentation efficiencies are a function of the total intensity of the product ions in the CID spectra; the relative abundances may or may not be affected.

To get a better understanding of the effect of internal energy on relative abundances of product ions, the intensity ratios of several product ions in the HE-CID spectrum of $(M+H)^+$ ions of piperidine were plotted as a function of collision gas pressure and CI reagent gas. For each ion and at each pressure ten scans were averaged and the relative intensity of the fragment ions were plotted.

Figure 3-7 shows the effect of varying the collision gas pressure and the CI reagent gas on several ion ratios from HE-CID of protonated piperidine. The ions used for these ratios range from metastable ions (m/z 30, 69) to ions formed

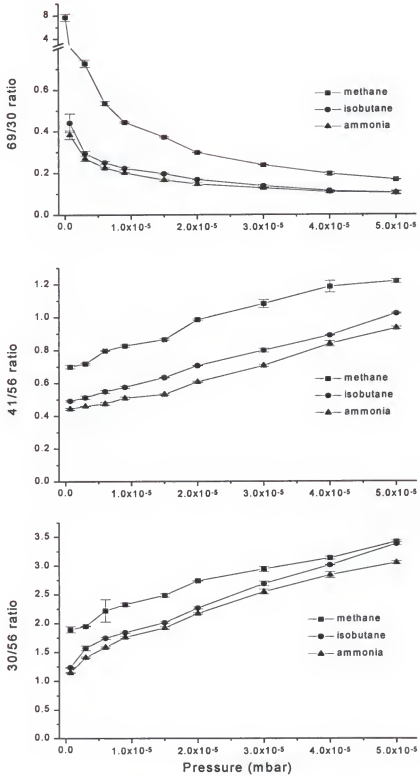

Figure 3-7. The effect of collision gas pressure (measured as analyzer pressure) and CI reagent gas on several fragment ion ratios from protonated piperidine. HE-CID 5keV, helium used as collision gas. m/z 30 and 69 are metastable ions.

purely during CID (m/z 41, 56). As can be observed, in all cases, at a given collision gas pressure the ion ratios are higher for ions formed by HE-CID of the $(M+H)^+$ ions produced by methane CI, followed by those of the ions formed by isobutane CI, in turn followed by those of the ions formed by ammonia CI. Recall that m/z 69 and 30 are metastable ions from $(M+H)^+$ of piperidine, and thus are formed by low activation energy pathways. Notice that the 69/30 ion ratio with methane CI is 2 to 20 times higher than for isobutane or ammonia CI at the same pressure. Clearly, internal energy has an enormous effect on this ratio. As collision gas pressure is increased, the 69/30 ratios get to a point where they level off and remain nearly constant. The behavior observed for the metastable ions was expected, since ion internal energies have been reported to have an effect on relative abundances of ions of low activation energies such as the metastable ions.

Ion ratios were also evaluated for ions that are formed only from CID processes (m/z 41 and 56) and from a combination of metastable and CID processes (m/z 30 and 56). For the graphs considering 41/56 and 30/56 ratios, and within the experimental error, it can be seen that there is a clear effect of the precollisional internal energy on the product ion ratios, as given by the order of the curves. In these graphs, methane is always the top curve, followed by isobutane, in turn followed by the curve obtained under ammonia CI. In general, even though these are not ions formed via low activation energy pathways, the effect of precollisional internal energy was not masked by the energy deposited by the CID process.

Calculation of ion ratios was also possible for ions resulting from the HE-CID of $(M+H)^+$ from pyridine. Metastable ions from pyridine were not observed, as shown before in Table 3-2, even when methane, which imparts approximately 4eV of internal energy, was used as CI reagent gas. The CID process, in contrast, produced ions at m/z 27, 28, 39 and 52. In Figure 3-8 the 28/52, 27/52 and 39/52 ion ratios are plotted as a function of collision gas pressure and CI reagent gas. Note that in all cases there is a clear separation among the curves obtained with methane, isobutane and ammonia CI. As can be seen, the methane CI curves are followed by the isobutane CI and in turn followed by ammonia CI. Indeed, the 28/52 ion ratio is approximately 2 times higher for pyridine $(M+H)^+$ ions produced by methane or isobutane CI than for those produced by ammonia. Clearly, produced ion ratios are significantly affected by choice of CI reagent gas. This indicates that the effect of precollisional internal energy is still observed under HE-CID conditions, even when the ions are not formed by low activation energy processes.

LE-CID vs. HE-CID

The effect of the collision gas pressure and collision energy on the appearance of CID spectra is generally more pronounced at low energies (< 100 eV) than at high energies[59] (keV). Thus, it should be informative to compare the effect of reagent gas identity and collision gas pressure on LE-CID with those on HE-CID.

LE-CID spectra were obtained with argon as collision gas for the $(M+H)^+$ ions from pyridine, pyrrolidine and pyrrole at different energies and collision gas

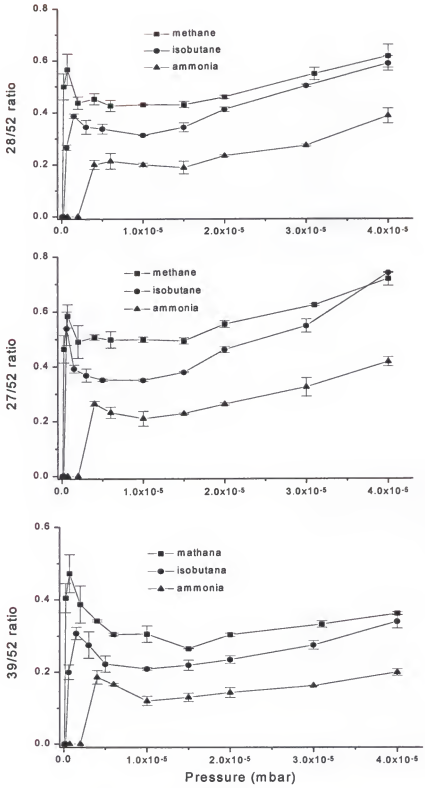

Figure 3-8. The effect of collision gas pressure (measured as analyzer pressure) and CI reagent gas on several fragment ion ratios from protonated pyridine. HE-CID 5keV, helium used as collision gas.

pressures. LE-CID of pyridine showed only one product ion, m/z 53, so no ion ratios could be calculated. LE-CID spectra of piperidine was not obtained due to instrumental problems. Thus for the two compounds pyrrolidine and pyrrole, it is possible to compare LE-CID and HE-CID ion ratios.

Decomposition of protonated pyrrolidine by low-energy CID showed intense ions at m/z 18, 30, 44 and 55. Recall that m/z 30 was a metastable ion in the HE-CID spectrum, and thus must arise from a low activation energy pathway. Ion ratios were calculated between m/z 55 and m/z 30 at both high- and low-collision energies. Figure 3-9 shows the effect of collision gas pressure and CI reagent gas on the 55/30 fragment ion ratios resulting from $(M+H)^+$ ions from pyrrolidine. The ratios in HE-CID (Figure 3-9 A) are consistent throughout the entire pressure range with ratios for methane CI higher than those of isobutane CI, in turn followed by those of ammonia CI. For LE-CID at 65 eV, as shown in Figure 3-9 B, ammonia CI shows the lowest ratios, but methane and isobutane CI curves overlap from approximately $6X10^{-6}$ to $1X10^{-5}$ mbar. Clearly, internal energy imparted during CI has a significant effect on the decomposition of pyrrolidine by both LE-CID and HE-CID spectra; the differences in internal energy from the ionization technique become less important, however, upon multiple collisions at high collision gas pressures in LE-CID.

Observations on the relative intensities of two product ions formed through competing reactions during CID of $(M+H)^+$ ions of pyrrole are shown below. Figures 3-10 A and 3-10 B show the relative intensities of ions m/z 41 and m/z 39 formed under high- and low-energy CID, respectively. As can be seen, for LE-

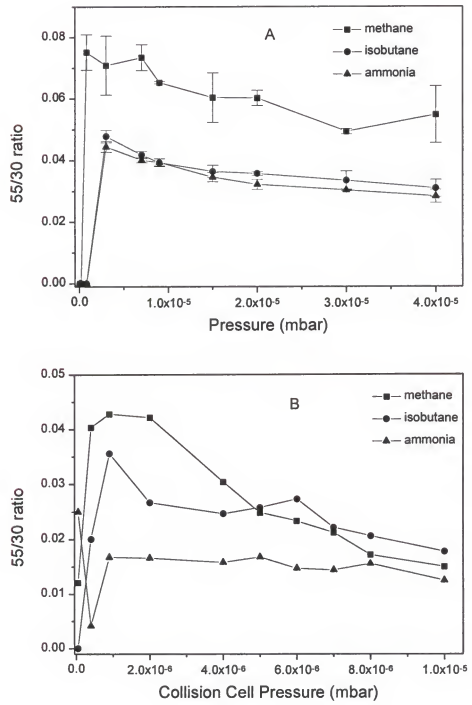

Figure 3-9. The effect of collision gas pressure (measured directly as analyzer pressure) and CI reagent gas on the 55/30 fragment ion ratio from protonated pyrrolidine. A. HE-CID 5keV, B. LE-CID 65 eV. m/z 30 is a metastable ion.

CID, m/z 41 is predominant over m/z 39 (i.e., the ratio is greater than 1) in all three CI experiments. The ratios of intensities for m/z 41 to m/z 39 range from 75:1 to 6:1. In contrast, for HE-CID, the relative intensity of these two ions is generally about 1:1, suggesting a more energetic process for the formation of m/z 39. Shown below are the neutral losses involved in the formation of m/z 39 and m/z 41, along with the proton affinities[143] of the neutrals that are lost.

$$(\text{Pyrrole} + H)^+ \xrightarrow[\text{PA=180 kcal/mol}]{-C_2H_3} C_2H_3N^+$$

m/z 68 m/z 41

$$(\text{Pyrrole} + H)^+ \xrightarrow[\text{PA=203.8 kcal/mol}]{-CH_3N} C_3H_3^+$$

m/z 68 m/z 39

According to Field`s rule,[147] the more favored neutral loss from $(M+H)^+$ in CI would be that of the lowest proton affinity. This has also been shown by McLafferty[148] in relative abundances of CID products resulting from competing reactions. Thus, if we compare the two reactions pathways that give origin to m/z 39 and m/z 41, we can see that the loss of C_2H_3 (PA=180 kcal/mol) to form m/z 41 would be more favored than the loss of CH_3N (PA=203.8 kcal/mol) to form m/z 39, as it is under LE-CID. It suggests that formation of m/z 39 ion involves a reaction channel available at higher energies, not only because its relative intensity is considerably higher in HE-CID than in LE-CID, but also because its relative intensity increases at higher collision gas pressures. Clearly,

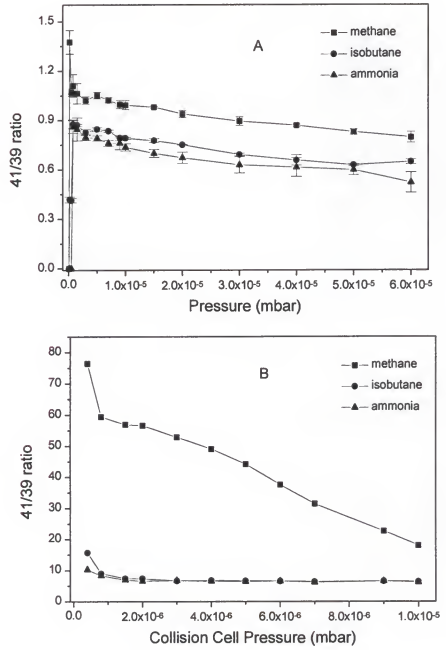

Figure 3-10. The effect of collision gas pressure (measured directly as analyzer pressure) and CI reagent gas on the 41/39 fragment ion ratio from protonated pyrrole. A. HE-CID 5keV, B. LE-CID 65 eV. m/z 41 is a metastable ion.

the product ion relative intensities in both high- and low-energy CID are affected by internal energy imparted during ionization. These effects are more pronounced in LE-CID, where the ratio varies by up to a factor of 10 as reagent gas is changed.

Conclusions

The $(M+H)^+$ ions of the five-membered ring heterocyclic compounds, pyrrole and pyrrolidine, have higher fragmentation efficiencies than the six-membered rings, which agrees with lower stability of the five-membered compounds; therefore, more fragmentation is induced in these systems.

The fragmentation efficiencies in HE-CID clearly correlate with the amount of internal energy deposited by the ionization technique for the five- and six-membered ring compounds studied.

For high- and low-energy CID of $(M+H)^+$ ions of pyrrolidine and pyrrole, the low-energy process is more sensitive to changes in internal energy. High-energy CID spectra include more abundant product ions from reaction channels that open up at high energies.

Neutralization-reionization studies and calculations have shown[149,150] that under isobutane and ammonia CI protonation of pyrrole occurs on the ring carbon atoms rather than on the nitrogen. In contrast, pyridine is protonated exclusively on the nitrogen under isobutane and ammonia CI; under methane CI, it can be protonated on the nitrogen or on the ring carbons. The difference in protonation sites may play a role in some of the differences observed in our experiments; this will be addressed in future studies.

CHAPTER 4
COMPARISON OF MALDI POST-SOURCE DECAY TO LOW- AND HIGH-ENERGY CID

Introduction

Matrix-assisted laser desorption ionization (MALDI)[3,4] was developed in the late 80s and has emerged as an extremely sensitive ionization technique for a variety of compounds. The use of a matrix in laser desorption enhances the desorption and ionization processes, facilitating the analysis of nonvolatile and labile analytes. Ions generated by MALDI are commonly analyzed with time-of-flight mass spectrometers (TOF-MS). These mass analyzers are convenient because of their compatibility with pulsed ionization techniques as well as their theoretically unlimited mass range, high ion transmission and simplicity. A major limitation of TOF-MS instruments is their relatively poor mass resolution. The coupling of reflectrons[151] to TOF-MS instruments has provided a remarkable improvement to the resolution problems. It has been demonstrated that the energy-resolving characteristics of reflectron TOF instruments make it possible to disperse and observe fragment ions that are formed in the drift region of a TOF-MS in an experiment analogous to tandem mass spectrometry.[152] This fragmentation, known as post-source decay (PSD),[153] apparently stems from a combination of excess internal energy imparted to the analyte ion during the

ionization event and multiple collisions with desorbed species during ion acceleration through the dense plume.[154]

The MALDI mechanism of ion formation is complex and involves both condensed-phase and gas-phase reactions. Several models have been developed to explain the desorption mechanism of large molecules in MALDI.[155,156,157] All these models include a fast heating step of thin layers of material, but involve different processes for energy deposition during desorption. The ionization mechanism of MALDI is not well understood; it seems to occur in a separate step in the expanding plume of desorbing materials as a result of matrix and analyte reactions. MALDI spectra are often dominated by matrix photoproducts, adduct ions, and protonated molecules. It has been proposed that excited-state protonated matrix molecules formed during this process act as proton donors for the analytes[158,159,160] during the ionization process. Thus, the internal energy of the ions formed in MALDI, in a similar way to ions formed by CI, should depend upon the exothermicity of the proton transfer reaction, which in turn depends on the matrix used. Other studies suggest that ion-molecule reactions between matrix molecular ions and analytes with the mediation of a radical ion are responsible for ionization.[161] Some authors have shown that the choice of matrix can strongly affect the extent of PSD. Karas and coworkers[158] reported that 3-hydroxypicolinic acid allowed desorption of intact glycoproteins with labile functional groups, while 4-hydroxy-α-cyanocinnamic acid induced strong metastable fragmentation. The use of so-called "cold" matrices such as

2,5-dihydroxybenzoic acid and DHAP/DAHC, a mixture of 2,6-dihydroxy acetophenone and diammonium-hydrogen citrate has also shown to minimize PSD fragmentation.[162] Matrices with low proton affinities such as 4-hydroxy-α-cyanocinnamic acid, have been shown to give high yields of multiply charged ions[163,164] which supports the hypothesis that gas-phase proton transfer reactions play an important role in the formation of ions during MALDI.

There have been several publications comparing MALDI-PSD spectra to CID spectra of ions formed by fast atom bombardment (FAB) and electrospray ionization (ESI). Rouse et al.[165] reported that for peptides, the fragments formed by MALDI-PSD and LSIMS-low-energy CID were remarkably similar. Kaufmann et al.[166] observed that in reflectron TOF-MS the cleavage pattern of PSD products of medium size peptides is different from that obtained by high-energy and low-energy CID of ions formed by FAB, LSIMS and ESI. Hsu and Gross[167] compared high-energy CID of Acyl-Coenzyme A $(M+H)^+$ ions from FAB and ESI to MALDI-PSD and concluded that these three methods yield similar CID spectra; they also concluded that MALDI-TOF analysis is 50-100 times more sensitive than FAB and 20 times more sensitive than ESI.

Here are reported comparative studies of liquid secondary ion mass spectrometry (LSIMS)-CID (high and low energy collision regimes) and MALDI-PSD in order to understand the energetics of the PSD and CID processes. An evaluation of several matrices and their role in inducing PSD is also shown.

Some of the matrices studied are considered "hot" matrices, which give extensive PSD, while others are known to induce little PSD.

Experimental

Bovine β-casomorphin, des-arg^9 bradykinin and tylosin were obtained from Sigma Chemical Co. (St. Louis, MO). Erythromycin A was purchased from ICN Pharmaceuticals Inc. (Costa Mesa, CA). These compounds were used as received without additional purification.

One nanomole per microliter stock solutions were prepared and used for LSIMS analysis. Bovine β-casomorphin and des-arg^9 bradykinin were dissolved in acetonitrile/water (70:30 v/v). Tylosin and Erythromycin A were dissolved in methanol. For MALDI experiments, these solutions were diluted with acetonitrile/water (70:30 v/v) to a final concentration of 10 pmol/μL.

MALDI-PSD

α-Cyano-4-hydroxy-cyanocinnamic acid (α-CHCA), 2,5-dihydroxybenzoic acid (DHB), 3-trans-indoleacrylic acid (IAA) and a 9:1 mixture of DHB with 2-hydroxy-5-methoxybezoic acid (HMBA) referred to as super-DHB (s-DHB) were supplied by Aldrich Chemical Co. (Milwaukee, WI). Structures of these compounds are shown in Figure 4-1. Saturated matrix solutions were made at a concentration of 10 mg/ml in a mixture acetonitrile/water (30:70 v/v).

Samples were prepared by the dried droplet method[4]. Ten microliters of the 10-pmol/μL analyte solutions were mixed with 5μL of matrix solution. One

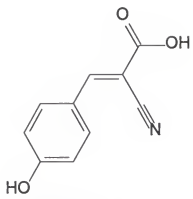

α-CHCA
PA=183 kcal/mol[a]

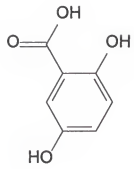

DHB
PA= 204 kcal/mol[a]

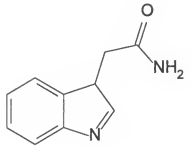

IAA
PA= 215 kcal/mol[a]

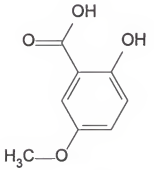

HMBA

Figure 4-1. Structures and proton affinities of the compounds used as MALDI matrices. α-CHCA: alpha-Cyano-4-hydroxycinnamic acid; DHB: 2,5-Dihydroxybenzoic acid; IAA: trans-3-Indoleacrylic acid; HMBA: 2-Hydroxy-5-methoxybenzoic acid. [a] proton affinity values taken from reference 185.

microliter of this mixture was deposited onto a stainless steel sample plate and air dried before analysis.

MALDI-PSD mass spectra were obtained on a Voyager RP Biospectrometry Workstation (PerSeptive Biosystems, Framingham, MA) fitted with a 337-nm nitrogen laser (3ns pulse). The extraction voltage was 20 kV. Precursor ions in PSD were selected with a resolution of 60, which was enough to differentiate $(M+H)^+$ from $(M+Na)^+$ ions. PSD spectra were generated by "stitching together" several reflectron TOF spectral segments, each produced by accumulating data from 128 laser shots and optimized for a certain range of mass-to-charge ratio of fragment ions. Time to mass conversion and calibration was obtained by using a 2 pmol/μL solution of human angiotensin I (Sigma).

LSIMS-CID

CID experiments were performed using a Finnigan MAT 95Q (BEoQ configuration) instrument (Finnigan MAT, San Jose, CA). Ions were generated by liquid secondary ion mass spectrometry (LSIMS) using a 15 keV cesium ion gun. 3-nitrobenzyl alcohol (NBA) supplied by Aldrich Chemical Co was used as matrix. Approximately 1-5 nmols of compound were loaded on a copper probe tip and mixed with 2 μL of matrix. An accelerating voltage of 4750 V was used.

High-energy CID was carried out in the second field-free region between the magnet and the electric sector. The precursor ion beam was attenuated by 50% with helium. For low-energy CID, the precursor ion beam was decelerated

to 50 eV (laboratory frame) in the octopole collision cell and attenuated by 50 % by collisions with argon.

Results and Discussion

High-and Low-Energy Collision-Induced Dissociation Spectra

Des-arg^9 bradykinin (H-RPPGFSPF-OH)

High- and low-energy CID spectra of the $(M+H)^+$ ion from des-arg^9-bradykinin produced by LSIMS are shown in Figure 4-2. There are sufficient ions in both spectra to obtain sequence information on the peptide. As is apparent from the peak assignments, the $(M+H)^+$ ions from des-arg^9 bradykinin fragment so that ions containing the N-terminus are dominant in both spectra, as indicated by the presence of mostly a-type ions. These ions have been shown to have a high energetic requirement,[168] which is favored in HE-CID. N-terminal cleavages are expected to dominate the mass spectra of peptides with arginine at the N-terminus[169] since this basic amino acid serves to localize the positive charge and to direct fragmentation.[170,171] Note that in the HE-CID spectrum the peaks are very broad due to the use of a kinetic energy analyzer as the second stage of mass analysis. This kinetic energy spread may cause problems in the interpretation and identification of the signals in the spectrum. The LE-CID spectrum (Figure 4-2 B) is rich in ions resulting from internal cleavages of the peptide backbone, such as those peaks identified as PG, PP, PGF, PPGF, etc., (which are useful in determining the sequence of the peptide) but most of them also seem to be present in HE-CID spectrum at relative abundances not all that

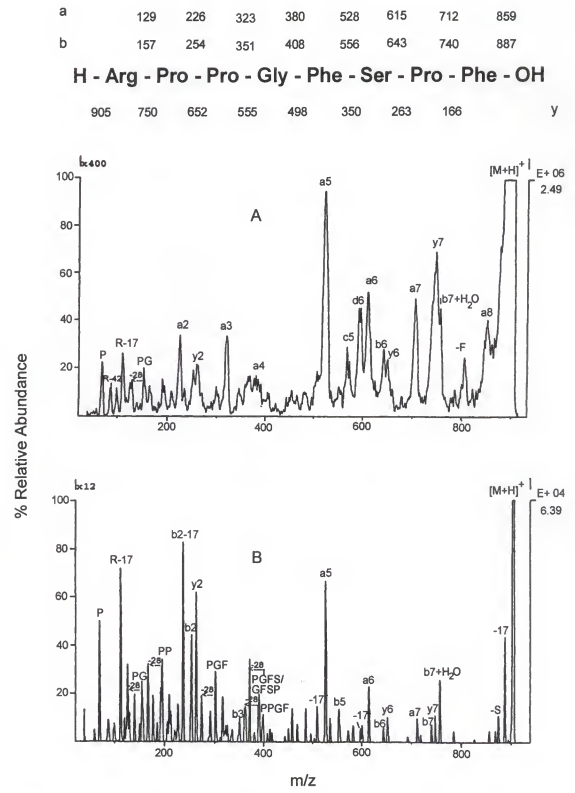

Figure 4-2. Product ion spectra of $(M+H)^+$ ions from des-arg^9 bradykinin (H-RPPGFSPF-OH) (m/z 904). A. HE-CID (5keV) B. LE-CID (50eV).

much smaller, just harder to see because of limited resolution. Internal fragment ions from peptides were first noticed in low-energy CID spectra by Hunt and coworkers.[172] In this collision energy regime a- and b-type series ions along with peaks at 17 Da lower due to the loss of ammonia from the N-terminal arginine are observed.

The collision process is more efficient at low energies than at high energies (note that the $(M+H)^+$ ion is 400 times off-scale in the HE-CID spectrum, vs. only 12 times off-scale on the LE-CID spectrum); more intense low mass ions are also observed in the LE-CID spectrum. The fact that mass analysis on the quadrupole mass filter is essentially independent of the ion kinetic energy makes it possible to obtain unit mass resolution in LE-CID. The presence of internal fragments and internal fragments at 28 Da lower is more pronounced in LE-CID. The generation of these ions requires a minimum of two amide bond cleavages, which is possible in these experiments as a result of multiple collisions and longer reaction times.

Bovine β-casomorphin (H-YPFPGPI-OH)

HE and LE- CID spectra of the $(M+H)^+$ ion from bovine β-casomorphin are shown in Figure 4-3. As can be seen, very abundant y_n-type fragment ions are observed in both spectra, which is expected for cleavages at amino acids adjacent to proline. The HE-CID spectrum allows the identification of the amino acid isoleucine[57] present at position 7 by showing a d_7 ion resulting from the loss of 14 amu from the corresponding a_7 ion. Charge-remote fragmentations that

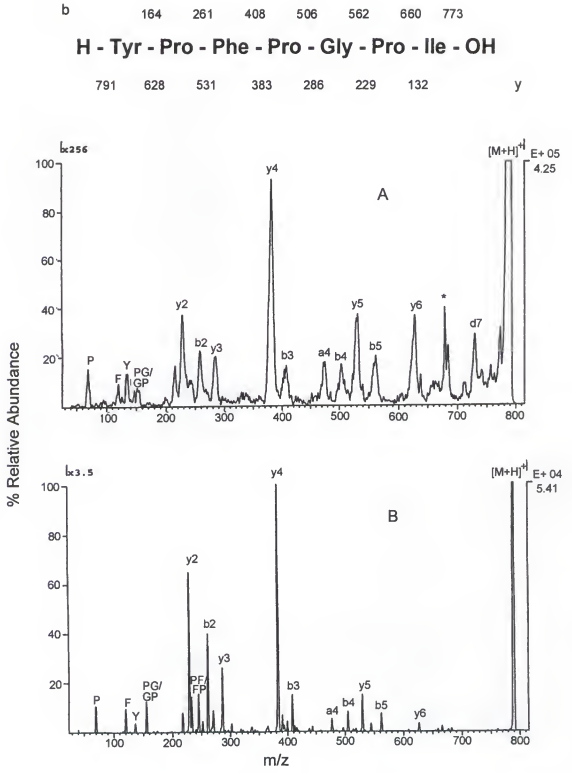

Figure 4-3. Product ion spectra of $(M+H)^+$ ions from bovine β-casomorphin (H-YPFPGPI-OH) (m/z 790). A. HE-CID (5keV) B. LE-CID (50eV).
* indicates product ion from isobaric matrix ion.

give origin to d-type ions are observed in HE-CID spectra of peptides.[173,174] High- and low-energy CID spectra of bovine β-casomorphin are remarkably similar; both exhibit fragmentation from both termini, sufficient to reveal the entire sequence. This behavior is expected for peptides lacking a strong basic terminal residue such as arginine, which can localize positive charges and direct the fragmentation on the peptide backbone.[75] Side chain fragmentations to give the d-type ions characteristic of isoleucine containing peptides were not observed in the low-energy spectrum, which agrees with previous reports suggesting high energy requirements for these cleavages.[175,176]

Tylosin

Tylosin is a macrolide antibiotic that consists of a 16-membered lactone aglycone ring with three sugars attached: mycarose, desosamine and mycinose. CID spectra from the $(M+H)^+$ ion of tylosin are shown in Figure 4-4. Note that the ions formed under these two collision energy regimes are similar. As can be seen from the scale factors in both spectra, the LE-CID process is more efficient, therefore, more intense low mass ions are observed in the LE-CID spectrum. In general, the principal decomposition products are derived from cleavages of the glycosidic bonds with charge retention on the amino sugar to form an ion at m/z 174 or from the loss of the terminal sugars to give the fragment Y_1; the bond cleavages are shown on the structure. The fragments observed are consistent with the decomposition of other macrolide antibiotics.[177] The B_2 ion (m/z 319), which contains the disaccharide moiety, is produced by charge retention on the

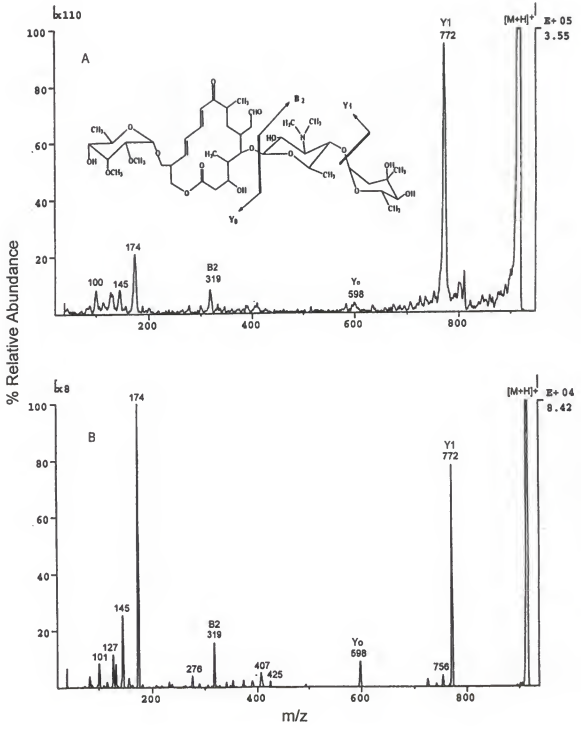

Figure 4-4. Product ion spectra of $(M+H)^+$ ions from Tylosin (m/z 916). A. HE-CID (5keV) B. LE-CID (50eV).

amino sugar. In low-energy CID, due to longer reaction times and multiple collision conditions, the B_2 fragment can in turn lose the sugar group, which contributes to the intense ion at m/z 174 observed in this spectrum (Figure 4-4 B). Lower mass peaks such as m/z 145 result from cleavages on the terminal sugar of the dissacharide portion. The loss of water from this peak is also observed in both spectra. The signal at m/z 407, more resolved in the LE- than in the HE-CID spectrum, seems to correspond to the aglycone ring after loss of the saccharide groups. Peaks due to successive loses of water from m/z 407 are also present in both spectra. A similar pattern has been observed in our laboratory by dissociation of protonated tylosin using infrared multiphoton dissociation (IRMPD) and CID in an ion trap mass spectrometer.[178] Low mass ions at m/z 145 are present in both HE- and LE- CID spectra and result from cleavages on the terminal sugar of the dissacharide. These ions are accompanied by ions corresponding to the loss of water and more sugar cleavages.

Erythromycin A

Erythromycin A is another macrolide antibiotic, consisting of two sugars, L-cladinose and D-desosamine, attached to a 14-membered lactone aglycone ring. $(M+Na)^+$ ions from erythromycin A (m/z 756) were formed in LSIMS by adding NaCl to the sample solution. $(M+Na)^+$ ions were used as precursor ions for high- and low-energy CID because $(M+H)^+$ ions were not observed in MALDI spectra and the main objective of these studies was to compare CID and PSD

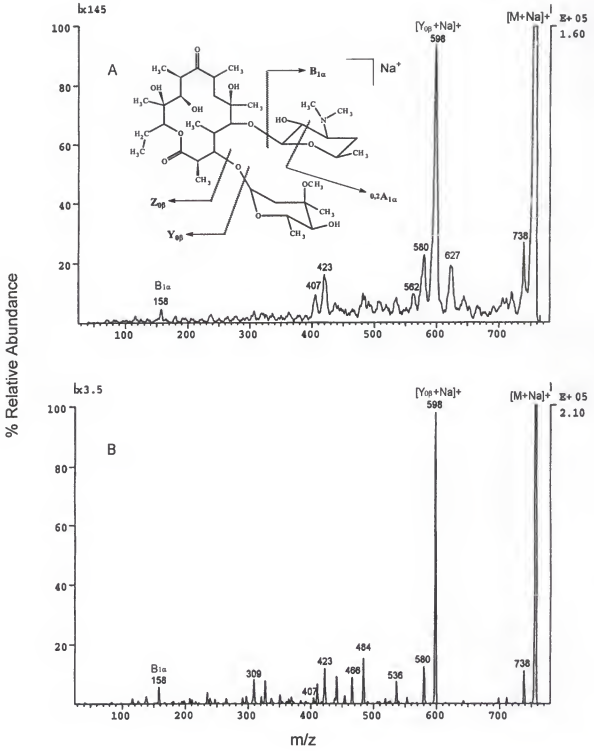

Figure 4-5. Product ion spectra of $(M+Na)^+$ ion from erythromycin A (m/z 756). A. HE-CID (5keV) B. LE-CID (50eV).

spectra. High- and low-energy CID spectra of erythromycin A are shown in Figure 4-5. It is evident that product ion spectra of $(M+Na)^+$ are very similar under low- and high-energy collisions. Apparently, Na^+ adducts with the aglycone ring and fragmentation seems to occur on the sugars. Loss of water from the $(M+Na)^+$ ion is observed; the major fragmentation pathway leads to a fragment at m/z 598 due to cleavage of the glycosidic bond of the amino sugar. Sequential losses of water are also observed in both spectra, but are more prominent in the high-energy spectrum. An ion at m/z 158 ($B_{1\alpha}$) for the (dehydro-amino sugar)$^+$ appears in both spectra. Ions at m/z 423, which are formed by at least two cleavages on both sugars, as well as at m/z 407 corresponding to the sodiated core aglycone, are also observed in both spectra. Cerny and coworkers[177] reported that cationization of erythromycin with other alkali metals shows similar ion abundances, which suggests metal-independent fragmentation. On these grounds, an ion at m/z 627 would be expected since it corresponds to the elimination of $C_7H_{15}NO$ (129 Da) from the amino sugar in similar way to the ions observed in the potasiated compound. As can be seen in Figure 4-5, such loss is only observed in the HE-CID spectrum, which indicates a highly energetic process is required to form this ion.

MALDI Post-Source Decay

Des-arg^9 bradykinin (H-RPPGFSPF-OH)

PSD spectra of $(M+H)^+$ ions of des-arg^9 bradykinin are shown in Figure 4-6. In general, the dissociation products are the same in all matrices used here.

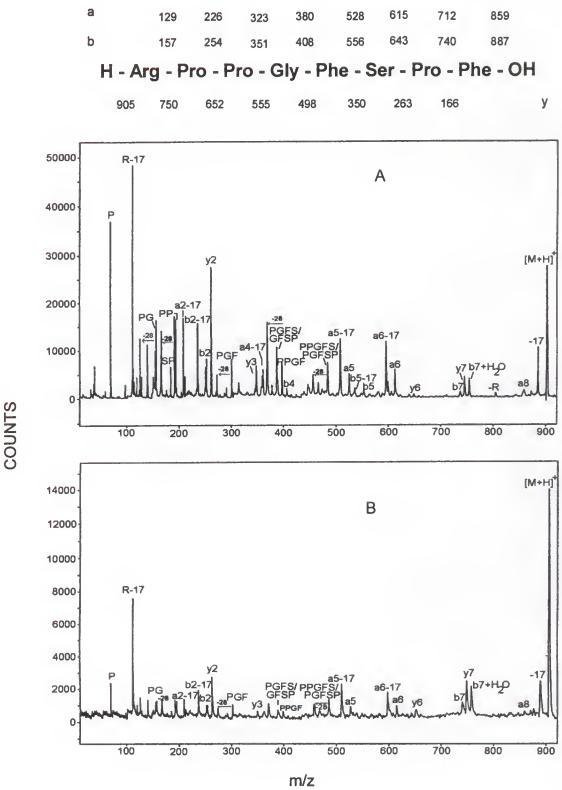

Figure 4-6 MALDI-PSD spectra of $(M+H)^+$ ions of des-arg^9 bradykinin (H-RPPGFSPF-OH) (m/z 904) with A. α-CHCA, B. DHB, C. IAA, D. s-DHB.

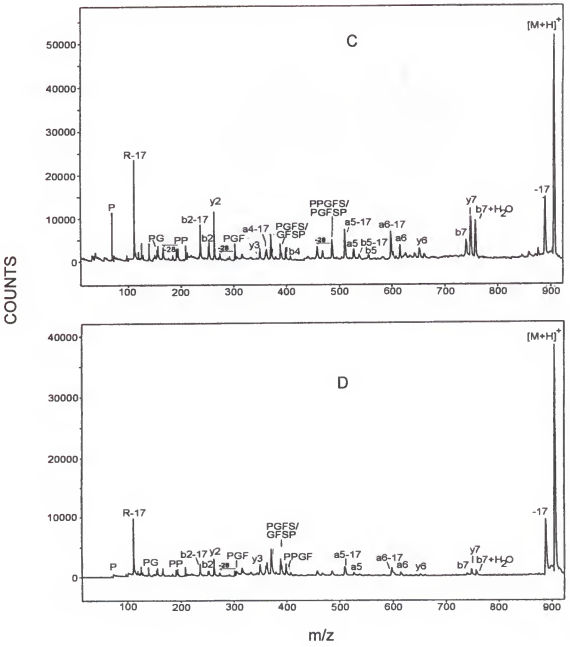

Figure 4-6 continued.

As can be seen, there are very abundant ions produced by internal bond cleavages and internal fragments – 28 Da, which are very useful in obtaining sequence information. Note that most of the internal fragments contain proline as the first amino acid, which is expected for peptides with proline at neither the N- nor the C-terminus.[169] A number of fragment ions from individual amino acid residues are identified as P (Pro), F (Phe) and R-17 from the arginine residue. Very abundant a_n, b_n, b_n-17 and almost a complete series of a_n-17 are also observed. These signals at 17 Da lower than the corresponding a- and b-type ions are believed to be due to the loss of ammonia from N-terminal arginine.[168] Precursor ions in PSD were selected with a resolution of 60. The possibility of a fraction of precursor ions is already deaminated cannot be excluded although these fragments are not observed in prompt fragmentation experiments. It has been assumed that the formation of a_n-17 and b_n-17 is a secondary process, which due to a relatively low rate constant, requires longer times to reach the yield obtained in PSD.[179] The fragment ions and their distributions are remarkably similar in LE-CID and MALDI-PSD, which indicate that similar internal energies are sampled by these two techniques.

Comparing the spectra taken in different matrices, the most striking difference is observed when α-CHCA is used (Figure 4-6 A). As can be seen, there is a remarkable increase in fragmentation when this matrix is used for des-arg^9 bradykinin. The spectrum obtained in α-CHCA is in excellent agreement with MALDI-PSD spectra reported in previous studies[162,165] for this compound.

Bovine β-Casomorphin (H-YPFPGPI-OH)

The spectra shown in Figure 4-7 allow comparison of PSD of the $(M+H)^+$ ion of bovine β-casomorphin using α-CHCA, DHB, IAA and s-DHB as matrices. There are not major differences in these spectra. All spectra have similar distributions of nearly complete series of y_n and b_n ions accompanied by some internal fragments. Immonium ions, characteristic of the amino acids present in the peptide, are also observed in the low mass region and are identified as P, F and Y (proline, phenylalanine and tyrosine, respectively). Note that a very intense y_4 ion dominates all spectra. In general, abundant y-type ions are observed as a result of cleavages adjacent to proline residues.[172] PSD and LE-CID spectra show very similar fragmentation pattern. It is evident that as in LE-CID (Figure 4-3) there are no ions indicating the presence of isoleucine in the PSD spectra; this suggests that PSD is not a very energetic process. Comparing the MALDI-PSD spectra taken in the four matrices, the mass spectrum obtained with s-DHB has the worst signal-to-noise ratio of all PSD spectra. It is important to mention that the normal MALDI spectrum taken in s-DHB had also the lowest relative intensity for $(M+H)^+$ ions of bovine β-casomorphin, compared to the spectra taken in the other three matrices. This means that the quality of the MALDI-PSD spectrum obtained with s-DHB as the matrix was affected by the few ions formed during the ionization process.

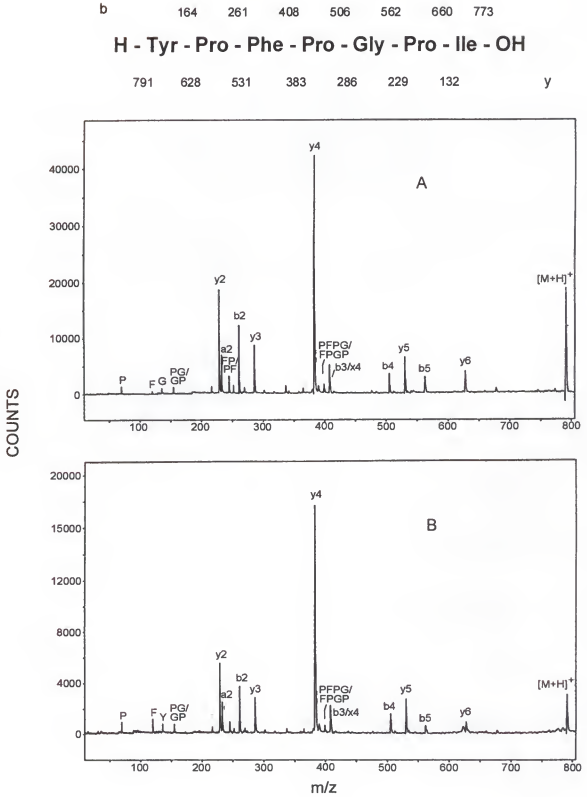

Figure 4-7. MALDI-PSD spectra of $(M+H)^+$ ions of bovine β-casomorphin (H-YPFPGPI-OH) (m/z 790) with A. α-CHCA, B. DHB, C. IAA, D. s-DHB.

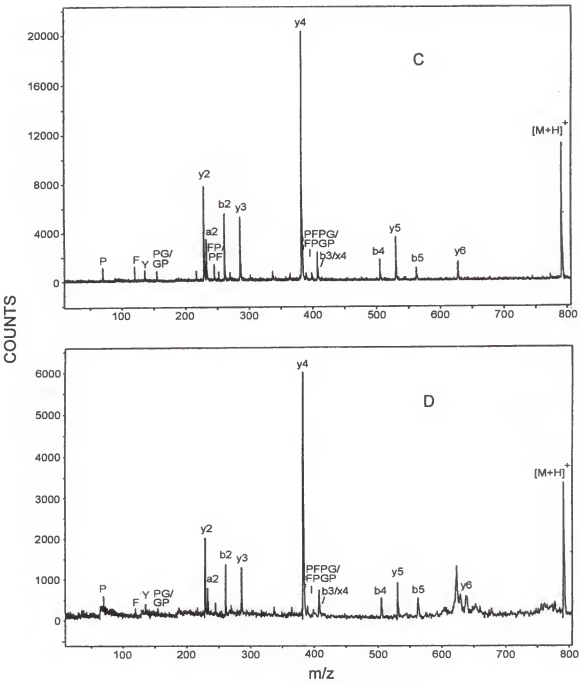

Figure 4-7. Continued.

Tylosin

PSD spectra of $(M+H)^+$ ions from tylosin in all matrices used in these analyses are shown in Figure 4-8. As can be seen, all spectra have the same ions and the fragmentation process seems very efficient (even more efficient than LE-CID) as indicated by the high intensity of the product ions with respect to the remaining precursor ion. The PSD spectra are characterized, as were the low- and high-energy CID spectra (Figure 4-4), by losses of the terminal sugar from the disaccharide moiety to give a fragment at m/z 772. Cleavage of the glycosidic linkage close to the aglycone ring produces an ion at m/z 598. A signal at m/z 309 is observed in all spectra and is produced by cleavage of the disaccharide from the aglycone ring with charge retention on desosamine. PSD of the $(M+H)^+$ ion of tylosin is dominated by an ion at m/z 174 which corresponds to the amino sugar and is formed by cleavage of two glycosidic bonds. Loss of water from this ion produces a signal at m/z 156. An intense signal at m/z 145 is observed in the PSD spectra, which has also been observed in chemical ionization spectra of tylosin and has been identified as coming from the terminal sugar on the disaccharide moiety of tylosin. Note that the peaks at m/z 407 due to the aglycone ring and the ions resulting from subsequent loses of water observed in the low-energy CID spectra (Figure 4-4) are less intense in MALDI-PSD.

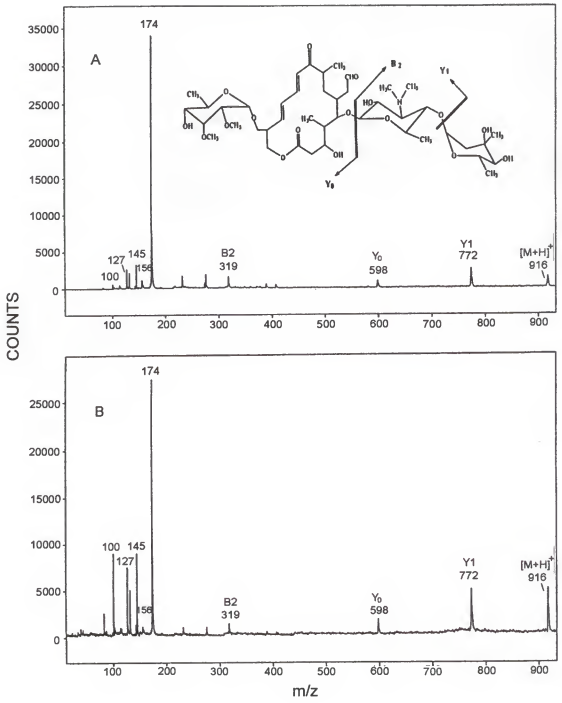

Figure 4-8. MALDI-PSD spectra of $(M+H)^+$ ions of tylosin (m/z 916) with A. α-CHCA, B. DHB, C. IAA, D. s-DHB.

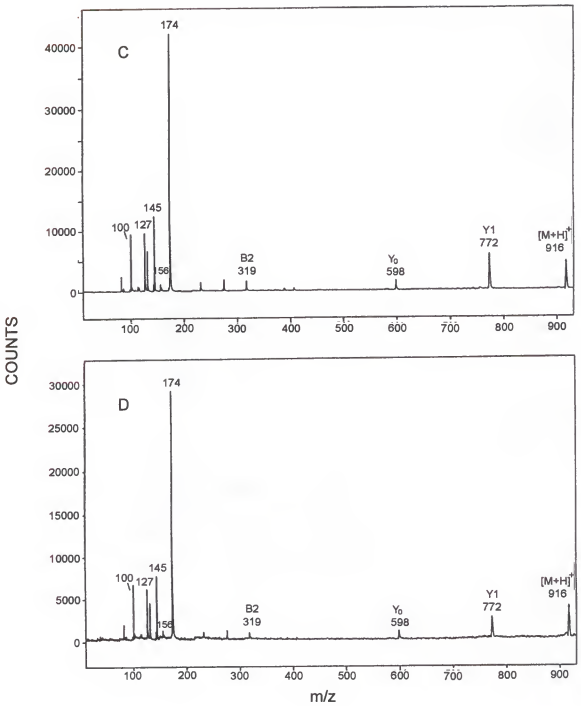

Figure 4-8. Continued.

Erythromycin A

$(M+H)^+$ ions of erythromycin A (m/z 734) were not present in the linear and reflectron MALDI spectra; instead, two peaks at m/z 756 and m/z 738 were observed. These ions were identified as the sodium adduct of erythromycin A and the corresponding loss of water from the sodiated species, respectively. Using DHB as matrix, Allison and coworkers[159] found that DHB tends to generate sodiated molecules of hexatyrosine even when no NaCl is added; they also showed that NaCl impurities in the matrix were responsible for this behavior. On the other hand, degradation of erythromycin A in aqueous solution has been described in the literature and it has been shown to destroy the antibiotic activity;[180] it has been demonstrated by ESI that the major reaction product in both acidic and basic solutions of erythromycin A is anhydroerythromycin A formed via an equilibrium of erythromycin and erythromycin enol ether coupled to a direct conversion from erythromycin to dehydroerythromycin.[181,182]

Because no protonated erythromycin A ions were produced by MALDI for PSD analysis, the sodiated adduct was selected instead. Figure 4-9 shows PSD spectra of $(M+Na)^+$ ions from erythromycin A taken in different matrices. It can be seen in these spectra that the major fragmentation pathway involves the loss of water from the precursor ion. Recall that precursor ion resolution in PSD is 60 and the possibility that a fraction of the precursor ions were dehydrated cannot be ruled out, especially because $(M+Na-H_2O)^+$ is observed in the normal MALDI spectrum. Ions are also produced by the cleavage of the glycosidic bond on the

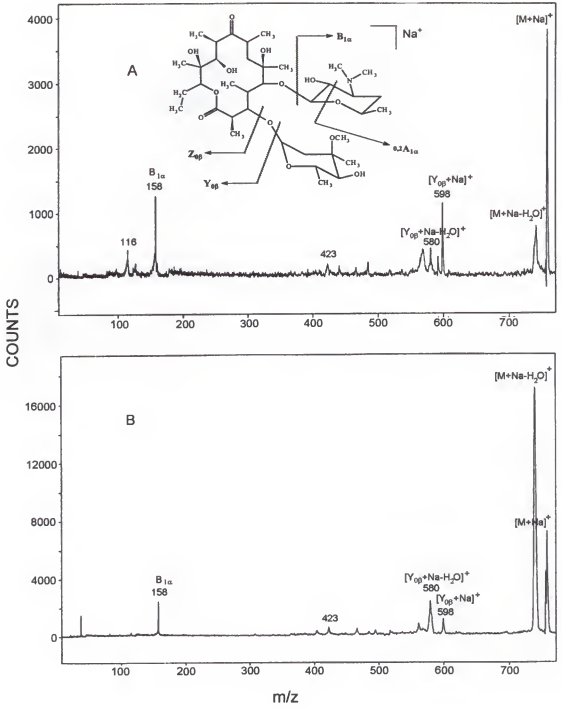

Figure 4-9. MALDI-PSD spectra of $(M+Na)^+$ ions of erythromycin A (m/z 756) with A. α-CHCA, B. DHB, C. IAA, D. s-DHB.

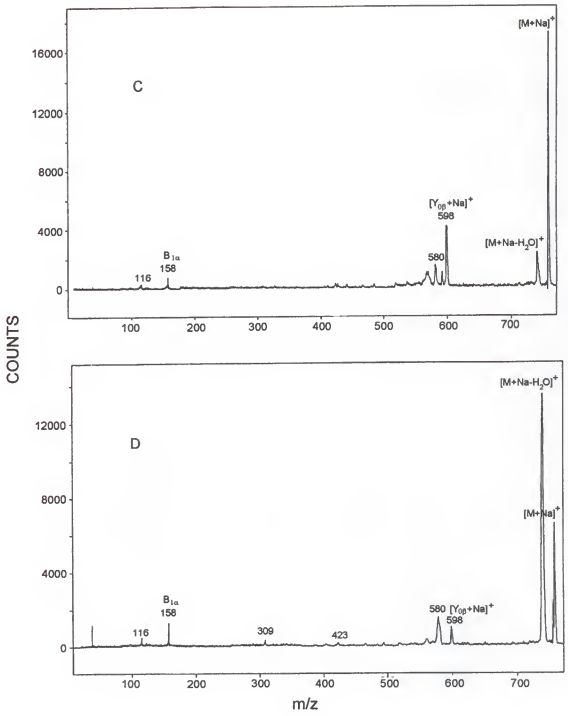

Figure 4-9. Continued.

non-amino sugar to produce a peak at m/z 598 (which was the major product ion in HE- and LE-CID (Figure 4-5)). Subsequent loss of water from this ion is also observed in the spectra at m/z 580. All spectra show a peak at m/z 158, which corresponds to the amino sugar moiety. Ring cleavage and loss of C_2H_2O from this amino sugar group produces an ion at m/z 116, which is present in the spectra. It is evident from these spectra that more intense ions corresponding to the loss of water from the sodiated species are obtained with DHB and s-DHB than with α-CHCA and IAA. The same is noticed for the loss of water from the $[Y_{0\beta}+ Na]^+$ ion, whose ion is more abundant in the "cooler" matrices DHB and s-DHB. In contrast to the other compounds studied, PSD spectrum of erythromycin taken in α-CHCA showed the poorest signal-to-noise ratio and the lowest intensity. It is important to mentioned that α-CHCA produced a low intensity MALDI spectrum, which resulted in few ions available for PSD and therefore a poor signal-to-noise ratio in PSD with this matrix is observed.

Effect of MALDI Matrix on PSD

For the protonated compounds studied we did not observe any effect other than enhancement of the intensity of product ions. For the sodiated compound, losses of water were significantly enhanced with DHB and s-DHB. In order to estimate the amount of fragmentation produced by PSD, the efficiency of the PDS process was calculated. In similar way to the calculations in the previous chapter, the fragmentation efficiency is given by the ratio of the intensities of the fragment ions to the intensities of all ions observed (precursor

plus fragment ions). Figure 4-10 summarizes the MALDI-PSD results. As indicated in the bar graph, the MALDI-PSD spectra taken with the four matrices show a large variation in the degree of ion activation. α-CHCA produces the most fragmentation for des-arg^9 bradykinin, which agrees with previous observations on other arginine-containing peptides.[183] If the proton transfer mechanism operates, the presence of a basic amino acid in the peptide seems to favor the proton transfer from matrix to analyte and therefore fragmentation is induced on the peptide backbone. α-CHCA is a high-energy transfer matrix that could be used to promote prompt fragmentation or metastable decay. In contrast, s-DHB shows the least fragmentation efficiency for des-arg^9 bradykinin. The observed suppression of fragmentation with s-DHB has been seen before and has been attributed to a greater disorder in the DHB lattice from the presence of the 5-methoxysalicylic acid, resulting in reduced internal energy and reduced metastable fragmentation.[184] IAA and DHB have similar fragmentation efficiencies although they have different proton affinities. Tylosin follows a similar trend even though the differences in the spectra are not as striking as in des-arg9 bradykinin. If proton transfer is the most important mechanism in ionization by MALDI and inducing PSD fragmentation, matrices with low proton affinities will be "hot", meaning more post-source decay is induced. The lower proton affinity of α-CHCA (PA, 183 kcal/mol)[185] in contrast to DHB (PA, 204 kcal/mol) indicates that α-CHCA will produce more fragmentation than DHB and that seems to be the case of des-arg^9 bradykinin and tylosin, but it does not

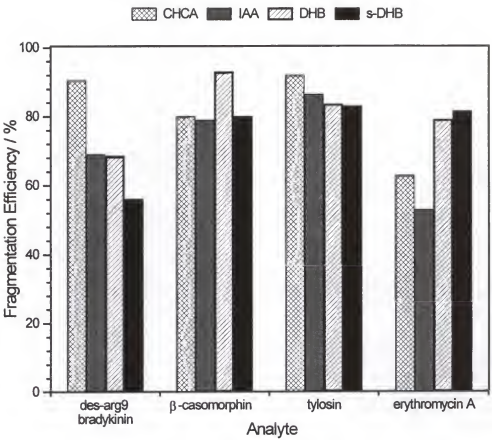

Figure 4-10. Dependence of PSD fragmentation on matrix composition.

apply to erythromycin A and bovine β-casomorphin, which somehow show a totally different behavior. As can be seen in the graph, the proton affinity of the matrix in PSD seems to have less effect than proton affinities of reagent gases in chemical ionization. Complications involve the MALDI matrix affecting crystalization and isolation of sample ions, effect on protonation (and perhaps adduction), and collisions with matrix molecules in the gas plume. UV absorption of matrix and analyte, as well as reactions with photofragments might also affect the PSD fragmentation. Further studies are needed to address these issues.

Conclusion

The results have shown that although dissociation efficiency is strongly analyte and matrix dependent, CID and PSD produced extensive structural information. There are differences in the fragmentation channels obtained under high- and low-energy CID. Internal fragments were prominent in low-energy CID and in PSD. Charge-remote fragmentation processes, important for the identification of isomeric amino acid residues leucine and isoleucine, were observed only in HE-CID spectra. Abundant a_n-17, b_n-17, and internal fragments-28 were obtained in low-energy CID and in PSD spectra. These fragments, produced by cleavages of at least two bonds, are favored by the longer reaction times obtained in these two types of processes and instruments. Fragmentation obtained in MALDI-PSD seems to correlate with LE-CID fragmentation patterns for the compounds studied.

The effect of the matrix on MALDI-PSD fragmentation is a complicated issue. Although proton affinity differences between matrices and analyte should have an effect on the amount of internal energy deposited in the precursor $(M+H)^+$ ions the effect is not always observed. Correlation between the proton affinity of the matrix and the PSD fragmentation is shown for des-arg^9 bradykinin and tylosin; however, this is not so apparent for bovine β-casomorphin. It seems that the presence of basic groups in the analyte favors proton transfer from matrix to analyte and therefore higher internal energies deposited in the precursor ion result in enhancing of PSD fragmentation. The PSD fragmentation of $(M+Na)^+$ ions of erythromycin A is not dependent on proton affinity of the matrix, since these are not protonated species.

CHAPTER 5
CONCLUSIONS AND FUTURE WORK

These studies emphasize the importance of understanding the influence of the different experimental parameters on MS/MS spectra. Several ionization techniques were compared in order to produce ions with different amounts of internal energy and to determine the role of precollisional internal energy in the appearance of MS/MS spectra. Metastable ions, high- and low-energy CID, as well as post-source decay experiments were performed to address the effect of internal energy.

Several ionization techniques and MS/MS instruments were used for the experiments described in Chapter 2. It was shown that internal energy can be added as thermal energy into the molecules during the fast heating process in DCI and that it can affect tandem mass spectra. Thus, the decomposition of $(M+H)^+$ from leucine enkephalin formed by DCI produced an intense A_4 ion resulting from the loss of CO from the corresponding B_4 ion. The results suggested that the intensity of A_4 might be enhanced as a result of thermal decomposition. A similar observation was made in the DCI spectra of isovalerylcarnitine in which an ion at m/z 232 appears as a result of pyrolysis. For these two compounds, the ions generated by LSIMS seemed to be "cooler"

than the ions generated by DCI, as indicated by the fewer ions in the MS/MS spectra of the ions generated by LSIMS. The possibility of having different structures formed by different ionization techniques was also addressed.

It would be interesting to perform MS/MS experiments on ions generated by atmospheric pressure chemical ionization (APCI) using different reagent gases to see if that might change the internal energy of the ions and also to see if the ions formed in APCI are the same as those formed by DCI. This would also offer the opportunity to explore the difference between gas-phase and condensed-phase ion chemistry if ESI, LSIMS, APCI and CI are compared. The ideal experiment would include the comparison of MS/MS spectra of ions generated by several ionization techniques in a single instrument so that instrumental discriminations are the same for all compounds.

The ions studied in Chapter 3 were formed by chemical ionization with different reagent gases since the internal energy of the ions formed in CI depends on the exothermicity of the proton transfer reaction between the conjugate base of the reagent gas and the analyte, which in turn is controlled by the proton affinity of the gas. The results showed a clear correlation between the energy deposited by the ionization technique and the fragmentation efficiency of the compounds studied. In general, ions generated by methane chemical ionization showed higher fragmentation efficiencies than ions generated by isobutane CI and by ammonia CI. It has been claimed (and disputed) that if ions formed by low activation energy pathways are ignored, the relative abundances of fragment ions in CID are unaffected by precollisional internal energy. It is

shown here that relative abundances are affected by internal energy deposited during ionization. Comparison of high- and low-energy CID showed that LE-CID spectra are more sensitive to internal energy changes and that precollisional internal energy differences are less important at high collision gas pressures in LE-CID. Internal energy differences arising from the ionization process were also observed under high-energy CID for the compounds studied. In HE-CID, ion ratios are shown to be at least two times higher for ions produced by methane or isobutane CI than for those produced by ammonia CI. In LE-CID these ratios can vary by up to a factor of 10 as the reagent gas is changed. Although the compounds used in these studies were rather small (< 100 Da), which might have helped to actually see an effect of precollisional internal energy on CID, the results are encouraging. Future work should involve the study of bigger molecules, isomers, and compounds with other functional groups in order to understand the details of the fragmentation process and to be able to compare different collision energy regimes.

In Chapter 4, post-source decay spectra observed in a reflectron TOF mass spectrometer were compared to high- and low- energy CID. PSD spectra showed to be similar to low-energy CID. Fragmentation efficiency of PSD is compound-dependent, but was approximately 70% for the compounds studied. PSD spectra did not display ions resulting from charge-remote fragmentation processes; the inability to access such pathways is expected for low-energy processes. PSD fragmentation was also evaluated as a function of the matrix used. MALDI PSD is much less affected by changing the matrix than is LSIMS

or CI. It was found that for the protonated ions of des-arg^9 bradykinin and tylosin, PSD increased when α-CHCA was used as matrix and was suppressed in the presence of s-DHB. In the case of bovine β-casomorphin, a peptide with no basic sites, there was not a clear correlation between proton affinity of the matrix and PSD. As for the sodiated species of erythromycin A, the internal energy is not expected to be dependent on proton affinity of the matrix, since there are no protonated species from the analyte. The degree of PSD was increased by the presence of s-DHB and DHB and was suppressed in α-CHCA and IAA. Although the proton affinity of s-DHB is unknown, it is presumably much higher than IAA and DHB, and higher, of course, than α-CHCA. If the ionization process in MALDI is directed by a protonation step, the exothermicity of that step will determine the degree of excitation of the precursor ions. Thus, molecules with strong basic sites, such as some of the compounds used here, will react with low-proton affinity matrices in a much stronger way, therefore facilitating the PSD process. It will be important to extend these studies to a series of antibiotics with and without amino sugar groups as well as to investigate the effect of cationization vs. protonation to determine if changing the matrix induces or reduces PSD. Future studies should also involve the use of a systematic group of peptides in which changes in PSD fragmentation with a particular matrix could be correlated to amino acid composition. In the experiments involving sodiated erythromycin A, it was observed that DHB and s-DHB produced a very intense peak corresponding to the loss of water. Studies

including the use of liquid matrices at different pH values should be important in determining the dehydration degree as a function of pH and matrix composition in general.

LIST OF REFERENCES

1. Barber, M; Bordoli, R. S.; Sedgwick, R. D.; Tyler, A. N. *J. Chem Soc. Chem. Commun.* **1981**, 325-327.

2. Aberth, W.; Straub, K. M.; Burlingame. A. L. *Anal. Chem.* **1982**, 54, 2029-2034.

3. Tanaka, K.; Waki, H.; Ido, Y.; Akita, S.; Yoshida, Y.; Yoshida, T. *Rapid Commun. Mass Spectrom.* **1988**, 2, 151-153.

4. Karas, M.; Hillenkamp, F. *Anal. Chem.* **1988**, 60, 2299-2301.

5. Fenn, J. B.; Mann, M.; Meng, C. K.; Wong, S. F.; Whitehouse, C. M. *Mass Spectrom. Rev.* **1990**, 9, 37-70.

6. Munson, M. S. B.; Field, F. H. *J. Am. Chem. Soc.* **1966**, 88, 2621-2630.

7. Bush, K. L.; Glish, G. L.; McLuckey, S. A. *Mass Spectrometry/Mass Spectrometry*. VCH Publishers, New York, **1988**.

8. Jennings, K. R. *Int. J. Mass Spectrom. Ion Phys.* **1968**, 1, 227-235.

9. Haddon, W. F.; McLafferty, F. W. *J. Am. Chem. Soc.* **1968**, 90, 4745-4746.

10. McLafferty, F. W.; Bente, P. F.; Kornfeld, R; Tsai, S. C.; Howe, I. *J. Am. Chem. Soc.* **1973**, 95, 2120-2129.

11. Porter, C. J.; Morgan, R. P; Beynon, J. H. *Int. J. Mass Spectrom. Ion Phys.* **1978**, 28, 321-333.

12. McLafferty, F. W.; Hirota, A; Barbalas, M. P.; Pegues, R. F. *Int. J. Mass Spectrom. Ion Phys.* **1980**, 35, 299-303.

13. Porter, C. J.; Proctor, C. J; Beynon, J. H. *Org. Mass Spectrom.* **1981**, 16, 62-67.

14. Van Koppen, P. A. M.; Illies, A. J.; Liu, S.; Bowers, M. T. *Org. Mass Spectrom.* **1982**, 17, 399-402.

15. Jarrold, M. F.; Illies, A. J.; Kirchner, N. J.; Bowers, M. T. *Org. Mass Spectrom.* **1983**, 18, 388-395.

16. Jackson, A. T.; Jennings, K. R.; Scrivens, J. H. *Rapid Commun. Mass Spectrom.* **1996**, 10, 1459-1462.

17. McLafferty, F. W. Ed. *Tandem Mass Spectrometry*, Wiley, New York, **1983**.

18. De Hoffmann, E. *J. Mass Spectrom.* **1996**, 31, 129-137.

19. McLafferty, F. W. *Org. Mass Spectrom.* **1993**, 28, 1403-1406.

20. Yost, R. A.; Boyd, R. K. in *Methods in Enzymology* vol 193, McCloskey, J. A. Ed, Academic Press, San Diego, **1990,** 154-200.

21. Johnson, J. V.; Yost, R. A. *Anal. Chem.* **1985**, 57, 758A-768A.

22. Yost, R. A.; Fetterolf, D. D. *Mass Spectrom. Rev.* **1983**, 2, 1-45.

23. Rosenstock, H. M.; Wallenstein, M. B.; Wahrhaftig, A. L.; Eyring, H. *Proc. Acad. Sci., USA* **1952**, 38, 667-678.

24. Forst, W. *Theory of Unimolecular Reactions*, Academic Press, New York, **1973**.

25. Robinson P. J.; Holbrook, K. A. *Unimolecular Reactions*, Wiley, London, **1972**.

26. Beynon, J. H.; Gilbert, J. R. *Applications of Transition State Theory to Unimolecular Reaction: An Introduction*, Wiley, New York, **1984**.

27. Vekey, K. *J. Mass Spectrom.* **1996**, 31, 445-463.

28. Vekey, K. in *Selected Topics in Mass Spectrometry in the Biomolecular Sciences*, Caprioli, R. M.; Malorni, A.; Sindona, G. Eds. NATO ASI Series vol 504, Kluwer Academic Publishers, Dordrecht, **1997**. 129-142.

29. Baer, T. in *Mass Spectrometry* vol 6, The Royal Society of Chemistry Burlington House, London, **1981**.

30. Cooks, R. G.; Beynon, J. H.; Caprioli, R. M.; Lester, G. R. *Metastable Ions.* Elsevier, New York, **1973**.

31. McLafferty, F. W.; Fairweather, R.B. *J. Am. Chem. Soc.* **1968**, 90, 5915-5917.

32. Cooks, R. G., Terwilliger, D. T.; Ast, T.; Beynon, J. H.; Keough, T. *J. Am. Chem. Soc.* **1975**, 97, 1583-1585.

33. DeKrey, M. J.; Mabud, Md. A.; Cooks, R. G., Syka, J. E. P. *Int. J. Mass Spectrom. Ion Proc.* **1985**,67, 295-303.

34. Dunbar, R. C. in *Gas Phase Ion Chemistry*, vol 2. M. T. Bowers, Ed. Academic Press, New York, **1979**.

35. Dunbar, R. C. in *Gas Phase Ion Chemistry*, vol 3. M. T. Bowers, Ed. Academic Press, New York, **1984**.

36. Freiser, B. S. *Int. J. Mass Spectrom. Ion Phys.*, **1978**, 26, 39-47.

37. Cody, R. B.; Freiser, B. S. *Anal. Chem.* **1979**, 51, 547-551.

38. Vekey,K.; Brenton, A. G.; Beynon, J. H. *Int. J. Mass Spectrom. Ion Proc.* **1986**, 70, 277-300.

39. Curtis, J. M.; Vekey,K.; Brenton, A. G.; Beynon, J. H. *Org. Mass Spectrom.* **1987**, 22, 289-294.

40. Vekey, K.; Brenton, A. G.; Beynon, J. H. *J. Phys. Chem.* **1986**, 90, 3569-3577.

41. Vekey, K.; Brenton, A. G.; Beynon, J. H. *Org. Mass Spectrom.* **1988**, 23, 31-36.

42. Hayes, R. N.; Gross, M. L. in *Methods in Enzymology* vol 193, McCloskey, J. A. Ed. Academic Press, San Diego, **1990**.

43. Cotter, R. J. *Mass Spectrom. Rev.* **1989**, 8, 445-483.

44. Hasted, J. B. *Physics of Atomic Collisions*, 2nd. ed. American Elsevier, New York, **1972**.

45. Cooks, R. G. Ed. *Collision Spectroscopy*, Plenum, New York, **1978**.

46. Levsen, K.; Schwarz, H. *Mass Spectrom. Rev.* **1983**, 2, 77-148.

47. Bordas-Nagy, J; Jennings, K. R. *Int. J. Mass Spectrom. Ion Proc.* **1990**, 100, 105-131.

48. McLuckey, S. A. *J. Am. Soc. Mass Spectrom.* **1992**, 3, 599-614.

49. Shukla, A. K.; Futrell, J. H. *Mass Spectrom. Rev.* **1993**, 12, 211-255.

50. Gross, M. L.; Tomer, K. B., Cerny, R. L.; Giblin, D. E. in *Mass Spectrometry in the Analysis of Large Molecules.* McNeal, C. J. Ed., Wiley, New York, **1986**.

51. Bordas-Nagy, J; Despeyroux, D.; Jennings, K. R. *J. Am. Soc. Mass Spectrom.* **1992**, 3, 502-514.

52. Ast, T.; Beynon, J. H.; Cooks, G. R. *J. Am. Chem. Soc.* **1972**, 94, 6611-6621.

53. Todd, P. J.; McLafferty, F. W. *Int. J. Mass Spectrom. Ion Phys.* **1981**, 38, 371-378.

54. Kim, M. S.; McLafferty, F. W. *J. Am. Chem. Soc.* **1978**, 100, 3279-3282.

55. Gross, M. L. *Int. J. Mass Spectrom. Ion Proc.* **1992**, 118/119 137-165.

56. Laramee, J. A.; Cooks, R. G. *J. Am. Chem. Soc.* **1981**, 103, 12-17.

57. Papayannopoulos, I. A. *Mass Spectrom. Rev.* **1995**, 14, 49-73.

58. Glish, G. ; McLuckey, S. A.; Ridley, T. Y.; Cooks, R. G. *Int. J. Mass Spectrom. Ion Phys.* **1982**, 41, 157-177.

59. Douglas, D. J. *J. Phys. Chem.* **1982**, 86, 185-191.

60. Harrison, A. G.; Lin, M. S. *Int. J. Mass Spectrom. Ion Phys.* **1983**, 51, 353-356.

61. Singh, S.; Harris, F. M.; Boyd, R. K.; Beynon, J. H. *Int. J. Mass Spectrom. Ion Proc.* **1985**, 66, 151-166.

62. Nacson, S.; Harrison A. G.; *Int. J. Mass Spectrom. Ion Proc*esses, **1985**, 63, 325.

63. McLuckey, S. A.; Ouwerkerk, C. E. D.; Boerboom, A. J. H.; Kistemaker, P. G. *Int. J. Mass Spectrom. Ion Proc.* **1984**, 59,85-101.

64. Wysocki, V.; Kenttamaa, H. I.; Cooks, R. G. *Int. J. Mass Spectrom. Ion Proc.* **1987**, 75, 181-208.

65. Shukla, A. K.; Qian, K; Howard, S. C.; Anderson, S, G.; Sohlberg, K. W.; Futrell, J. H. *Int. J. Mass Spectrom. Ion Proc.* **1989**, 92,147-169.

66. Qian, K.; Shukla, A. K.; Futrell, J. H. *J. Am. Chem. Soc.* **1991**, 113, 7121-7129.

67. Martinez, R. I.; Ganguli, B. *J. Am. Soc. Mass Spectrom.* **1992**, 3, 427-444.

68. Yost, R. A.; Enke, C. G.; McGilvery, D. C.; Smith, D.; Morrison, J. D. *Int. J. Mass Spectrom. Ion Phys.* **1979**, 30, 127-136.

69. Nystrom, J. A.; Bursey,M. M.; Hass, J. R.; *Int. J. Mass Spectrom. Ion Proc.* **1983/1984**, 55, 263-274.

70. Alexander, A. J.; Boyd, R.K *Int. J. Mass Spectrom. Ion Proc.* **1989**, 90, 211-240.

71. Charles, M. J.; Marbury, G. D. *Anal. Chem.* **1991**, 63, 713-721.

72. Gaskell, S. J.; Reilly, M. H. *Rapid Commun. Mass Spectrom.* **1988**, 2, 139-142.

73. Poulter, L.; Taylor, L. C. E. *Int. J. Mass Spectrom. Ion Proc.* **1989**, 91, 183-197.

74. Alexander, A. J.; Thibault, P; Boyd, R. K. Curtis, J. M.; Rinehart, K. L. *Int. J. Mass Spectrom. Ion Proc.* **1990**, 98, 107-134.

75. Bean, M. F; Carr, S. A.; Thorne, G. C.; Reilly, M. H.; Gaskell, S. J. *Anal. Chem.* **1991**, 63, 1473-1481.

76. Claeys, M.; Van den Heuvel, H.; Chen, S.; Derrick, P. J.; Mellon, F. A.; Price, K. R. *J. Am. Soc. Mass Spectrom.* **1996**, 7, 173-181.

77. Nizigiyimana, L.; Van den Heuvel, H; Claeys, M. *J. Mass Spectrom.* **1997**, 32, 277-286.

78. Rafferty, T. L.; Gallagher, R. T.; Derrick, P. J.; Heck, A. J. R. Duncan, A.; Robins, S. P. *Int. J. Mass Spectrom. Ion Proc.* **1997**, 160, 377-386.

79. Bruins, A. P.; Jennings, K. R.; Evans, S. *Int. J. Mass Spectrom. Ion Phys.* **1978**, 26, 395-404.

80. Morgan, R. P.; Beynon, J. H.; Bateman, R. H.; Green, N. B. *Int. J. Mass Spectrom. Ion Phys.* **1978**, 28, 171-191.

81. McLafferty, F. W.; Todd, P. J.; McGilvery, D. C.; Baldwin, A. *J. Am. Chem. Soc.* **1980**, 102, 3360-3363.

82. Hass, J. R.; Green, B. N.; Bott, P. A.; Bateman, R. H. In *Proceedings of the 32nd ASMS Conference on Mass Spectrometry and Allied Topics*, San Antonio, TX **1984**, 380.

83. Proctor, C. J.; Kralj, B; Brenton, A. G.; Beynon, J. H. *Org. Mass Spectrom.* **1980**, 15, 619-631.

84. Yost, R. A.; Enke, C. G. *J. Am. Chem. Soc.* **1978**, 100, 2274-2275.

85. Schoen, A. E.; Amy, J. W.; Ciupek, J. D.; Cooks, R. G.; Dobberstein, P.; Jung, G. *Int. J. Mass Spectrom. Ion Proc.* **1985**, 65, 125-140.

86. McLuckey, S. A.; Glish, G. L; Cooks, R. G. *Int. J. Mass Spectrom Ion Phys.* **1981**, 39, 219-230.

87. Glish, G. L.; McLuckey, S. A.; Ridley, T. Y.; Cooks, R. G. *Int. J. Mass Spectrom. Ion Phys.* **1982**, 41, 157-177.

88. Ciupek, J. D.; Amy, J. W.; Cooks, R. G.; Schoen, A. E. *Int. J. Mass Spectrom. Ion Proc.* **1985**, 65, 141-157.

89. March, R. E; Hughes, R. J. *Quadrupole Storage Mass Spectrometry*. Wiley, New York, **1989**.

90. March, R. E.; Todd, J. F. J. Eds. *Practical Aspects of Ion Trap Mass Spectrometry* vol 1-3, CRC Press, Boca Raton, FL **1995**.

91. Easterling, M. L.; Amster, I. J. in *Selected Topics in Mass Spectrometry in the Biomolecular Sciences*. Caprioli, R. M.; Malorni, A.; Sindona, G. Eds. NATO ASI Series vol 504, Kluwer Academic Publishers, Dordrecht, **1997**, 287-314.

92. Kofel, P.; Schlunegger, U. P. in *Selected Topics in Mass Spectrometry in the Biomolecular Sciences*. Caprioli, R. M.; Malorni, A.; Sindona, G. Eds. NATO ASI Series vol 504, Kluwer Academic Publishers, Dordrecht, **1997**, 263-286.

93. Nemirovskiy, O. V.; Gooden, I. K.; Ramanathan, R.; Gross, M. L. in *Selected Topics in Mass Spectrometry in the Biomolecular Sciences*. Caprioli, R. M.; Malorni, A.; Sindona, G. Eds. NATO ASI Series vol 504, Kluwer Academic Publishers, Dordrecht, **1997,** 183-211.

94. Morris, H. R.; Paxton, T; Dell, A; Langhorne; J; Berg, M.; Bordoli, R. S.; Hoyes, J.; Bateman, R. H. *Rapid Commun. Mass Spectrom.* **1996**, 10, 889-896.

95. Schwartz, J. C.; Kaiser, R. E.; Cooks, R. G.; Savickas, P. J. *Int. J. Mass Spectrom. Ion Proc.* **1990**, 98, 209-224.

96. Clayton, E.; Bateman, R. H. *Rapid Commun. Mass Spectrom.* **1992**, 6, 719-720.

97. Bateman, R. H.; Green, M. R.; Scott, G.; Clayton, E. *Rapid Commun. Mass Spectrom.* **1995**, 9, 1227-1233.

98. Johnstone, R. A. W.; Rose, M. E. *Mass Spectrometry for Chemists and Biochemists*, Cambridge University Press **1996**, chapter 9.

99. Genuit, W.; Nibering, N. M. M. *Int. J. Mass Spectrom. Ion Proc.* **1986**, 73, 61-80.

100. Wahrhaftig, A. L. In *Gaseous Ion Chemistry and Mass Spectrometry*. Jean H. Futrell, Ed. Wiley, New York **1986**.

101. Vekey, K.; Somogyi, A.; Wysocki, V. H. *Rapid Commun. Mass Spectrom.* **1996**, 10, 911-918.

102. Takayama, M.; Fukai, T.; Nomura, T.; Nojima, K. *Rapid Commun. Mass Spectrom.* **1989**, 3, 4-6.

103. Macfarlane, R. D.; Torgerson, D. F. *Science* **1976**, 191, 920-925.

104. Hakansson, P.; Kamensky, I.; Sundqvist, B.; Fohlman, J.; Peterson, P; Mc Neal, C. J.; Macfarlane, R. D. *J. Am. Chem. Soc.* **1982**, 104, 2948-2949.

105. Hillenkamp, F.; Karas, M. In *Methods in Enzymology* McCluskey, J. A. Ed. Academic Press, San Diego, **1990**, Chapter 12, 280-295.

106. Beckey, H. D. *Principles of Field Ionization and Field Desorption Mass Spectrometry*, Pergamon, Oxford, **1977**.

107. Blakley, C. R.; Vestal, M. L. *Anal. Chem.* **1983**, 55, 750-754.

108. Gaskell, S. J. *J. Mass Spectrom.* **1997**, 32, 677-688.

109. Curtis, J. M.; Bradley, C. D.; Derrick, P. D.; Sheil, M. M. *Org. Mass Spectrom.* **1992**, 27, 502-507.

110. Sheil, M. M.; Kilby, G. W.; Curtis, J. M.; Bradley, C. D.; Derrick, P. D. *Org. Mass Spectrom.* **1993**, 28, 574-576.

111. Kilby, G. W.; Sheil, M. M., *Org. Mass Spectrom.* **1993**, 28, 1417-1423.

112. Gaskell, S. J.; Reilly, M. H.; Porter, C. J. *Rapid Commun. Mass Spectrom.* **1988**, 2, 142-145.

113. Roepstorff, P.; Fohlman, J. *Biomed. Mass Spectrom.* **1984**, 11, 601.

114. Westmore, J.B.; Alauddin, M.M. *Mass Spectrom. Rev.* **1986**, 5, 381-465.

115. Bjorkman, S. *Biomed Mass Spectrom.* **1982**, 9, 315-322.

116. Dass, C *J. Mass Spectrom.* **1996**, 31, 77-82.

117. Sunner, J. *Org. Mass Spectrom.* **1993**, 28, 805-823.

118. Katakuse, I; Desiderio, D. M. *Int. J. Mass Spectrom. Ion Phys.* **1983**, 54, 1-15

119. Alexander, A.J.; Boyd, R. K. *Int. J. Mass Spectrom. Ion Proc.* **1989**, 90, 211-240.

120. De Pauw, E. In *Methods of Enzymology*, vol 193 McCluskey, J. A. Ed., Academic Press, San Diego **1990**, 201-214.

121. Dass, C.; Desiderio, D. M. in *Proceedings of the 40th ASMS Conference on Mass Spectrometry and Allied Topics*, Washington, DC, **1992**, 1937.

122. Guevremont, R.; Boyd, R. K. *Rapid Commun. Mass Spectrom.* **1988**, 2, 1-5.

123. van Dongen, W. D.; Ruijters, H. F. M.; Luinge, H. J.; Heerma, W.; Haverkamp, J. *J. Mass Spectrom.* **1996**, 31, 1156-1162.

124. Ballard, K. D.; Gaskell, S. J. *Int. J. Mass Spectrom. Ion Proc.* **1991**, 111, 173-189.

125. Meot-Ner, M.; Dongre, A. R.; Somogyi, A.; Wysocki, V. H. *Rapid Commun. Mass Spectrom.* **1995**, 9, 829-836.

126. Schnier, P.D.; Price, W. D.; Strittmatter, E. F.; Williams, E. R. *J. Am. Soc. Mass Spectrom.* **1997**, 8, 771-780.

127. Millington, D. S.; Roe, C. R.; Maltby, D. A. *Biomed. Mass. Spectrom.* **1984**, 11, 236-241.

128. Van Bocxlaer, J. F.; Claeys, M.; Van den Heuvel, H; De Leenheer, A. P. *J Mass Spectrom.* **1995**, 30, 69-80.

129. Yergey, A. L.; Liberato, D. J.; Millington, D. S. *Anal. Biochem.* **1984**, 139, 278-283.

130. Liberato, D. J.; Millington, D. S.; Yergey, A. L. In *Mass Spectrometry in the Health and Life Sciences*, Burlingame, A. L.; Castagnoli, N. Ed. Elsevier, Amsterdam. **1985**, chapter 24, 333-348.

131. Duran, M; Ketting, D.; Dorland, L.; Wadman, S. K. *J. Inh. Metab. Dis.* **1985**, 8, suppl. 2, 143-144.

132. Harrison, A. G. *Chemical Ionization Mass Spectrometry* CRC Press, Boca Raton, FL, **1992**.

133. Bone, W. M.; Hunt, D. F.; Marasco, J. M. In *Proceedings of the 30th ASMS Conference on Mass Spectrometry and Allied Topics*, Honolulu, **1982**, 566.

134. Gaskell, S. J.; Guenat, C.; Millington, D. S.; Maltby, D. A.; Roe, C. R. *Anal. Chem.* **1986**, *58, 2801-2805.*

135. Fetterolf, D. D.; Yost, R. A. *Int. J. Mass Spectrom. Ion Phys.* **1982**, 44, 37-50.

136. Johnson, J. V.; Yost, R. A. ; Kelley, P. E.; Bradford, D. L. *Anal. Chem.* **1990**, 62, 2162-2172.

137. Talrose, V. L.; Lyubimova, A. K. *Dokl. Akad. Nauk SSSR* **1952**, 86, 909.

138. Field, F. H. *J. Am. Chem. Soc.* **1961**, 83, 1523-1534.

139. Field, F. H.; Franklin J. L.; Munson, M. S. B. *J. Am. Chem. Soc.* **1963**, 85, 3575-3583.

140. Munson, M. S. B.; Franklin J. L.; Field, F. H.; *J. Am. Chem. Soc.* **1964**, 68, 3098.

141. Field, F. H. *J. Am. Soc. Mass Spectrom.* **1990**, 1, 277-283.

142. Chapman, J. R. *Practical Organic Mass Spectrometry*, Wiley, Chichester **1993**.

143. *NIST Chemistry Webbook, NIST Standard Reference Database*, Number 69, March **1998** on-line release, http//webbook.nist.gov/chemistry.

144. Schoots, A. C.; Leclerq, P. A. *Biomed. Mass. Spectrom.* **1979**, 6, 502-507.

145. Brenton, A. G. *J. Mass Spectrom.* **1995**, 30, 657-665.

146. Kitson, F. G.; Larsen, B. S.; McEwen, C. N. *Gas Chromatography and Mass Spectrometry*, Academic Press, San Diego, **1996**.

147. Field, F. H. In *Mass Spectrometry*, Maccoll, A., Ed.; MTP Publishers, London, **1972**, 133-181.

148. McLafferty, F. W.; Turecek, F. *Interpretation of Mass Spectra*. University Science Books, Mill Valley, CA **1993**.

149. Nguyen, V. Q.; Turecek, F. *J. Mass Spectrom.* **1996**, 31, 1173-1184.

150. Nguyen, V. Q.; Turecek, F. *J. Mass Spectrom.* **1997**, 32, 55-63.

151. Mamyrin, B. A.; Karataev, V. I.; Shmikk, D. V.; Zagulin, V. A. *Sov. Phys. JETP.* **1973**, 37, 45-48.

152. Tang, X.; Ens, W.; Standing, K.G.; Westmore, J.B. *Anal. Chem.* **1988**, 60, 1791-1799.

153. Spengler, B.; Kirsch, D.; Kaufmann, R. *J. Phys. Chem.* **1992**, 96, 9678-9684.

154. Spengler, B.; Kirsch, D.; Kaufmann, R. J.; Jaeger, E. *Rapid Commun. Mass Spectrom.* **1992**, 6, 105-108.

155. Johnson, R. E.; Sundqvist, B. U. R. *Rapid Commun. Mass Spectrom.* **1991**, 5, 574-578.

156. Vertes, A.; Gigbels, R.; Levine, R. D. *Rapid Commun. Mass Spectrom.* **1990**, 4, 228-233.

157. Hillenkamp, F; Karas, M.; Beavis, R. C.; Chait, B. T. *Anal. Chem.* **1991**, 63, 1193A-1203A.

158. Karas, M.; Bahr, U; Strupat, K.; Hillenkamp, F.; Tsorbopoulos, A.; Pramanik, B. N. *Anal. Chem.* **1995**, 67, 675-679.

159. Liao, P. C.; Allison, J. *J. Mass Spectrom.* **1995**, 30, 408-423.

160. Chiarelli, M. P.; Sharkey, A. G.; Hercules, D. M. *Anal. Chem.* **1993**, 65, 307-311.

161. Ehring, H; Karas, M.; Hillenkamp, F. *Org. Mass Spectrom.* **1992**, 27, 472-480.

162. Stimson, E.; Truong, O.; Richter, W. J.; Waterfield, M. D.; Burlingame, A. L. *Int. J. Mass Spectrom. Ion Proc.* **1997**, 169/170, 231-240.

163. Jorgensen, T. J. D.; Bojesen, G.; Rahbeknielsen, H. *European Mass Spectrom.* **1998**, 4, 39-45.

164. Beavis, R. C.; Chaudhary, T; Chait, B. T. *Org. Mass Spectrom.* **1992**, 27, 156-158.

165. Rouse, J. C.; Yu, W.; Martin, S. A. *J. Am. Soc. Mass Spectrom.* **1995**, 6, 822-835.

166. Kaufmann, R.; Spengler, B.; Lützenkirchen, F. *Rapid Comm. Mass Spectrom.* **1993**, 7, 902-910.

167. Hsu, F-F.; Gross, M. L. in *Proceedings of the 44th ASMS Conference on Mass Spectrometry and Allied Topics,* Portland, OR. **1996**, 921.

168. Vachet, R. W.; Winders, A. D.; Glish, G. L. *Anal. Chem.* **1996**, 68, 522-526.

169. Johnson, R.S.; Martin, S.A.; Biemann, K. *Int. J. Mass Spectrom. Ion Proc.* **1988**, 86, 137-154.

170. Wada, Y.; Matsuo, T.; Papayannopoulos, I. A.; Costello, C. E.; Biemann, K. *Int. J. Mass Spectrom. Ion Proc.* **1992**, 122, 219-229.

171. Papayannopoulos, I. A. *J. Am. Soc. Mass Spectrom.* **1996**, 7, 1034-1039.

172. Hunt, D. F.; Yates, J. R., III; Shabanowitz, J.; Winston, S.; Hauer, C. R. *Proc. Natl. Acad. Sci. U. S. A.* **1986**, 83, 6233-6237.

173. Biemann, K. *Biomed. Mass Spectrom.* **1988**, 16, 99-111.

174. Johnson, R. S.; Martin, S. A.; Biemann, K.; Stults, J. T.; Watson, J. T. *Anal. Chem.* **1987**, 59, 2621-2625.

175. Alexander, A. J.; Thibault, P.; Boyd, R. K. *Rapid Commun. Mass Spectrom.* **1989**, 3, 30-34.

176. Martin, S. A.; Johnson, R. S.; Costello, C. E.; Biemann, K. In *Analysis of Peptides and Proteins*, McNeal, C. J.; Ed; Wiley, Chichester, **1988** 135-150.

177. Cerny, R.L.; MacMillan, D.K.; Gross, M.L.; Mallams, A.K.; Pramanik, B.N. *J. Am. Soc. Mass Spectrom.* **1994**, 5, 151-158.

178. Boue, S. M. Ph. D. Dissertation, University of Florida, **1997**.

179. Kauffmann, R.; Kirsch, D.; Spengler, B. *Int. J. Mass Spectrom. Ion Proc.* **1994**, 131, 355-385.

180. Yudi, L. M., Baruzzi, A. M.; Solis, V. *J. Electroanal. Chem.* **1993**, 360, 211-219.

181. Pariza, R. J.; Freiberg, L. A. *Pure Appl. Chem.* **1994**, 66, 2365-2368.

182. Volmer, D. A.; Hui, J. P. M. *Rapid Commun. Mass Spectrom.* **1998**, 12, 123-129.

183. Sunner, L.W.; Edmonson, R.D.; Kinsel, M.G.; Hamon, R.; Sulikowski, G.; Russell, D.H. in *Proceedings of the 43rd ASMS Conference on Mass Spectrometry and Allied Topics*, Atlanta, GA, **1995**, 1250-1251.

184. Tsarbopoulos, A.; Karas, M.; Strupat, K.; Pramanik, B. N.; Nagabhushan, T. L. Hillenkamp, F. *Anal. Chem.* **1994**, 66, 2062-2070.

185. Burton, R.D.; Watson, C.H.; Eyler, J.R.; Lang, G.L.; Powell, D.H.; Avery, M.Y. *Rapid Commun. Mass Spectrom.* **1997**, 11, 443-446.

BIOGRAPHICAL SKETCH

Maria del Pilar Ospina Mejia was born in Caicedonia, Colombia on September 26, 1967, to Jose Ospina and Haydee Mejia. In August of 1983, she graduated from secondary school from Colegio Bolivariano while still being 15. Maria wanted to be a medical doctor or a pharmaceutical chemist (in Colombia, these are not considered graduate degrees) but did not get accepted into the institutions she had applied even though she had been salutatorian in her class. She was driving her parents crazy and they decided to send her to Cali, Colombia where she started as an audit at the Universidad del Valle (Univalle) in the spring of 1984. She attended medical school classes and also calculus, physics and chemistry classes (designed for chemistry majors) as preparation for the entrance examination of the university. Maria was accepted to Univalle for the fall of 1984 and graduated as a chemist in February of 1989 after a three-month internship at Hoechst Colombiana.

Maria worked at Univalle for about two and a half years. She was in charge of performing mass spectrometry and gas chromatography analysis and assisting undergraduates with laboratory practices in these areas. Maria was then lured into doing research at the Centro Internacional de Agricultura Tropical (CIAT), where she worked on liquid chromatography of plant extracts and gel electrophoresis of proteins. At that time, her head had already started flashing

the word graduate school. After being at CIAT for about five months, she was offered the opportunity of working as a research assistant in the Spectroscopic Services Laboratory of the University of Florida doing mass spectrometry. This was made possible thanks to Dr. William R. Dolbier, whom she had met while working at Univalle and recommended her for the position. The idea of working for one year and then applying to graduate school sounded sufficiently attractive and she took the chance. While working in this laboratory, she completed the requirements and was granted admission into the graduate program of the Department of Chemistry at UF. She began graduate school in January of 1993 and continued working as a research assistant in the Spectroscopic Services Laboratory for four more years. Maria investigated the effect of internal energy on collision-induced dissociation spectra under the direction of Drs. Richard A. Yost and David H. Powell. Upon graduation, Maria will work as a postdoctoral fellow at the Centers for Disease Control and Prevention in Atlanta, Georgia.

I certify that I have read this study and that in my opinion it conforms to acceptable standards of scholarly presentation and is fully adequate, in scope and quality, as a dissertation for the degree of Doctor of Philosophy.

Richard A. Yost, Chairman
Professor of Chemistry

I certify that I have read this study and that in my opinion it conforms to acceptable standards of scholarly presentation and is fully adequate, in scope and quality, as a dissertation for the degree of Doctor of Philosophy.

David H. Powell
Associate Scientist of Chemistry

I certify that I have read this study and that in my opinion it conforms to acceptable standards of scholarly presentation and is fully adequate, in scope and quality, as a dissertation for the degree of Doctor of Philosophy.

Samuel O. Colgate
Professor of Chemistry

I certify that I have read this study and that in my opinion it conforms to acceptable standards of scholarly presentation and is fully adequate, in scope and quality, as a dissertation for the degree of Doctor of Philosophy.

John R. Eyler
Professor of Chemistry

I certify that I have read this study and that in my opinion it conforms to acceptable standards of scholarly presentation and is fully adequate, in scope and quality, as a dissertation for the degree of Doctor of Philosophy.

John P. Toth
Associate Scientist in Food Science
and Human Nutrition

This dissertation was submitted to the Graduate Faculty of the Department of Chemistry in the College of Liberal Arts and Sciences and to the Graduate School and was accepted as partial fulfillment of the requirements for the degree of Doctor of Philosophy.

December, 1998

Dean, Graduate School